AD

AVSCOM REPORT NO. 77-27

PRODUCTION ENGINEERING MEASURES PROGRAM MANUFACTURING METHODS AND TECHNOLOGY

INFLUENCE OF GRAIN REFINEMENT ON THE STRUCTURE AND PROPERTIES OF CAST NICKEL-BASE SUPERALLOY TURBINE COMPONENTS

A.F. Denzine, T.A. Kolakowski, W.M. Matlock and J.F. Wallace

CASE WESTERN RESERVE UNIVERSITY
10900 Euclid Avenue
Cleveland, Ohio 44106

May 1977

AMMRC CTR 77-15

FINAL REPORT - CONTRACT NO. DAAG46-74-C-0009

Prepared for
U.S. ARMY AVIATION SYSTEMS COMMAND
St. Louis, Missouri 63166

ARMY MATERIALS AND MECHANICS RESEARCH CENTER
Watertown, Massachusetts 02172

This project was accomplished as part of the U.S. Army Manufacturing Technology program. The primary objective of this program is to develop, on a timely basis, manufacturing processes, techniques, and equipment for use in production of Army Materiel.

The findings in this report are not to be construed as an official Department of the Army position, unless so designated by other authorized documents.

Mention of any trade names or manufacturers in this report shall not be construed as advertising nor as an official indorsement or approval of such products or companies by the United States Government.

DISPOSITION INSTRUCTIONS

Destroy this report when it is no longer needed.
Do not return it to the originator.

(18) USAAVSCOM, AMMRC (19) 77-27, CTR-77-15

UNCLASSIFIED

SECURITY CLASSIFICATION OF THIS PAGE (When Data Entered)

REPORT DOCUMENTATION PAGE	READ INSTRUCTIONS BEFORE COMPLETING FORM
1. REPORT NUMBER: AVSCOM Report No. 77-27	2. GOVT ACCESSION NO. / 3. RECIPIENT'S CATALOG NUMBER
4. TITLE (and Subtitle): INFLUENCE OF GRAIN REFINEMENT ON THE STRUCTURE AND PROPERTIES OF CAST NICKEL-BASE SUPERALLOY TURBINE COMPONENTS.	5. TYPE OF REPORT & PERIOD COVERED: Final Report, 10 Sept 1973-15 May 1977 / 6. PERFORMING ORG. REPORT NUMBER: AMMRC-CTR-77-15
7. AUTHOR(s): A.F. Denzine, T.A. Kolakowski, W.M. Matlock and J.F. Wallace	8. CONTRACT OR GRANT NUMBER(s): DAAG46-74-C-0009
9. PERFORMING ORGANIZATION NAME AND ADDRESS: Case Western Reserve University, 10900 Euclid Avenue, Cleveland, Ohio 44106	10. PROGRAM ELEMENT, PROJECT, TASK AREA & WORK UNIT NUMBERS: D/A Project: 1728036, AMCMS Code: 4097, Agency Accession:
11. CONTROLLING OFFICE NAME AND ADDRESS: U.S. Army Aviation Systems Command, St. Louis, Missouri 63166, Attn: DRSAV-EXT P.O. Box 209	12. REPORT DATE: May 1977 / 13. NUMBER OF PAGES: 106
14. MONITORING AGENCY NAME & ADDRESS (if different from Controlling Office): Army Materials and Mechanics Research Center, Watertown, Massachusetts 02172	15. SECURITY CLASS. (of this report): Unclassified / 15a. DECLASSIFICATION/DOWNGRADING SCHEDULE: -

16. DISTRIBUTION STATEMENT (of this Report)

Approved for public release; distribution unlimited.

17. DISTRIBUTION STATEMENT (of the abstract entered in Block 20, if different from Report)

18. SUPPLEMENTARY NOTES

19. KEY WORDS (Continue on reverse side if necessary and identify by block number)

Cast Nickel Superalloys
Cast Grain Size Control
Low Cycle Fatigue
Stress Rupture Properties
Tensile Properties
Fatigue-Creep Properties

20. ABSTRACT (Continue on reverse side if necessary and identify by block number)

The influence of refinement of the cast grains on the mechanical properties of three nickel base superalloys (713LC, MAR-M-246 and C103) was determined. The investigation was conducted because improvements in the fatigue properties of integrally cast rotors for helicopters was desired. Grain refinement of all three alloys was accomplished by a controlled thermal cycling technique together with a boron addition to the melt. This refinement practice was successfully adapted to a

DD FORM 1 JAN 73 1473 EDITION OF 1 NOV 65 IS OBSOLETE

UNCLASSIFIED

SECURITY CLASSIFICATION OF THIS PAGE (When Data Entered)

492 49

production rotor casting. This grain refinement increased by a factor of 2 to 4 the number of cycles to failure in low cycle fatigue of 713LC and MAR-M-246. The fatigue behavior of C103 was insensitive to grain size. The yield strength of 713LC and MAR-M-246 was increased 10 ksi but the tensile strength and ductility slightly decreased by grain refinement. The 1800°F stress rupture properties of the refined alloys were slightly superior to the unrefined alloys at high stress levels and equal to or slightly inferior at low stress levels. At 1850°F and lower stress levels, the stress rupture properties of MAR-M-246 were somewhat reduced compared to the unrefined structure.

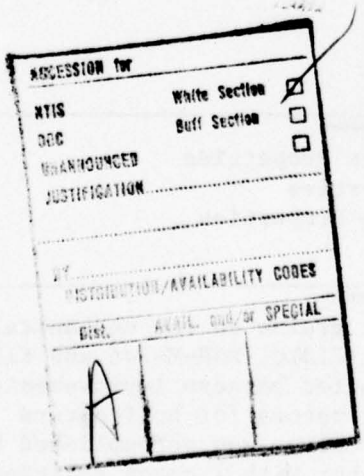

SUMMARY

This investigation studied the influence of refinement of the cast grains on the mechanical properties of nickel base superalloys (713LC, MAR-M-246 and C103). The purpose was to improve the service life of T-63 rotors which now have their service life limited by fatigue in the rim sections. The rotor is presently produced from MAR-M-246 by a vacuum investment casting process. The conventional casting techniques employed in its manufacture result in large columnar grains which cause an anisotropic fatigue behavior. The primary emphasis of the investigation was to improve the fatigue properties although other properties including the tensile, stress rupture, combined fatigue-creep, thermal fatigue and oxidation behavior were studied.

For 713LC and MAR-M-246, grain refinement was initially accomplished on a small laboratory furnace by the addition of 0.1%B and 0.1%Zr to the melt which was heated to about 2850°F. The melt was then partially solidified in the crucible, reheated and poured with a 50-100°F superheat into simple slab molds preheated to 1650°F. The resulting equiaxed structure had grain sizes ranging from ASTM #2 (713LC hub) to ASTM #4 (MAR-M-246 rim). These compared to unrefined grains about 100 times larger. For alloy C103 (an alloy that contains about 1% Hf) the formation of hafnium borides at temperatures above 2804°F prevented the formation of other borides which served as substrates for heterogeneous nucleation. A technique was developed with a maximum melt temperature in the range of 2635°F to 2804°F which allowed these effective borides to form in preference to HfB. The C103 melt was then partially solidified, remelted, and poured with a 50-100°F superheat into a slab mold preheated to 1650°F to yield an equiaxed structure of grain size ASTM #3 3.5.

Further development of the grain refining technique resulted in eliminating the 0.1%Zr addition so that only 0.1%B was added and establishing proper time-temperature cycles to achieve refinement in the variety of section thicknesses in the T-63 rotor. Thin section castings including thermal fatigue blades and tubular (0.060 inch wall) stress rupture specimens were cast successfully employing this grain refinement technique. A production melting unit (Austenal Division of Howmet Corporation) was used to cast grain refined MAR-M-246 rotors of acceptable quality and soundness.

The mechanical properties including tensile properties, low-cycle fatigue resistance, combined fatigue-creep lives, thermal fatigue and oxidation properties, and stress rupture behavior were determined for the unrefined (baseline, columnar), fine columnar, and refined (equiaxed) structures of the three test alloys. The number of cycles to failure in low-cycle fatigue of 713LC and MAR-M-246 were improved above the baseline structure by a factor of 2-4 upon grain refinement. The low-cycle fatigue performance of the fine columnar structure (obtained with CoO coated

olds) was inferior to both the equiaxed and baseline structures. The fatigue performance of C103 was insensitive to grain morphology.

The cycles to failure obtained during the fatigue-creep test which utilized a 90 second hold time at the maximum strain showed significantly longer lives at equivalent strains for grain refined 713LC and MAR-M-246 compared to the coarse columnar grained cast structure. The fatigue-creep properties of C103 were little affected by grain refinement. The slope of the strain amplitude-fatigue life test with the hold time is steeper than the conventional fatigue life curves. At high strain amplitudes the lives are similar to the conventional fatigue test for MAR-M-246 and longer for coarse grained 713LC and C103 indicating a hardening effect from the creep component in the latter two alloys.

Grain refinement produced an increase of 10 ksi in the yield strength of 713LC and MAR-M-246 and a slight decrease in tensile strength. Both the yield and tensile strengths of C103 decreased as a result of grain refinement. The ductility was also lowered a small amount in the refined compared to the baseline or unrefined condition. Thermal fatigue tests on a burner rig failed to crack baseline or refined specimens of all three alloys. Weight loss measurements indicate a higher oxidation rate for grain refined samples of MAR-M-246 and C103.

The 1800°F stress rupture properties of refined alloys were slightly superior to baseline (columnar) alloys at relatively high stress levels and equal to or slightly inferior, in the case of 713LC, to baseline stress rupture properties at lower stress levels. The stress rupture tests at the higher temperature of 1850°F and lower stress level of 20.0 ksi indicated slightly shoter lives of 68.7 hours for refined MAR-M-246 alloy compared to the 88.4 hour lives with the coarse columnar structure.

It was concluded that the grain refining process developed could be employed successfully to produce integrally cast rotors. These grain refined rotors would have superior fatigue properties and adequate stress properties at the service temperatures and stress levels presently found in operating engines.

PREFACE

This project was accomplished as part of the US Army Aviation Systems Command Manufacturing Technology program. The primary objective of this program is to develop, on a timely basis, manufacturing processes, techniques, and equipment for use in production of Army material. Comments are solicited on the potential utilization of the information contained herein as applied to present and/or future production programs. Such comments should be sent to: US Army Aviation Systems Command, ATTN: DRSAV-EXT, P.O. Box 209, St. Louis, MO 63166.

The authors wish to express their appreciation to the individuals who contributed to this work: the personnel at AMMRC including Perry Smoot, the Technical Supervisor of the project, Mr. E. Scott Nichols of Allison Division of Detroit Diesel, Mr. W.M. Garcia and Mr. R. Ransom of the Austenal Division of Howmet Corporation, La Porte, Indiana, and Dr. R. Ashbrook and Mr. J. Johnston at NASA, Lewis Research Center.

TABLE OF CONTENTS

TABLE OF CONTENTS
... Continued ...

INTRODUCTION

Gas turbines are now used in a variety of aircraft, marine, industrial and vehicular applications as well as high performance military aircraft. Since the early 1960's a trend of rapidly rising turbine inlet temperatures has occurred (1*) because of the increase in efficiency (2). The growing demands of advancing gas turbine engine technology have, since the early 1940's, required the development of high strength heat-resistant materials. To keep pace with the increasing temperature in recent years, improved technology has led to the development of alloys capable of higher strengths at these elevated temperatures. These approaches have included directionally solidified alloys and eutectics, superalloy powder metallurgy, dispersion strengthening, and processing improvements. However, the disparity which exists between alloy capability and the rise in inlet temperature has not been offset completely by advancements in component cooling concepts, so a need for improved materials remains.

A. Service Considerations

While the high temperature capability of an alloy is most commonly expressed in terms of a temperature to produce rupture in 100 hours at a given stress, several additional properties must be considered. The choice of which properties are most critical depends on the location in the gas turbine under consideration. This study will be restricted to the hot section of the gas turbine engine, with emphasis on improving the properties of the turbine rotor.

A rotor is customarily divided into three general areas; the hub, the rim, and the blades. As shown in Figure 1, the hub section is located near the axis of the disc. In the hub section, operating temperatures are low (approximately 500°F) but stresses from centrifugal loads are high. High tensile strength and good low-cycle fatigue resistance are primary requirements in the hub section. The rim section is the outer region of the disc in the area of blade attachment. In this region temperatures of 1400°F (760°C) add hot corrosion resistance to the fatigue and tensile requirements. In the blade section, where operating temperatures are the highest, up to 1800°F (980°C), stress rupture life is of primary importance. The blade root is subjected to temperatures of 1400-1600°F and stresses of 40,000 to 80,000 psi (3), and requires strength, creep ductility and low-cycle fatigue strength. Steep thermal gradients of 500°F along a blade span in normal engine operation add to the combination of fatigue and creep. Since these parts are in contact with high-temperature combustion products of high oxygen content, good oxidation resistance is mandatory. Resistance to surface degradation by hot corrosion (oxidation in combination with

---

*Numerical notations refer to literature listed under references.

sodium, sulfur, vanadium, and other fuel or air contaminants) is also an important requirement.

All three sections of the rotor are subjected to mechanically and thermally induced cyclic strain. The mechanical strains have a high mean strain (from the centrifugal loading) with a low alternating strain from vibrations of the spinning rotor. The frequency of the cyclic strain in the hub and rim depends upon rotational speed, while the blade and blade root experience higher frequencies from airfoil twist and bending.

The thermally induced cyclic strain arises during acceleration and deceleration of the turbine. During acceleration, turbine blade leading and trailing edges heat up faster and expand more than the cooler mid-chord region. This nonuniform heating results in internal stresses which are compressive in the hotter regions and tensile in the cooler regions. Following acceleration is an equilibrium period during which a nearly uniform temperature is present across the blade. On deceleration, the leading and trailing edges cool more rapidly than the center region resulting in tensile stresses in the cooler edges and compression in the hotter center. This sequence is shown schematically in Figure 2 (4). By a similar mechanism, the rim is subjected to thermal cyclic strain when the engine is started and stopped.

In the preceding discussion, the service requirements were treated for the general case of a gas turbine rotor. In this study, a particular gas turbine rotor will be examined. The rotor (Figure 3) is designed for use in the small T-63 gas turbine which provides power for OH6A and OH58A army helicopters. Currently, the T-63 first stage turbine rotor is being replaced after 1000 hours of service because of the appearance of thermal fatigue cracks in the rim section as indicated by arrows in Figure 1. Considerable economic gain would be realized if the fatigue properties could be improved and service life of the rotor could be extended to 2000 hours or more.

The T-63 rotor achieves a temperature of approximately 1400°F at the rim, the blades encounter considerably higher ($\sim$ 1800°F) temperatures. The temperature decreases when moving toward the axis to no more than 500°F in the hub section. The engine burns a standard grade (Jet-A) jet fuel and produces 320 horsepower.

B. Rotor Development: Alloys and Processes

The T-63 rotor is currently being produced as an integral wheel (blades and disc are a single piece) using a vacuum investment casting process. Several nickel base superalloys are used to produce the rotors: 713C, 713LC and MAR-M-246. Before proceeding with the details of T-63 rotor production, a brief review of the evolution of superalloys and related processes is in order.

In the early 1940's the first precipitation hardening nickel-base (80% nickel, 20% chromium) alloys were developed. Precipitation hardening was achieved by the alloying addition of aluminum and titanium which formed the γ (gamma prime) precipitate in the FCC (γ) matrix. The γ' phase is the FCC coherent intermetallic phase Ni_3 (Al,Ti). During the late 1940's molybdenum was added as a solid-solution and carbide forming strengthener, and the alloys were used extensively in the production of forged turbine blades. Processing, at this point, was limited to air-melted wrought nickel-base alloys.

By the late 1950's, increasing turbine operating temperature was limited by the capabilities of wrought alloys. The introduction of vacuum induction melting greatly improved the quality and properties of the existing alloys. Vacuum melting removes oxygen and nitrogen from the melt, preventing their reaction with aluminum and titanium to form oxide and nitride inclusions. Titanium and aluminum are thus retained for subsequent γ' formation. Alloys of greater strength were available by varying the composition, but no methods were available to forge alloys with such exceptional strength at high temperatures. The needed strength was made available by induction melting and investment casting wholly under vacuum. The vacuum investment casting made it possible to closely control alloy composition, maintain dissolved gases at low levels and facilitate mold filling. This resulted in the use of lower metal pour temperatures, allowing greater control of grain size.

With these improvements, a new family of nickel-base superalloys evolved, specifically designed for high temperature capability and for production as vacuum investment cast parts. The microstructure of these alloys consists of an FCC solid-solution matrix, carbides, and the coherent intermetallic phase, γ'. These alloys are strengthened principally by aluminum, titanium, columbium, and tantalum, which combine with nickel to form the FCC γ'. Additions of cobalt raise the γ' solvus temperature, thus improving strength at high temperatures. Carbides are the principal second phases. Various carbides exist, depending on alloy composition and heat treatment. Carbon (added at levels of about 0.05 to 0.2%) reacts with refractory elements present to form primary MC carbides (large blocky-spherical particles) which decompose to form lower carbides such as $M_{23}C_6$ and M_6C, which are located at the grain boundaries. Strength is also increased by elements in solid-solution, the most effective of which are molybdenum, tungsten and chromium. Aluminum and chromium provide oxidation resistance, and chromium and titanium are effective in imparting hot-corrosion resistance. Small additions of boron and zirconium greatly improve stress-rupture properties. Boron, in the form of an M_3B_2 boride, is present at the grain boundaries. The most recent alloys include the addition of 1-2% hafnium which alters carbide, grain boundary, and γ' morphologies to improve the transverse ductility of columnar grained castings (5-9). The role of various elements in superalloy analyses is summarized in Table I. With increasing operating temperatures and higher stresses, additional strength at higher temperatures was required. This was accomplished by variations

in processing. Dispersion hardening was obtained by powder metallurgy procedures with the use of thoria dispersed nickel and nickel-chromium alloys. The Y_2O_3 dispersed alloys were developed later. These had the combined advantage of the strength of TD nickel above 1500°F (815°C) and γ' strengthening at lower temperatures. Variations in the thermo-mechanical processing cycles of conventional superalloy forgings show promise of improving performance at temperatures below 1400°F (760°C).

In 1966, advances were made in the control of the direction of solidification, enabling the production of investment castings containing columnar grains oriented parallel to the major stress axis. This grain orientation greatly improves resistance to intergranular fracture at elevated temperatures, thus improving creep strength, ductility, and thermal fatigue resistance (10-13). As a further improvement, grain boundaries have been eliminated as the sites of crack initiation and chemical segregation by casting single crystals using the unidirectional solidification techniques with control of grain seeding. This procedure has shown advantages in terms of stress-rupture properties and corrosion resistance.

A class of composite materials that offers the possibility of improvement in high temperature performance are the in-situ composites, specifically the directionally solidified eutectics. These materials generally have an aligned two phase structure consisting of a hard, brittle reinforcement phase in a matrix of a more ductile materials. The aligned structure is formed during unidirectional solidification from a homogeneous liquid phase (14).

The main emphasis of alloy and process development has been to improve the stress-rupture properties and thermal fatigue resistance in blade sections. For the T-63 rotor under consideration in this study, failure was not occurring from a stress rupture or thermal fatigue condition in the blades but from combined thermal and mechanical fatigue in the rim and hub. This situation occurs because the conditions of use of the T-63 rotor are such that the fatigue properties in the rim are more critical than the stress rupture properties in the blades. The nickel base alloys are used in fatigue applications because their endurance limit is maintained at elevated temperatures although some problems with their fatigue behavior do occur (15). The fatigue behavior is a consequence of the planar slip mode which is operative to approximately 1400°F (760°C). Fatigue life is then governed by the fast crack propagation rates along planar slip bands and through carbide phases. Therefore, to attain the ultimate in fatigue properties, structural heterogeneities should be eliminated and slip dispersed.

The approach toward improving stress-rupture properties has been to control the solidification behavior to minimize the grain boundary material oriented normal to the major stress direction; the extreme example of this is single crystals. Solidification control can also be used to improve fatigue properties by the production of a uniform,

fine equiaxed grain size. Improved low-cycle fatigue resistance with a reduction in grain size has been obtained in work involving wrought nickel-base superalloys (1,16,17). A similar increase in tensile properties occurs with inoculated and refined cast alloys (18).

A homogeneous fine equiaxed structure has the considerable advantage of providing uniform properties in all directions compared to the greater variation in the anisotropic properties of a columnar grained material. Also, the fine grains tend to disperse slip and to minimize the effects of segregation and structural heterogeneities by reducing their degree and extent.

C. Solidification and Grain Refinement Principles

The parameters which must be controlled to refine the cast structure can be deduced from known principles of solidification. The transformation from the liquid to the solid state is a two-step process involving the nucleation of stable particles in the melt and the subsequent growth of these particles.

The nucleation phase can be a difficult step in the process (even though the solidification of all commercial alloys occurs by heterogeneous nucleation) because of the surface energy between the nucleus and the melt. This energy is primarily supplied by the bulk free energy difference between the two phases involved and requires undercooling to produce nucleation. Continued growth, once the effect of undercooling has been overcome, requires the removal of heat from the system, since the evolving heat of fusion raises the temperature at the liquid-solid interface.

A concentration gradient of solute generally forms at the liquid-solid interface during the growth of nuclei in alloy metals. This variation in composition occurs because the solute content in the solid particles rejected from the melt differs from that in the co-existing liquid. The concentration gradient in the liquid next to the advancing interface produces a corresponding gradient in the liquidus temperature distribution curve (19-20), leading to the well known phenomenon of constitutional supercooling of the liquid adjacent to the interface. When a sufficiently shallow thermal gradient is obtained, independent nucleation in the melt ahead of the liquid-solid interface occurs. The growth of the initial solid (usually columnar) crystals will be stopped by contact with the new equiaxed crystals. This situation is favored by low thermal gradient to rate of solidification ratios or $G/R^{1/2}$, high solute content and low equilibrium distribution coefficients of the solute elements. Interruption of the growth of columnar crystals can also be obtained by other mechanisms but the constitutional supercooling plus separate nucleation phenomena appear to be the operative mechanisms in this study.

Refinement of the as-cast structure requires that nucleation occur at a large number of sites and that extensive growth of crystals be

avoided. It follows that grain refinement necessitates both ease of nucleation and inhibition of the continued growth of crystallites in the melt. Rapid nucleation can be achieved through numerous methods including, chill action, thermal cycling, mechanical vibration, rotation, convection, and inoculation. Chilling promotes nucleation at the mold wall but does not, in itself, provide the additional nuclei required for a fine equiaxed structure unless accompanied by a very low superheat. Thermal cycling involves the partial solidification of a suitable alloy which is then remelted and poured quickly and with minimal superheat. In certain alloys, carbide and other phases are sluggish in dissolving during remelting, and can act as nucleation sites resulting in grain refinement. Mechanical vibration has been widely studied as a means of achieving grain refinement (19-25). The effect occurs because of fragmentation of dendrite arms to act as substrates or by cavitation. The disadvantages to this technique include the complexity of equipment to vibrate a heated mold in a vacuum furnace and the tendency to break molds. Rotation of the mold during solidification has also been used to control grain size and structure (10,26). In this case, the refinement is attributed to fragmentation of existing crystals which then float into the molten zone and act as nuclei. The effect of natural convection has been studied in terms of its potential in structure control (27). Refinement is rationalized in terms of a "raining down" of melted off dendrite fragments.

Inoculation, or the addition of stable substrates for heterogeneous nucleation, has been one of the more effective techniques for grain refinement when utilized along with constitutional supercooling. Inoculation generally refers to the addition of a substance to the melt which provides finely distributed particles on which nucleation of the parent solid can readily occur. These substances may be added to the crucible before melting, to the melt itself, or in the form of a prime-coat on the mold. The mechanism by which inoculants reduce the work of nucleation (and thus the critical nucleus size) can be rationalized in terms of interfacial energies (28). The interfacial energy between the substrate and the nucleus is substantially less than between the liquid and nucleus. This fact plus the ability of rough surfaces on substrates to lower the number of atoms required to provide a stable nucleus and to reduce the surface area in contact with the liquid account for the lower interfacial energy for nucleation attained by inoculation.

The criteria that an inoculant must possess to perform as a stable substrate for hetergeneous nucleation are not entirely established. A partial list of the prerequisites is as follows (19,22,28):

1. Good matching between the crystal structure of the parent solid and the inoculating particle to reduce interfacial energy at this contacting surface.

2. Stability of the particle at the freezing point of the parent material.

3. Density of the particle must be such that it is not subject to appreciable gravity segregation.

4. The substrates must be fine particles which are well dispersed.

5. Surfaces of the substrates must be clean (free of oxides or other components).

6. Substrates with rough surfaces reduce the surface energy of the system.

In addition to the presence of stable substrates for nucleation sites, effective grain refinement depends upon the constitutional supercooling produced by solute concentrations at the advancing interface, so that the liquidus temperature in the vicinity of the substrate will decrease below the nucleation temperature. The thermal conditions that favor constitutional supercooling include a high growth rate and a shallow thermal gradient. The conditions favoring grain refinement based on inoculation and grain growth restriction from constitutional supercooling can be summarized as follows:

1. Availability of sites of easy nucleation which are well distributed throughout the melt.

2. Low pouring temperature and a preheated mold to guarantee a shallow temperature gradient in the liquid.

3. The presence of suitable solute alloys.

Grain refinement by inoculation has been successfully applied to a number of alloy systems. Most frequently used are additions which form the desired substrate after a chemical reaction in the melt, thereby providing a clean, reactive surface. Form, et al (19) describe the addition of Co, W, and Fe powders to copper, TiC and ZrC to steel, and FeSi to gray iron. The refinement of steel by Ti addition (29), and austenitic stainless steel by addition of Zr (22) and CaCN (30) has been documented. Cerium has been found to be an effective inoculant for certain nickel and aluminum alloys (31). Within the abundance of information that exists in the literature, the use of elements such as Ti, Zr, C and B appear to be most favored for use as inoculants since they form compounds such as TiC, TiB, ZrC and ZrB in the melt.

Inoculation at the casting surface is also a useful technique for grain refinement. Metallic oxides such as CoO in the form of a prime coat in investment molds will be reduced to Co (when in contact with the molten metal) which acts as an inoculant. Using this technique, the surface of the casting will appear to have a fine equiaxed structure, but internally a columnar structure is present with grain size increasing toward the center of the casting.

D. Mechanical Testing

To evaluate the suitability of a material for turbine application, appropriate mechanical property data must be accumulated. The mechanical tests must be chosen to simulate the service conditions in terms of operating temperature, environment and type of loading. For an integral rotor, loading conditions and temperatures vary considerably from the blades to the hub, making it impossible to run a single type of test to assess the suitability of the material accurately. For the T-63 rotor, tensile, mechanical fatigue and stress rupture data are necessary for material evaluation. A detailed description of these tests is presented in Experimental Procedures.

E. Objectives

Integrally cast turbine rotors are used in army helicopter engines, such as the T-63 engine. Some problems have been encountered in the past with thermal fatigue cracking of the rim of the T-63 first stage turbine rotor. The present work was undertaken to overcome these problems with the following specific objectives.

1. Develop a technique for structure control of cast rotor rim, hub, and blade sections.

2. Test the effect of structural control on properties, using a combination of tensile, low-cycle fatigue, combined fatigue-creep, thermal fatigue-corrosion, and stress rupture tests.

3. Adapt the technique to a production facility for limited production of rotors with controlled structure and properties.

EXPERIMENTAL PROCEDURES

A. Alloy Selection

The three alloys chosen for use in this study were 713LC, MAR-M-246, and C103 with their compositions listed in Table II. These alloys were selected to fulfill the following criteria:

1. Alloys tested should represent materials currently used in the production of cast turbine components.

2. The selected alloys should provide a range of composition to insure that the grain refinement technique developed will have a relatively wide application.

3. Baseline properties of these alloys (yield strength, tensile strength, elongation, stress-rupture properties, corrosion resistance, etc.) should vary over a range typical of the family of cast superalloys.

4. Traditional, well-established alloys through "state-of-the-art" materials should be represented.

713LC has had widespread use for a number of years in the production of turbine components, including the T-63 rotor. It has a rather lean composition compared to most superalloys, with no cobalt or tungsten and low carbon. This alloy is the least expensive of the three tested and is considered easy to cast (23) in production applications. The alloy was obtained in the form of 3" diameter remelt stock from Special Metals Corporation, New Hartford, New York.

MAR-M-246 has also had widespread use in the production of turbine components, replacing 713LC in some applications including a revised design of the T-63 rotor. Compositionally, MAR-M-246 differs from 713LC by its increased carbon (0.15% compared to 0.05% for 713LC) and the presence of 10% cobalt and 10% tungsten which improve some properties and increase the cost per pound of the alloy. MAR-M-246 has increased strength and reduced ductility (compared to 713LC) at temperatures up to 1800°F (32-33). This alloy was supplied in the form of 2.75" diameter remelt stock from the Alloy Division of Howmet Corporation, Dover, New Jersey.

C103 is a recently developed experimental superalloy. The most significant change in the alloy is the addition of 1% hafnium to increase transverse ductility and improve hot corrosion resistance. While aluminum plus titanium is maintained at approximately 7% for all three alloys, 4.0% titanium is used in C103 compared to 0.75-1.5% for 713LC and MAR-M-246. Further, columbium plus tantalum are increased in C103 from 1.5 to 5.0% to offset the reduction in tungsten (from 10.0% to 5.0%). This alloy was supplied in the form of 2.75" diameter remelt stock from Detroit Diesel, Allison Division, General Motors, Indianapolis, Indiana.

B. Investment Mold Design

Investment molds were designed to simulate the thermal processing of the hub, rim, and blade sections of the T-63 rotor. These molds were designed and produced for casting to permit the development, evaluation, and perfection of structure control techniques separately on each of the three section before using the more expensive rotor molds. The design of the simulated sections was based on the drawing of the T-63 rotor shown in Figure 3. The most important parameter to be controlled is solidification time, which is proportional to $(V)^2/(SA)^2$ (V=casting volume, SA=surface area of casting), which therefore varies for the hub, rim, and blade sections. The molds must also be designed such that sound castings can be produced. The molds taper inward from the top to the bottom to insure proper feeding and are adequately risered. The

volume of the casting plus the volume of the riser is limited to a maximum of eighteen cubic inches or the maximum volume of the crucible available for this study. The geometry of the casting must be such that a maximum number of specimens can be obtained to minimize heat-to-heat variations in properties. Finally, the mold-riser-pouring basin assembly must fit into the mold heater within the furnace.

The hub and rim molds designed to meet these qualifications are shown in Figures 4 and 5. The molds were produced at a commercial plant (Sherwood Refractories Co.) supplying the turbine component industry, using seven layers of zircon flour slurry. Half of the molds had a CoO prime coat. The specimens used in tensile, fatigue, and combined creep-fatigue tests were machined from hub and rim molds. The thermal fatigue-oxidation specimens and tubular stress rupture specimens were cast in clusters with six specimens arranged under a riser on each mold. Details of specimen design are presented subsequently.

The design of the two types of rotor molds employed in this study was identical to that commonly used in the industry. Flat stress rupture paddles were cast in place of blades on a seven and one half inch diameter rotor. This type of casting permitted the evaluation of the stress rupture properties of the alloys with grain morphologies which simulate the structures obtained in integrally cast rotor blades. The T-63 rotor mold used to cast final rotors was the DD 536-A mold cast by Austenal Division of Howmet Corporation, La Porte, Indiana. The rotor molds were made of seven to nine layers of zircon flour slurry and had a prime coat of CoO.

C. Casting Technique

All of the experimental, simulated section castings were produced in a small experimental vacuum induction furnace; the rotor castings were made in the production unit (Austenal Division of Howmet Corporation). For heats from the small furnace, the charge (remelt stock plus additions) is melted in a stabilized zirconia crucible which is placed within a graphite susceptor. Power is supplied by a 275 KVA, 960 cycle motor-generator set with appropriate controls. The six pound charge is melted in approximately fifteen minutes and can then be poured by tipping the furnace toward the mold positioned in the mold preheating oven.

For a typical heat, the technique used is as follows. After loading the charge, the furnace is evacuated to a pressure of 10-25 microns (during the production casting of rotors, a vacuum of 8-20 microns is used (23)) requiring a pump down time to 8-12 hours using a mechanical roughing pump. The mold preheating oven is started and controlled to $\pm 15°F$. The charge is then heated, and as melting begins the furnace is back-filled with 1/2 atmosphere of argon to prevent the loss of high vapor pressure elements and reduce bubbling at the surface of the melt. The superheat is measured within $\pm 25°F$ using a Pt-Pt 10% Rh immersion thermocouple. When the desired superheat is achieved, the furnace is

poured in approximately one second. The vacuum is then broken, and an exothermic "hot-top" compound is placed on top of the riser to assure soundness and avoid nucleation from particles falling from the top surface. The mold preheating oven is then turned off and the casting allowed to cool in the furnace.

Several hub and rim castings and all of the rotor castings were produced on the production melting unit at Howmet. The furnace is rated at 90KW and operates at 3000 cycles per second. A fourteen pound charge can be melted in approximately five minutes. After melting and following the selected thermal superheating and thermal cycling, the interlock between the melt chamber and the mold chamber is opened and the molten charge is poured into a preheated mold. The interlock is then closed and the vacuum is broken in the mold chamber only.

Before proceeding with the development of a grain refinement technique, the values of mold preheat temperature and melt superheat temperature were established. A matrix of heats was produced with mold preheat temperature varying from 1500°F to 1900°F and melt superheat varying from 200°F to 350°F. The combination of a 1650°F mold and a 250°F superheat was selected for use as baseline conditions. This selection was based on the as-cast structure which produced an average grain size (coarse columnar morphology) and secondary dendrite arm spacing that was similar to those for the T-63 rotor produced on a commercial basis. This combination of mold temperature and superheat also results in the best as-cast mechanical properties (33).

With a casting process established for the production of baseline heats, a series of variations from the basic technique were evaluated in terms of their effect on control of grain size and morphology. A detailed description of the techniques used and their effect on the microstructure are provided in the Results and Discussion section since these techniques have to be discussed in terms of the resulting structures. In brief, the hub and rim molds were altered, using a CoO prime coat to produce fine columnar grains. The alloy compositions were changed by the addition of small amounts of cerium, calcium cyanamide, nickel-boron powder, boron and zirconium to the melt. The maximum melt temperature was carefully controlled to insure the production of the proper substrates. Thermal cycling techniques with pouring temperatures as low as 50°F were also employed. The end result was the attainment of coarse columnar, fine columnar, and fine equiaxed structures depending on the casting technique employed. These techniques were applied to the production of hub, rim and blade sections and later to the production of rotors.

D. Mechanical Testing

The schedule of mechanical testing is summarized in Table III. Hub and rim sections were subjected to tensile and low cycle fatigue tests (strain controlled) at temperatures consistent with in-service

operating temperature (room temperature, 1000°F, 1400°F for rim specimens; room temperature and 500°F for hub specimens).

A threaded end hourglass specimen (Figure 6) was designed for use in the tensile, strain cycle fatigue and fatigue-creep tests at room and elevated temperature. The design is similar to that used in previous studies (34-36). Specimen dimensions were limited by the dimensions of the casting to a maximum length of 2.750" and maximum diameter at the thread of 0.500", with a minimum diameter of 0.250". The stress concentration factor from this shape was calculated to be 1.027 at the outside diameter. The hourglass geometry of the gage section was chosen after consideration of the advantages and disadvantages of that design (34). The advantages are: controlling and measuring the strain at the fracture cross-section; utilization of large compressive strains without buckling; a limited length over which the temperature has to be controlled closely; reducing the significant test section; and ready location of the diametral strain sensors with allowance for their accurate measurement.

Mechanical fatigue and tensile tests were performed on an M.T.S. closed loop servo-hydraulic testing facility. The movement of the axial ram was controlled by diametral strain measured by the movement of two quartz rods located across the diameter of the specimen. This strain was then converted electronically into axial strain fed into the PDP-11 computer of the M.T.S. unit. Conversion of diametral strain to axial strain required an input of Poisson's ratio or Young's modulus into the plastic strain computer. These values were obtained for each material at each grain size on a Baldwin machine which can be calibrated directly using hanging weights for load calibration and a rod of known taper driven through a U-type strain gage for strain calibration.

For high temperature testing, heat was supplied from a double wound induction coil. The temperature was controlled to ± 9°F by a thermocouple located directly beneath the coil near the top of the hourglass. A second thermocouple was attached at the minimum diameter, between the two quartz rods.

Axial alignment of the load cell, specimen, and ram was achieved through the use of a Wood's metal grip at the bottom of the specimen. After the specimen was inserted, the grip was heated until the Wood's metal became molten. The specimen was then free to float and axially align itself when a small load was applied; the Wood's metal was then allowed to solidify and, thereby, properly located the specimen.

The mechanical fatigue tests were conducted in a strain control mode, with a zero mean strain. To determine the strain levels for the tests, the shape of the ε vs. N curve was estimated first. This was accomplished by using the data from a monotonic tensile test, a single strain controlled fatigue test, and an incremental step test (36).

Selection of a suitable cyclic frequency was based on the capabilities of the testing system, which is usually limited by the dynamic characteristics of the extensometer. Frequencies are limited to those levels which do not disrupt isothermal conditions because of adiabatic heating. Further, poor hysteresis records result when the X-Y recorder is driven excessively fast. For these tests, the cyclic frequency was varied from 0.3 Hz to 0.5 Hz depending on the strain range. At higher strain amplitudes, a lower frequency was used to maintain a nearly constant strain rate for all strain ranges. The cyclic frequency selected is within the range used in previous studies (36) where no significant difference in fatigue life was observed for frequencies of 0.1 to 10 Hz.

A one-channel block program was used to produce the fatigue-creep cycle. The load was applied as a sinusoidal wave function with respect to time and began the first cycle in the third quadrant or compression direction from the zero stress and strain origin. The first channel block program cycled the specimen through the third, fourth and first quadrants of the sine function or from zero strain to maximum compression to zero strain to maximum tension. At this point the computer held the specimen at the maximum tensile strain for 90 seconds. After completion of the hold time, a second channel block program returned the specimen to zero strain. After a few cycles, a stabilized hysteresis loop was generated. Apart from the 90 second hold time, the cycle was completed in 0.5 seconds.

The tensile hold time of 90 seconds was chosen to produce significant stress relaxation in each cycle while allowing the tests to be completed in a reasonable length of time. Comparing the test frequency of the present study, .01 Hz, to earlier (37,38,39) strain range partitioning results, indicates the creep component of the cycle, $\Delta\varepsilon_{cc}$ as approximately 10%. The half-cycle strain ranges investigated were 0.3 to 0.6% which produced failure within 1 to 10^4 cycles. These ranges were comparable to those used to establish the conventional low-cycle fatigue data.

The thermal fatigue performance of simulated blade specimens was evaluated using the specimen shown in Figure 7. Testing was conducted on the thermal fatigue facility at NASA Lewis Research Center. This type of equipment is typically used to simulate the environment of a jet engine and is widely used in the evaluation of turbine alloys. The paddle specimens were quickly heated in the blast of a jet burning a mixture of Jet-A grade jet fuel and air to a temperature of 1800°F at Mach 0.3 and then quickly cooled to 1000°F in an air blast at Mach 0.7. To assure uniform heating, the sample holder was rotated in the blast at 450 rpm. All specimens were weighed before testing and were weighed and inspected at ten hour intervals. The test temperature was monitored using an optical pyrometer which was calibrated by placing a thermocouple on a dummy specimen. The test cycle had a duration of 2.5 minutes, with two minutes heating and 30 seconds cooling. A total of 2400 cycles was run in the 100 hour test duration. This technique is similar to that used by other investigators (14).

Both tubular and flat specimen stress rupture tests were performed on Satec Model LD creep units. The tubular specimens illustrated in Figure 8 were tested in air at 1800°F ±3°F and the flat specimens shown in Figure 9 were tested in air at 1850°F ±3°F. Temperatures were controlled with chromel-alumel thermocouples. Tests were made at constant load with initial stress levels of 17.62 to 38.18 ksi for tubular specimens and 20.00 ksi for flat specimens.

Specimen strain was measured for selected stress levels by monitoring load train motion with a LVDT with the output measured on a chart recorder. This provided a record of axial displacement vs. time. Minimum creep rates were calculated from the slope of the straight section of the creep curve which followed the primary creep portion. All specimens were tested to failure and elongations to failure were measured with dividers and a ruler.

E. Microstructural Analaysis

A major portion of the microstructural examination of castings and test specimens was performed using light microscopy and standard metallographic techniques. The etchant had the following composition: 150 ml methanol, 50 ml HCl, and 2.5 grams $CuCl_2$. The grain size and shape, gamma prime size and distribution, grain boundary morphology and the morphology of carbides, borides and other phases were evaluated.

The light microscopy study was augmented by the electron microprobe which was used to investigate the partitioning of alloying elements. A Materials Analysis Company Model 400 S microprobe was employed in this study. The three spectrometer system was operated at 20 KeV using $K\alpha_1$ radiation.

RESULTS AND DISCUSSION

A. Structure Control of Superalloy Castings

As described in Experimental Procedures, a mold preheat temperature of 1650°F in combination with a superheat of 250°F was selected for use in the production of baseline heats of the three alloys. This selection provides a structure similar to that present in the T-63 rotor produced on a commercial basis. The macrostructure of a typical commercial rotor is shown in Figure 10. The macrostructure of a baseline heat of 713LC is shown in Figure 11a, with a coarse columnar structure and grains up to 0.5" diameter. A nearly identical structure is obtained from baseline heats of MAR-M-246 and C103 with a slight increase in maximum grain size for hub molds compared to rim molds.

To obtain a fine columnar structure, an investment mold inoculated with a prime coat of cobaltous oxide (CoO) was employed. Using alloy

713LC and thermal conditions identical to those for a baseline heat, the structure shown in Figure 11b was produced. As the molten metal comes into contact with the mold wall, the CoO is reduced to Co which acts as a substrate for nucleation at the surface. The very fine columnar grains at the surface changes to extended growth of those grains oriented most favorably for growth, resulting in the grain size increasing toward the center of the casting. A similar result was obtained for MAR-M-246 and C103 cast in inoculated rim molds.

To obtain a fine equiaxed structure requires that nucleation occur at a large number of sites. As discussed in the Introduction, inoculation together with constitutional supercooling has been found to be the most effective technique for grain refinement, with Ti, Zr, B, and C most widely used as inoculants and the solute segregation at the solid-liquid interface provided by the solute elements present in the alloy. For the alloys under consideration, titanium and carbon contents are closely controlled to allow the formation of a suitable proportion of gamma prime and carbides for optimum mechanical properties but sufficient latitude is available for additions of these elements as inoculants without major microstructural changes. Using an inoculated mold preheated to 1600°F, additions of 0.1 wt. % Zr (in sponge form) and 0.1 wt. %B (elemental powder wrapped in nickel foil packets) were made to a crucible charged with 713LC.

To obtain refinement, suitable substrates must be formed in the melt. The Ti-B-C ternary phase diagram (Figure 12) (40) serves only to approximate solid state transformation temperature in certain highly segregated regions of the Ni rich systems being considered. It is apparent from Figure 12 that the melt must be heated to temperatures above the 1510°C (2750°F) isotherm (shaded or cross hatched) to form TiB and TiC. Melt temperatures in excess of the similarily shaded 2160°C (3920°F) isotherm are required to form TiB_2. Based on this approximation, the melt temperature was established in the range of 2850°F-2900°F since higher temperatures are regarded as extremely detrimental to crucible life and significantly lower temperatures probably would not permit the formation of TiB and TiC. After this temperature range is achieved, the charge is allowed to cool in the crucible for 10-25 minutes (until solidification has progressed sufficiently to freeze the top metal completely over) to provide substrates of TiC and TiB. The charge is then reheated and poured quickly with a 50-100°F superheat. This freezing and remelting has the advantage of facilitating temperature control on the pour temperature. When this thermal cycling technique was performed on 713LC without any added boron or zirconium, no effect was observed on the grain macrostructure. However, when 0.1%B and 0.1%Zr were added to the charge and the thermal cycle was performed, grain refinement was obtained.

The macrostructure resulting from this casting technique is shown in Figure 13a. This is a fine equiaxed structure with a grain size of ASTM #3. The same technique was then applied to the larger hub mold,

resulting in the structure shown in Figure 13b. This fine equiaxed structure with a thin columnar region at the surface has a grain size of ASTM #2. This technique was applied to alloy MAR-M-246 hub and rim molds to obtain even finer equiaxed structures with equiaxed grain sizes of ASTM #4 and ASTM #3.5 for the rim and hub sections, respectively. The additional refinement in this alloy compared to that of 713LC is attributed to the higher carbon and refractory content of MAR-M-246.

The application of the previously described technique proved unsuccessful with rim sections of alloy C103. A coarse columnar structure similar to that in Figure 11a was produced. In alloy C103 the most significant alloying addition (compared to 713LC and MAR-M-246) is 1% hafnium. Since the existing grain refinement theory is based on the formation of titanium and zirconium borides and carbides in the melt (which then act as substrates for heterogeneous nucleation), it is significant that a higher negative free energy of formation exists for hafnium borides and carbides than for the titanium and zirconium counterparts (Table IV) (41). The hafnium in the alloy would be expected to react preferentially with the boron and carbon, reducing the amount available to the titanium and zirconium. The hafnium borides and carbides apparently do not act as effective substrates for reasons that will be discussed later.

To verify the presence of hafnium as the source of the problem, a heat was made using alloy MAR-M-246 and a 1% addition of hafnium. The casting technique employed was that which previously produced refinement in MAR-M-246. Instead of the previous fine grained equiaxed structure, coarse equiaxed grains result with a region of fine columnar grains at the surface.

A comparison of the Ti-Zr-B and Ti-HF-B (40) ternary phase diagrams (again only serving as approximations in a highly alloyed, Ni-rich system) in Figures 14 and 15 indicates that the titanium and zirconium borides begin to form upon cooling from temperatures above the 1445°C (2635°F) minimum shown in Figure 14. However, the hafnium borides can begin to form upon cooling from temperatures above about 1540°C (2804°F) as shown in Figure 15. Therefore, heating to the intermediate temperature range between 2635°F and 2804°F is designed to result in the formation of effective substrates of titanium or zirconium borides with a minimal loss of substrates from the presence of hafnium because the boron is not tied up as hafnium borides that apparently fail to serve as substrates.

Using boron and zirconium as inoculants and a cobaltous oxide coated rim mold, a C103 heat was made by heating to approximately 2660°F, cooling and then pouring with a 50°F superheat. The casting surface was composed of fine columnar grains because of the action of the mold inoculant and the body of the casting was equiaxed with an average grain diameter of 0.07". While this structure is not as fine grained as those of 713LC or MAR-M-246, it represents a significant improvement compared to previous attempts with C103 in this

investigation. A second heat was made under the same conditions with the maximum temperature increased to the upper limit (2804°F) suggested by the phase diagram approximations. The structure was wholly equiaxed, with an average grain diameter of 0.004" (ASTM #3.5). The same technique was then applied to an inoculated hub mold and the structure was wholly equiaxed with an average grain diameter of 0.005" (ASTM #3).

B. Production of Test Castings and Rotors

The grain refinement technique utilized on the simulated mold section castings employed alloying additions of 0.1%B plus 0.1%Zr and a thermal cycling between 2800°F for 713LC and MAR-M-246 or 2635 to 2804°F for C103 and the melting temperature of the various alloys. After this cycling a low pouring temperature with 50 to 80°F superheat and low mold temperature of 1650°F was utilized. In addition, the melt chamber was back-filled with 1/2 atmosphere of argon after melting had started. During the production casting of integrally cast rotors in a commercial melting unit, these alloying additions and thermal cycling can be readily accomplished but the low pouring and mold temperatures and argon back-fill would interfere with filling the thin blade sections of the rotor. Zirconium additions could lead to hot tearing problems.

Since MAR-M-246 alloy is now used for production rotors, this composition was the one investigated. Two experimental heats of MAR-M-246 were cast from the small size furnace into rim molds to determine whether the zirconium addition and argon back-fill were necessary to grain refine in the experimental furnace. The results showed that grain refinement was obtained without zirconium additions with only 0.1%B added. However, the argon back-fill proved to be necessary in this laboratory furnace. These results indicate that titanium borides are the primary substrates for heterogeneous nucleation of the nickel solid solution phase. Poor vacuum conditions once melting begins (pressure approximately 200 microns and an excessively high leak rate) in the small size experimental furnace may have contaminated the surface of these substrates without argon back-fill. A 1/2 atmosphere back-fill reduces the leak rate of outside air to a very low level and minimizes the available oxygen for substrate contamination. The production melting unit was capable of much better vacuum conditions (less than one micron and very low leak rates). An argon back-fill was later proven to be unnecessary for grain refinement on this unit.

The tubular stress rupture specimens were cast on the laboratory casting facility. An argon back-fill was used, 0.1%B was added and thermal cycling was employed in grain refined heats. Problems with filling the long, thin tubular specimens made higher pouring and mold temperatures necessary. Mold temperature was held at 1900°F, baseline heats were poured with 250°F superheat and refined heats were poured with 150°F superheat. The baseline heats had long columnar grains oriented perpendicular to the specimen axis which often extended across the entire tubular cross-section. The refined heats exhibited an equi-

axed structure with grain diameters of approximately 0.005-0.010 inch. These equiaxed grains are slightly larger than the 0.004 inch diameter grains obtained previously in rim molds because of the higher pour and mold temperatures that were needed to fill the thin tubular specimen molds.

The remainder of the casting work was conducted on the production facility at Austenal Division of Howmet Corporation, La Porte, Indiana using MAR-M-246. Two series of hub and rim molds (heats 1-10 and heats 11-16) were cast to establish an optimum refinement technique. Tables V and VI summarize the preliminary results of these heats. The temperatures referred to in these two tables were obtained with an optical pyrometer. A check of the melting temperature of MAR-M-246 using the optical pyrometer showed the alloy to melt at 2250°F. Previous experience with MAR-M-246 on the experimental furnace using an immersion thermocouple indicated that the alloy melts at approximately 2350°F. This discrepancy caused the reported temperatures in Tables V and VI to be somewhat low. In addition the time required to reach the maximum temperature of the thermal cycle was not controlled or even measured in these heats while it had been consistently 20 minutes in heats made on the experimental facility. The lack of cycle time and temperature control were responsible for the inconsistent success in grain refining MAR-M-246 in these preliminary production heats.

Only heats #3 and #10 showed a wholly equiaxed structure. However, this series of heats provided considerable useful information. Heat #3 demonstrated again that grain refinement could be obtained without a zirconium but not without a boron addition. Heat #10 confirmed that refinement was possible without an argon back-fill and that only a boron addition and proper time and temperature control of the thermal cycle were necessary. Based on these results, the formation of titanium borides to act as potent substrates for heterogeneous nucleation appears to be dependent on both time and temperature. These two parameters were carefully controlled in subsequent production heats to duplicate the conditions used successfully on the experimental casting facility. This duplication required that the maximum temperature of the thermal cycle was reached in approximately twenty minutes.

The next series of heats employed MAR-M-246 cast in T-63 rotor molds. Table VII shows the results of the six heats. A photograph of one of the rotors (sectioned for structure examination) is shown in Figure 16. The first rotor (serial number J 311) was cast as a control sample. Conventional production techniques of Austenal Division of Howmet were used to obtain a corase columnar structure (Figure 17). The other five rotors were grain refined (Figure 18) by the following modified technique.

a. Add 0.1%B (powder wrapped in Ni foil) to the charge.

b. Thermal cycle to melting temperature plus 375-450°F in approximately 20 minutes.

c. Cool the melt until partial solidification had occurred.

d. Reheat and pour with 10-25°F superheat into an 1800°F mold.

This technique resulted in a consistent fine equiaxed structure with an approximate grain diameter of 0.004 inch and is the recommended refinement technique. The low pour and mold temperatures caused incomplete fill in the blade sections of the rotors. Three additional grain refined MAR-M-246, T-63 rotors were poured into 2100°F molds at superheats of +20, +50 and +100°F (not listed in Table VII). The rotors poured at +20 and +50°F superheat also failed to fill in the blade sections properly. However, the rotor poured at +100°F superheat was completely filled. The grain structure remained wholly equiaxed with an average grain diameter of 0.004-0.006 inch.

The 7 1/2 inch diameter test rotors with stress rupture paddles in place of blades were also cast with MAR-M-246 in 2100°F molds at the production facility. A baseline (columnar) rotor was cast using conventional practice. The macrostructure in the paddle is identical to that of a conventionally cast T-63 rotor blade (similar to Figure 11a). A refined (equiaxed) test rotor was cast using the modified grain refinement technique and a superheat of +100°F. The refined structure in the stress rupture paddles is identical to that observed in grain refined T-63 rotor blades (similar to Figure 13a).

C. Microstructural Analysis

A microstructural analysis was performed on these castings with the objective of investigating the following features: gamma prime size and distribution, carbide and boride morphology and grain boundary structure. Figures 19 a and 19b depict a low and high magnification view of a baseline heat (non-inoculated mold, 1600°F, +200°F superheat) of alloy 713LC. In Figure 19a the γ' phase ($Ni_3(Al,Ti)$) is distinguishable from the matrix by the surface texture. The grain boundaries are smooth and rounded. In Figure 19b, the γ' phase is more evident, occupying a volume fraction of between 60-70%. Two types of carbides are visible, the large, blocky MC carbides, and the irregular, elongated $M_{23}C_6$ carbides at the grain boundaries. This structure is unchanged with the addition of a CoO mold wash. The grain refinement technique to produce equiaxed grains produces a grain boundary carbide and boride network in the microstructure of alloy 713LC as indicated in Figure 19c, This 713LC refined structure has been compared to MAR-M-246 in the refined condition as shown in Figure 19d. Both a cellular and script morphology of $M_{23}C_6$ carbides is evident with a higher volume fraction of MC carbides compared to 713LC because of the higher carbon and refractory content in MAR-M-246. Grain boundaries in this alloy are smooth and angular, and gamma

prime volume fraction is comparable to that of 713LC.

Micrographs of a baseline heat of alloy C103 are shown in Figures 20a and 20b. The structure of the γ and γ' phase is different compared to the other alloys, since it occurs in globular islands of γ/γ' eutectic. The grains are populated with angular hexagonal carbides as shown in 20b. A micrograph of this alloy in the refined condition in Figure 20c indicates the convoluted grain boundary geometry resulting from the presence of the γ/γ' eutectic islands. The grain boundary carbides have assumed more of a cellular morphology as experienced with the other alloys following refinement. The microstructure of C103 has undergone some change during the grain refinement. Most significant is the increase in volume fraction of the γ/γ' eutectic with a decrease in the number and size of the angular carbides within the grains.

An electron microprobe analysis was performed on grain refined rim sections of the three alloys to investigate the partitioning of the major alloying elements. Qualitative results were obtained in the form of x-ray modulation micrographs. In alloy 713LC the carbides are depleted in terms of nickel, with titanium rich MC carbides and chromium and molybdenum rich $M_{23}C_6$ carbides as predicted by reaction equation:

$$MC + \gamma \rightarrow M_{23}C_6 + \gamma' \qquad \text{or}$$

$$(Ti,Mo)C + (Ni,Cr,Al,Ti) \rightarrow Cr_{21}Mo_2C_6 + Ni_3(Al,Ti)$$

Little information was gained on the partitioning of Ta and Zr or B and Al. A similar result is present in alloy MAR-M-246 with carbides lean in terms of Ni and Co and Ta, Zr and Ti partitioned to the MC carbides. The $M_{23}C_6$ carbides are rich in Cr, Mo and W with little information available on B and Al. In alloy C103, the hafnium is partitioned in two important locations: higher concentrations of Hf are present in the γ/γ' eutectic phase compared to the matrix; and this element is also concentrated in the angular primary carbides characteristic of hafnium-modified alloys.

These results provide information on the difficulty experienced with grain refining the hafnium-modified alloys. Assuming that carbides and borides result in stable substrates for nucleation, smooth angular carbides could fail to provide the surface roughness requirement and a poor crystallographic match occurs between the crystal structure of the parent solid and the substrate particle. The lattice parameter of HfC at 4.64 Å is 32% larger than that of the nickel matrix at 3.52 Å.

D. Mechanical Testing

1. Tensile Tests

The influence of anisotropy on tensile properties was studied by a

series of tests to relate the stresses and strains in "hard" and "soft" grains to the "hard" or "soft" orientation for controlling the test. The terms "hard" and "soft" refer to regions of high and low modulus of elasticity, respectively. To obtain an axial strain $e=(ed_1/\nu)$, using subscripts S = soft, H = hard, d = diametral, ν = Poisson's ratio, and E = elastic modulus, the following table is generated:

EXTENSOMETER CONTROLLING IN SOFT ORIENTATION

	"Soft" Grain	"Hard" Grain
Axial Strain	$\frac{1}{\nu_S} e_{d_1}$	$\frac{1}{\nu_S} e_{d_1} \frac{E_{d_S}}{E_{d_H}}$
Axial Stress	$\frac{1}{\nu_S} e_{d_1} E_{d_S}$	$\frac{1}{\nu_S} e_{d_1} \frac{E_{d_S}}{E_{d_H}} E_{d_H}$

EXTENSOMETER CONTROLLING IN HARD ORIENTATION

Axial Strain	$\frac{1}{\nu_H} e_{d_1} \frac{E_{d_H}}{E_{d_S}}$	$\frac{1}{\nu_H} e_{d_1}$
Axial Stress	$\frac{1}{\nu_H} e_{d_1} \frac{E_{d_H}}{E_{d_S}} E_{d_S}$	$\frac{1}{\nu_H} e_{d_1} E_{d_H}$

From these relations, the maximum stress is equal in hard and soft grains when controlling in the hard orientation. The maximum strain occurs in the soft grains when controlling in the hard direction. It would then be predicted that failure would initiate in the soft grains with the test controlled in the hard orientation. This behavior was confirmed by conducting a pair of fatigue tests on samples from the same heat, with nearly equal anisotrophy, positioning one sample in the hard orientation and one in the soft orientation. The specimen tested in the soft orientation had nearly double the fatigue life of its counterpart.

The orientation used to control fatigue and tensile tests of coarse grained samples exerts a significant effect on the results and has to be selected prior to testing. Using the hard orientation results in conservative estimates which may not accurately reflect the properties of a larger section. Using the soft orientation results in a consistently optimistic performance. The use of an "average" orientation has been chosen since the results will be somewhat conservative but will still reflect the scatter characteristic of the coarse grained material. It may be difficult to locate an average orientation since the properties

may change discontinuously when moving from a hard to a soft grain. In such cases, the hard orientation is chosen as the test direction as a conservative measure.

The tensile test results of rim and hub molds are summarized in Tables VIII and IX respectively. This data represents specimens from rim molds which were tested at room temperature, 1000°F and 1400°F with baseline and refined grain morphologies. Columnar grained specimens were tested at room temperature only since the properties were inferior. Also included in these tables are data from hub mold specimens tested at room temperature and 500°F (baseline and refined). The tabulated data represents the average of a minimum of two tests unless otherwise indicated.

The yield strength and tensile strength of all three alloys are generally insensitive to increasing test temperature. The yield strength of baseline heats increases from about 110 ksi for 713 LC to 125 ksi for MAR-M-246 and 130 ksi for C103. Grain refinement results in an increase in yield strength of 713LC to 120 ksi and MAR-M-246 to 135 ksi with a slight decrease in tensile strength for these alloys. The yield strength of C103 decreases to 128 ksi and tensile strength also is lowered as a result of grain refinement. The fine columnar grained structures are lower in both tensile and yield strengths compared to their baseline and refined counterparts. The ductility of the three alloys decreases at temperatures above 1200°F. Alloy 713LC has considerably greater ductility (12% elongation) than MAR-M-246 at 5% and C103 at 6% in both the baseline and refined states because of the relatively small volume fraction of carbides in this low carbon alloy. Grain refinement results in a small decrease in ductility for these alloys at these test temperatures which is attributed to the increase in brittle constituents such as networks of borides and altered carbide morphologies. The columnar grained castings have greater ductility than refined castings but less than baseline castings because the columnar grain boundaries are aligned normal to the major stress axis but do not contain the boride and altered carbides present in the grain refined structure.

The modulus of elasticity and Poisson's ratio as determined by conventional methods are summarized in Table X. Poisson's ratio is .316 for the three alloys; the elastic modulus at room temperature increases from 29.7 x 10^6 psi for 713LC to 31.53 x 10^6 psi for MAR-M-246 and 32.11 x 10^6 psi for C103. The modulus of elasticity of the three alloys decreases at 1400°F with the average decrease from about 31 x 10^6 psi at room temperature to about 24 x 10^6 psi at 1400°F.

2. Low Cycle Fatigue Tests

Room temperature strain-life curves of rim mold specimens are shown in Figure 21. Several trends are apparent as described below.

1. The baseline material shows considerably greater scatter than the

columnar or refined materials as a result of the anisotropy effects. An accurate assessment of the limits of the scatter band requires testing a greater number of specimens; these limits of the scatter band are essential to designers since the lower limit must be employed in the design.

2. The baseline properties of the alloys are superior in performance to their fine grained columnar counterparts because of the orientation of the fine columnar grains with their major axes normal to the tensile axis of the specimen.

3. For alloys 713LC and MAR-M-246, the slopes of the fatigue curves follow the relation (42)

$$(2N_f)^x \quad \Delta e_T = K$$

with K varying from 0.032 for 713LC columnar to 0.07 for MAR-M-246 refined and x = 0.24. Alloy C103 has a considerably shallower slope and does not conform to this behavior.

4. The performance of baseline MAR-M-246 and baseline 713LC is nearly identical. Columnar grained MAR-M-246 has a distinct advantage over columnar 713LC.

5. The fatigue performance of refined 713LC and MAR-M-246 is superior to their respective columnar or baseline grain structures. At a strain amplitude of 0.003, refined MAR-M-246 has a factor of four increase in cycles to failure compared to baseline MAR-M-246. Refined 713LC has fatigue life increased 1.8 times that of baseline 713LC at the same strain amplitude.

6. The shallow slope of the 3 strain-life curves for C103 indicates that this alloy is extremely sensitive to small changes in grain morphology, with columnar, baseline and refined data falling on nearly the same line.

The poor strength behavior of the columnar grained alloy in room temperature fatigue and room and elevated temperature tensile tests predicates the elimination of this grain morophology in future testing. Emphasis is, therefore, focused on the performance of baseline and refined material.

The 1000°F (538°C) fatigue performance of rim mold material is shown in Figure 22. The relative positions of the fatigue curves are unchanged with respect to the room temperature data. The slopes of the 713LC and MAR-M-246 baseline curves have decreased somewhat with the following parameters; x = 0.224 for MAR-M-246 and 713LC refined, and x = 0.21 for MAR-M-246 and 713LC baseline (coarse columnar).

This slope change can be rationalized in terms of the variation in ductility with temperature for the materials tested. At 1000°F, the elongation of 713LC baseline has decreased from 15% to 12%, with MAR-M-246 baseline dropping from 8.7% to 5.0%. Refined 713LC, refined MAR-M-246, and C103 baseline and refined show a much smaller decrease in ductility

over the same temperature range. The mechanism by which this decrease in ductility affects the slope of the fatigue curve can be explained in terms of the elastic and plastic strain contributions to the total strain life-curve. At low strain amplitudes the fatigue performance is dependent mainly upon the strength of the material since the straining is almost totally elastic. At higher strain amplitudes, the dominance of the elastic factor is reduced as the amount of plastic straining increases. The importance of material ductility, as reflected by the fatigue ductility exponent and coefficient, increases with increasing plastic strain. Therefore, the reduced ductility present at 1000°F results in decreased high strain fatigue life with low strain fatigue life unaffected, thereby reducing the slope of the fatigue curve.

The fatigue curves for rim material tested at 1400°F are shown in Figure 23. Several significant features are apparent in this figure.

1. The performance of refined MAR-M-246 and refined 713LC is superior to that of baseline heats of those materials.

2. The slopes of all six fatigue curves are reduced compared to the 1000°F data. This is again the result of a ductility loss, with the minimum in the ductility versus temperature curve (Table VIII) occurring at 1400°F. The reduced slopes have the parameters $x = 0.20$ for 713LC and $x = 0.18$ for MAR-M-246.

3. At high strain amplitudes, 713LC has considerably better fatigue life than MAR-M-246 or C103. This is attributed to the ductility of 713LC which, at 1400°F, is three times that of MAR-M-246 or C103. At lower temperatures 713LC had nearly double the ductility of MAR-M-246, but the strength advantage of MAR-M-246 was sufficient to compensate for its inferior ductility.

4. At low strain levels MAR-M-246 has the superior fatigue life. Since the straining is elastic in this region, the strength of MAR-M-246 dominates.

5. At low strain levels, the fatigue life of MAR-M-246 and C103 is superior (at 1400°F) to that at room temperature. At 1400°F, the decrease in the modulus of elasticity (Table X) results in less stress required to achieve a given strain. Since the fatigue test is being conducted in a strain control mode, specimens at the same strain level are subject to less stress at 1400°F than at room temperature. While the modulus decreases with temperature, the yield strengths of these alloys are essentially constant up to 1400°F (Table VIII). Therefore, under wholly elastic strain conditions, fatigue life at 1400°F will be superior to that at room temperature.

Room temperature strain-life curves of hub mold specimens are shown in Figure 24. The data has very close agreement with that of room temperature rim molds. For MAR-M-246 and 713LC, refined specimens have

superior fatigue performance compared to their baseline counterparts. The fatigue parameters for room temperature hub mold specimens are X = 0.24 and K = 0.072 for MAR-M-246 refined and K = 0.051 for 713LC baseline. Again, C103 has a much shallower slope of the $\Delta\varepsilon_T/2$ vs. $2N_f$ curve than 713LC or MAR-M-246.

The 500°F fatigue performance of hub mold material is shown in Figure 25. At this low test temperature, the fatigue curves are nearly identical to those at room temperature. This is the expected result since no significant changes occur in tensile properties at 500°F compared to room temperature as shown by the data in Tables VIII and IX.

The fatigue curves for each of the alloys at various test temperatures and grain morphologies are shown in Figures 26, 27 and 28 for 713LC, MAR-M-246, and C103 respectively. For 713LC (Figure 26), the decrease in slope of the fatigue curves with increasing test temperature is apparent for both baseline and refined materials. Baseline material is more susceptible to the slope change as it experiences a greater decrease in ductility with increasing temperature.

The behavior of MAR-M-246 is significantly different as shown in Figure 27. The slopes of the fatigue curves decrease with increasing temperature. However, the baseline and refined curves, at a given temperature, remain nearly parallel. The high temperature, low strain behavior of MAR-M-246 is interesting since the reversals to failure exceed those for room temperature specimens at the same strain amplitude.

C103 has the unique characteristic of being insensitive to changes in test temperature or grain morphology (Figure 28) with extreme sensitivity to changes in strain amplitude. At low strain amplitudes this material is comparable to the other alloys in terms of fatigue life but at strain amplitudes in excess of 0.004.

3. Combined Fatigue-Creep Tests

The results of the fatigue-creep tests conducted at 1400°F for the three alloys are contained in Figures 29, 30 and 31. In general, several trends are evident.

1. The slopes of the fatigue-creep curves are steeper than the conventional fatigue data. This indicates that the hold-time reduces the cycles to failure at lower strain amplitudes - higher life values. The creep damage is most evident in the high-cycle region at the longer test times. An exception to this was refined 713LC.

2. Both 713LC and MAR-M-246 demonstrate significantly longer lives in the refined than baseline condition in the fatigue-creep test. C103 shows only very limited effect of the grain morphology on fatigue-creep behavior. The data for the refined alloy indicates slightly better

fatigue-creep behavior. This is in agreement with earlier fatigue tests which showed C103 is insensitive to test temperature and grain size.

3. The fatigue creep data at shorter lives and high strain amplitudes are generally similar to conventional fatigue properties for MAR-M-246 and have longer lives than conventional fatigue for baseline 713LC and C103.

In the conventionally cast baseline condition both 713LC and MAR-M-246 undergo a reduction in life with the hold times test at long lives compared to the standard fatigue data. At about 10^3 reversals, the life is reduced by a factor of 2.5 for both alloys. This is comparable to the reduction by a factor of 5 reported for MAR-M-200 columnar grained material tested in tension-tension at 1400°F (43). This data for Reference 43 was obtained using a test frequency of 0.033 cps and this reduction factor was cited near 10^3 reversals. This reduction of 5 in life is comparable to the present work since the test temperature of 1400°F is low and the amount of life reduction is not excessive. At a higher temperature of 1700°F, the same reference reports a reduction in life of two orders of magnitude.

The influence of grain morphology on the hold time test properties is evident in Figures 29 through 31. The fatigue-creep properties of refined 713LC and MAR-M-246 were improved over the baseline condition, indicating that the fine grains were not detrimental to creep at this temperature. A similar effect for creep in nickel-base superalloys has been reported in the literature. It has been shown for MAR-M-200 at 1400°F that single crystals and coarse columnar grains demonstrate larger primary creep strains than polycrystalline material (44). The creep deformation at 1400°F in MAR-M-200 and similar advanced nickel-base superalloys is reported to occur by viscous glide of stacking fault pairs with a net Burgers vector of a <112> (45). The dislocation glide occurs over relatively large distances along the same slip plane producing relatively heterogeneous deformation. The grain boundaries in the refined material act as barriers to slip and intersections with adjacent grains limit the glide distance (44). At temperatures over 1550°F the dislocation distribution is more homogeneous causing interactions at smaller glide distances so that both coarse and fine grain materials show similar primary creep strains.

The grain boundaries of the refined alloys contain greater amounts of discontinuous carbide and boride phases as shown by the photomicrographs (Figures 19 and 20), because of the addition of boron and zirconium during refinement. These phases improve creep properties by inhibiting grain boundary sliding; however, grain boundary sliding would not be expected at 1400°F.

Although the literature indicates that hold times reduce the number of cycles to failure, the equivalent performance of MAR-M-246 and improved

life of 713LC and C103 at high strain amplitudes (life less than 3×10^2 reversals) is not too surprising. A large number of the tests reported in the literature have been at temperatures where creep is the predominant mode. At 1400°F, the creep rate of nickel-base superalloys is low. Other studies (46) have shown for the cast nickel-base superalloy Udimet 500 that a cyclic-hardening effect occurs at decreasing test frequencies (i.e. increasing creep effects) at less than 10^2 cycles at a test temperature of 730°C (1350°F). This trend reverses itself at 790°C (1450°F); at higher temperatures and the lower frequency does produce lower life. The cyclic-hardening at lower temperatures is attributed to a strain-aging effect.

To determine whether strain-aging did account for the greater life in the low-cycle region, the highest strain amplitide hysteresis loops for baseline and refined 713LC were examined. It was expected that strain-aging would cause an increase in the modulus between the initial and final stabilized cycles and be most apparent in baseline 713LC. No significant change in modulus was observed; however, the width of the loops tended to decrease after a few cycles, indicating less inelastic strain or an increase in yield strength. Another approach was tried by comparing the hardness of the fractured specimens in the heated test section to that of the unheated, essentially unstrained, threaded portion for both short and long life specimens. The results shown in Table XI indicated that the greatest increase in hardness in the heated test section from strain-aging occurred with 713LC. This difference in hardness usually decreased with increasing test time, indicating that the greatest effect should occur after a few cycles. Both 713LC and C103 indicated a larger increase in hardness than the slight increase for MAR-M-246. This is consistent with the observed hold time results since these indicated that MAR-M-246 maintained equivalent life compared to conventional fatigue whereas baseline 713LC and C103 demonstrated an improvement at less than 10^3 reversals.

A summary of the results of the hold time tests for each of the alloys in the refined condition is shown in Figure 32. These data illustrate that refined 713LC has substantially higher life at all strain amplitudes compared to MAR-M-246 and C103. At a strain amplitude of 0.004, the life of 713LC is greater by a factor of 7 than for MAR-M-246 and C103. This improvement is attributed to the greater ductility of 713LC at 1400°F indicated by the tensile test results in Table VIII and IX. This higher ductility allows the alloy to absorb the effects of creep damage. In addition the higher strain-aging response of this alloy imparts strength during cycling.

4. Thermal Fatigue and Corrosion Testing

Thermal fatigue testing of baseline and refined blade specimens of the three alloys was performed on a burner rig with air velocity of Mach 0.3. The samples were cycled between 1800°F and 1000°F with 2400 cycles accumulated during the 100 hour test duration. Examination of

the specimens revealed that none formed thermal fatigue cracks during the test. This specimen is similar to a blade shape and does not have a shape that produces severe thermal gradients with high thermal stresses.

The test was interrupted periodically and the specimens were examined for cracks and were reweighed to measure the corrosion rate. A plot of the weight change versus exposure time is shown in Figure 33. All of the specimens gained weight in the first 10-20 hours as oxide layers built upon the specimen surface. After reaching a maximum, the weight began to decrease as surface scale was removed by the gas flow. From this figure, several conclusions can be drawn:

1. After exposure times of 30 to 70 hours depending on the alloy, the rate of weight loss approaches a "steady state" value where the formation and loss of oxide scales are at equal rates.

2. Grain refinement produces an increase in weight loss for MAR-M-246 and C103, with refined and baseline 713LC nearly equal.

3. The rate of weight loss is significantly greater for C103 than for the other alloys.

The scaling of oxide layers was confined mainly to the leading edge of the blade in the region of gas impingement. A study of the corroded layers at the leading edge of a 713LC baseline specimen was conducted at the point of maximum test temperature in the center along the length of the blade. The principal features are an oxidized layer 0.001" thick with a depleted zone beneath it. The gamma prime in the alloy appears to have coarsened somewhat from the high temperature exposure.

A grain refined thermal fatigue specimen of alloy 713LC was also studied. The scaling was confined to the curved edge of the blade and did not extend to the face of the blade whereas the scaling of the baseline specimen does occur on the face. The corroded layer was thicker (0.002" maximum) at some locations on the refined specimen and the depleted zone and coarsened gamma prime were similar to those of the baseline specimen.

An electron microprobe study of this surface layer was performed. The layer is heavily concentrated with Cr and Ni with some concentration of Ti and Al. A region of chromium depletion is apparent, with evidence of some aluminum depletion at the metal-scale interface. No appreciable concentration of sulfur is visible in the base metal or scale.

Baseline MAR-M-246 is little affected by thermal fatigue exposure. Only a shallow (>0.001") discontinuous scale forms on this alloy. A shallow scale is also present on the refined samples with increased loss

of material at the leading edge. The microstructure has the characteristic coarsened gamma prime, but does not show any evidence of the formation of sigma or other embrittling phases commonly formed after high temperature exposure. Electron microprobe analysis of this scale on MAR-M-246 indicates a heavy concentration of nickel and chromium in the surface layer in addition to a build-up of aluminum and titanium. A thin (0.0005") layer at the metal-scale interface is depleted in chromium and aluminum. No significant sulfur concentration is present in the scale. The microprobe results obtained for 713LC and MAR-M-246 are consistent with those reported in the literature (47-49). In thermal fatigue tests involving higher temperatures, longer durations and exposure to sea salts, sulfur played a more dominant role.

Severe corrosion was apparent on the C103 baseline specimens that were tested. The corrosive attack extends over half of the face of the blade with some damage at the trailing edge. This condition deteriorates with the refined C103 sample where the majority of the blade surface is affected. A relatively shallow surface scale was present which overlies a prominent depleted zone. The surface layers were rich in Ni, Cr and Ti, with no visible depletion of Al.

5. Stress Rupture Tests

The results of the as cast, tubular stress rupture tests are listed in Table XII; the stress vs. life curves are shown in Figures 34-36 and summarized in Figure 37. At high stress levels and lives of less than about 15 hours, the refined 713LC has longer stress rupture life than the baseline alloy (Figure 34). However, at lower stress levels (less than about 25.0 ksi) the curves cross with baseline rupture lives longer than refined. The elongations to failure of both the refined and baseline alloy exhibit a maximum (Table XII) at approximately 23.0-25.0 ksi. At higher stress levels the refined elongations are greater than the baseline elongations; at lower stress levels (where the baseline lives are superior) the baseline elongations exceed the refined elongations. At these low stress levels (20.56 ksi), the minimum creep rate of the refined 713LC is approximately three times that of the baseline 713LC. This faster creep rate and reduced ductility at low stress levels are responsible for the crossing of the stress vs. time to rupture curves in baseline and refined 713LC.

Figure 35 shows the stress rupture behavior of baseline and refined MAR-M-246. Again, at high stress levels, the refined material shows significantly longer stress rupture lives than the baseline material. The two curves converge at about 110 hours and 26.5 ksi. However, they do not cross over as in the case of 713LC. The elongations listed in Table XII do not show the sharp maximum seen in 713LC. The elongations of the refined MAR-M-246 are greater at higher stress levels than the baseline alloy and they converge at lower stress levels along with the time to rupture. The minimum creep rate of the refined MAR-M-246 at

30.0 ksi is approximately three times that of baseline MAR-M-246. The flat stress rupture specimen tests performed on refined and baseline MAR-M-246 were conducted at a lower stress level (20.0 ksi) and a higher temperature. The results of these tests are discussed later in this section of the report.

The stress rupture behavior of baseline and refined C103 is shown in Figure 36. The results are similar to those obtained with MAR-M-246 but the curves are generally lower and converge at about 110 hours and 20.5 ksi. Considerably more scatter is evident in the data for the C103 alloy. The elongations (Table XII) of the refined material are significantly higher at all stress levels than the baseline material. As was the case with MAR-M-246, no maximum in elongation is observed over the stress range tested. The minimum creep rate (at 30.0 ksi) of refined C103 is about three times that of baseline C103. The minimum creep rates of both the baseline and refined C103 are approximately one half of the baseline and refined minimum creep rates of MAR-M-246 at the same stress level. This behavior is attributed to the convoluted, interlocking grain boundaries in alloy C103.

Figure 37 is a summary of the 1800°F tubular stress rupture life results. Alloy MAR-M-246 is clearly superior to the other two alloys; C103 has similar stress rupture properties to 713LC at the higher stress levels but is superior to 713LC at the lower stress levels. Based on these results and those observed earlier, MAR-M-246 in the refined condition appears to be the best material for rotor production and was selected. MAR-M-246 is presently being used for the production of T-63 rotors. The casting of grain refined MAR-M-246 rotors has already been discussed in a previous section of this report.

Although the creep strength expressed in terms of minimum creep rate of baseline material is higher than that of refined material in all three test alloys, the times to rupture of the refined alloys are longer than baseline alloys at relatively high stress levels. This effect has already been attributed to the increased creep ductility of the refined material at these stress levels. The grain structure of the baseline tubular stress rupture specimens was columnar with the long axis of the grains oriented perpendicular to the specimen and principal stress axis. The refined specimens had equiaxed grains with grain diameters of 0.005-0.010 inch. These structures are similar to those observed in the critical zone of stress rupture in baseline and refined turbine rotor blades. The location of this critical zone is demonstrated in Figure 38 (50).

The importance of grain boundaries that are perpendicular to crack growth direction (and thus parallel to the stress axis) in the enhancement of rupture life is implicit in the work on directionally solidified cast superalloys and elongated grain, dispersion hardened structures. Columnar grains which are oriented perpendicular to the major stress axis

produce lower rupture lives and creep ductility in superalloys when compared to columnar grains oriented parallel to the stress axis in directionally solidified or equiaxed structures (11). The results obtained in this study support this theory despite the increased grain boundary area of the refined alloys over the baseline alloys. This increased grain boundary area causes a higher creep rate by a factor of approximately three because of enhanced diffusional creep. Diffusional creep can be broken into two distinguishable components: when bulk diffusion dominates, it is called Nabarro-Herring creep; and when boundary diffusion dominates, it is known as Coble creep. No attempt has been made to distinguish between the two in this study. Despite the enhanced diffusional creep, the detrimental effects of unfavorably oriented columnar grain boundaries on rupture life and creep ductility make equiaxed grains superior at high stress levels.

In addition to the grain boundary orientation effects discussed above, the increased boron level in the refined alloys is considered to have influenced their creep properties. Trace additions of boron, zirconium and magnesium to superalloys can increase life 13 times, elongation 7 times, rupture stress 1.9 times and n, stress dependence of creep rate, from 2.4 to 9.0 (51). Although each of the three test alloys contain base levels of 0.005-0.020% boron, the refinement technique adds 0.100% or approximately a tenfold increase. This added boron both forms substrates for heterogeneous nucleation and boron segregates at the grain boundaries. The skeletal grain boundary borides found in grain refined 713LC and shown in Figure 19 support this theory.

While some mechanisms to explain the boron effect on stress rupture properties in nickel base superalloys have been offered (51,52), considerable differences of opinion still exist. Most hypotheses hinge on the unusual size of the boron atom (about three-fourths the size of the usual substitutional elements, Fe, Cr, Co, Ni, Mn and V, but somewhat larger than the interstitials H, C and N). Boron atoms segregate to grain boundaries where, because of their odd size, they are accomodated by natural lattice imperfections or holes which result from orientation differences between neighboring grains. The obvious result is that boron slows down diffusion through the grain boundaries.

Since boron atoms in the grain boundaries block short-circuit diffusional paths, they can be expected to disrupt normal grain boundary precipitation kinetics. This leads to the development of discontinuous rather than continuous grain boundary precipitates in several alloys. Also boron has been shown to retard the formation of depleted grain boundaries (carbides surrounded with an all γ or all γ' zone). These depleted zones can develop on boundaries transverse to stress during creep and cause reduced life and ductility. In γ' - free alloys, boron slows down carbide precipitation in grain boundaries and shunts carbon into the grains (53,54). The one general mechanism that is consistent with the above observations is that boron retards grain boundary diffusion.

The tubular stress rupture tests discussed above served largely as a screening test to determine which of the three alloys was most suitable for rotor production. The decision to cast refined MAR-M-246 rotors was based on the significant improvement in low cycle fatigue properties that this alloy displayed upon refinement and its superior stress rupture properties (Figure 37). The converging of refined and baseline MAR-M-246 stress rupture curves at low stress levels suggested that under extreme creep conditions (high temperatures and low stresses) the refined alloy might sacrifice too much in stress rupture properties to be acceptable for rotor production. Flat stress rupture paddles cast in place of rotor blades on baseline and refined MAR-M-246 test rotors were tested to determine whether this was the case.

Stress rupture tests were run at 20 ksi and 1850°F, and the results on flat baseline and refined MAR-M-246 paddle specimens are shown in Table XIII. The average life of the baseline specimens (88.4 hours) is longer than that of the refined specimens (68.7 hours). Refined creep elongations were greater than baseline elongations. Minimum creep rates of refined alloy were approximately twice the minimum creep rates of baseline alloy.

Based on these results, it appears that under conditions of very high temperatures and relatively low stress levels, refined stress rupture properties in MAR-M-246 rotors are slightly inferior to baseline properties. The enhanced diffusional creep which results from increased grain boundary area in the refined alloy has overcome the grain boundary orientation and boron effects which caused improved stress rupture properties in refined alloy at lower temperatues and higher stress levels. It should be noted however, that the severe creep conditions employed in these tests are not representative of conditions in the critical zone for stress rupture in a turbine rotor blade shown in Figure 38. In the T-63 rotor the maximum blade temperature is about 1800°F (at the blade tip) and the rim operates at about 1400°F; the critical zone probably experiences temperatures of approximately 1500-1700°F. Bearing this in mind, the stress rupture properties of a refined MAR-M-246 rotor could be as good as baseline MAR-M-246 rotor stress rupture properties under service conditions. Also it has already been shown that the fatigue properties of the refined alloy are superior to the fatigue properties of the baseline alloy. The complex loading and temperature distribution conditions in an integrally cast rotor suggest that the refined alloy may well have overall advantages. The final evaluation of refined versus baseline rotor performance obviously requires service testing.

CONCLUSIONS

This investigation was conducted to determine the influence of grain refinement and microstructural control on the significant properties of

nickel-base superalloys for use in integrally cast turbine rotors such as the T-63 commercial rotor produced in investment molds. The alloys selected were 713LC, MAR-M-246, and C103 and the properties studied were tensile at room temperature to 1400°F, low cycle, strain controlled mechanical fatigue at room temperature to 1400°F, combined fatigue-creep at 1400°F, stress rupture at 1800 and 1850°F in air, thermal fatigue, and hot oxidation resistance. This investigation yielded the following conclusions:

1. A grain refinement technique was developed to attain a fine equiaxed grain structure compared to the conventional commercial coarse columnar grains throughout the various sections of the integrally cast rotors. T-63 rotors of good quality were successfully cast with this fine structure throughout. The technique consists of adding 0.1% boron powder wrapped in nickel foil to the charge followed by thermal cycling the melt. This cycling was to raise the temperature of 713LC and MAR-M-246 molten alloys to over slightly 2800°F and to between 2635 and 2804°F for C103 in approximately twenty minutes followed by cooling the melt until partial solidification has occurred. The alloy is then reheated and poured into an 1800-2100°F mold with about a 100°F superheat. Refinement is attributed to the formation of titanium borides which act as stable substrates for heterogeneous nucleation.

2. Grain refinement produced an increase of 10 ksi in the yield strength of 713LC and MAR-M-246 with a slight decrease in tensile strength. Both the yield and tensile strengths of C103 decrease following grain refinement. Grain refinement also resulted in a small decrease in the ductility of each alloy at the given test temperature.

3. Grain refinement produced an increase in low cycle, strain controlled fatigue life by a factor of 2-4 compared to baseline material for alloys 713LC and MAR-M-246. These improved properties could potentially be used to improve service life. Baseline specimens exhibit considerable scatter because of anisotropy. Fine columnar castings are decidedly inferior to baseline or refined castings. As the test temperature increases, the slopes of the strain-life curves decrease as a result of the lower ductility at elevated temperatures. At low strain amplitudes, fatigue life increases with increasing temperature. The fatigue performance of C103 is insensitive to changes in test temperature and grain morphology, but it is extremely sensitive to strain amplitude.

4. The cycles to failure during the fatigue-creep test which contained a 90 second hold time in the fatigue cycle are significantly longer for 713LC and MAR-M-246 with a grain refined, fine equiaxed compared to coarse grained columnar structure. Comparison of each of the refined alloys in the hold time test showed 713LC was superior in life to MAR-M-246 or C103 by a factor of 7 at 10^3 reversals. Alloy C103 shows only a very slight improvement in fatigue-creep behavior resulting from refinement.

5. The 1800°F stress rupture tests conducted on coarse grained columnar and fine equiaxed nickel-base superalloys indicated that grain refinement produced slightly better stress rupture properties at high stress levels than coarse columnar structures with the long grain axis oriented perpendicular to the stress axis. At stress levels greater than about 23.0 ksi and lives of less than about 15 hours, grain refined 713LC has longer stress rupture lives than the coarse columnar alloy. However, at lower stress levels, the curves cross over and the rupture lives are longer for the coarse columnar than fine equiaxed grains. At high stress levels grain refined MAR-M-246 and C103 have longer rupture lives than the baseline alloys; the behavior of the two structures converge at a life of about 110 hours and a stress of 26.5 ksi for MAR-M-246 and 20.5 ksi for C103. The stress rupture properties of MAR-M-246 in the as cast condition are superior to those of the other two alloys at 1800°F. The superior rupture lives of refined alloys over baseline alloys (at high stress levels) are attributed to the higher level of boron in the refined alloys and to grain boundary orientation effects.

6. At a higher temperature of 1850°F and lower stress level of 20.0 ksi the stress rupture properties of large columnar grained MAR-M-246 was slightly longer at 88.4 hours compared to 68.7 hours for fine grained equiaxed MAR-M-246. The minimum creep rates of the refined alloy were approximately twice the minimum creep rates of the coarse columnar MAR-M-246; creep elongations of the refined structure were 9.5% compared to 5.9% for the coarse columnar structure.

7. Conventional thermal fatigue in a burner rig did not produce thermal fatigue cracks in baseline or refined specimens of the three test alloys. The oxidation rate (as measured by weight change) was increased for grain refined samples of C103 and MAR-M-246 but the same for 713LC.

8. The structural control technique was proven by adapting it to a production facility for limited production of rotors with controlled structure and properties.

9. As appropriate, this process to control structure and properties may now be further developed and used in pilot production to increase the life of army turbine wheels.

RECOMMENDATIONS

The purpose of this project was to develop a technique for structure control of integrally cast rotor hub, rim, and blade sections for turbine engines similar to the Army T-63 engine. Integral cast turbine wheels are used in army engines such as the T-63. A problem that is reducing the service life for the T-63 engine is thermal fatigue cracking of the rim. This investigation was undertaken to correct this thermal fatigue cracking by structure control. This cracking results because of the large grain

size and possible anisotropy in fatigue behavior exhibited by these as cast grains in the nickel base superalloys at this rim location. These grains are columnar and somewhat longer than wide with a breadth of about 0.25 inches. Grain refinement of the cast structure should have the capability of changing these grains to an equiaxed structure with a diameter of about 0.004 inches. These finer equiaxed grains would essentially provide isotropic behavior in the rim location and should improve the fatigue properties of the rim.

After the successful development of this grain refinement process for production, the production implementation of this procedure requires both that the other significant properties of the rim, blade and hub sections are not influenced deleteriously (at least to a significant degree) and that the process of grain refinement be feasible in production without undue scrap or production delays. This project first developed the grain refining technique for three modern nickel base superalloys; the alloys investigated were 713LC, MAR-M-246 and C103. The technique consisted of the addition of 0.1% boron and controlled thermal cycling to produce what are believed to be titanium boride substrates for heterogeneous nucleation of the grains during solidification. This technique changed the grain structure from the coarse columnar grains presently being obtained on the commercially cast rotors to a fine equiaxed structure. The width of the columnar grains now being obtained in the hub, rim and blade sections was reduced from 0.200, 0.100 and 0.030 inches respectively to equiaxed grains of 0.006, 0.006 and 0.004 inch diameters by this grain refining procedure.

The grain refining technique resulted in a significant improvement in the low cycle fatigue behavior of both the 713LC and MAR-M-246 and had no significant effect on the low cycle fatigue properties of C103. This improvement was apparently produced by elimination of the anisotropic behavior of the large columnar grained structure. The effect that this grain refinement had on stress rupture properties in the blade sections of the rotor depended on the temperature and stress level. At lower temperatures and higher stress levels grain refinement increased the stress rupture life; at the highest temperature of testing (1850°F) and lower stress levels (20 ksi) the stress rupture properties were reduced slightly compared to the unrefined coarse columnar structure. The primary emphasis in this stress rupture testing was placed on the MAR-M-246 because it is being used commercially to cast T-63 rotors. Grain refinement increased the yield strength and reduced the tensile strength and elongation slightly for 713LC and MAR-M-246. For C103 all three tensile properties were reduced slightly. None of the unrefined or refined specimens of the three superalloys exhibited thermal fatigue cracking under the test conditions. Grain refinement increased the oxidation rate of MAR-M-246 and C103 and had little effect on the 713LC. On balance the most significant improvement in mechanical properties is the higher fatigue strength of the 713LC and MAR-M-246 as a result of grain refinement; this property is most significant because fatigue cracking can limit service life. Considered in the light of service conditions, the effect on stress rupture properties appears to be small. The influence

of grain refinement on oxidation behavior requires further study to establish its significance.

The grain refining technique established on laboratory equipment and simulated section sizes was successfully translated to the production of T-63 first stage turbine rotors by the manufacture of grain refined rotors at the Austenal Division of Howmet Corporation in La Porte, Indiana. These rotors were produced utilizing regular production investment molds, melting, and casting facilities. The alterations in the manufacturing process required for grain refinement were the addition of 0.1% boron; thermal cycling between about 2800°F and the melting temperature and pouring with about 100°F superheat; and increasing the mold temperature from 1800°F to 2100°F. The increased time required for these changes in practice was approximately twelve minutes more per casting (from about 6 to 18 minutes). The final rotor produced was sound and of acceptable quality. The grain refinement attained was consistent throughout the refined castings.

The results of this project show that grain refinement of production integrally cast rotors of nickel base superalloys is commercially feasible. The fatigue properties were improved; the stress rupture properties were reduced to only a slight extent under some conditions; and the oxidation resistance was lowered somewhat. This indicates that the grain refining process has the potential of producing better integrally cast rotors. Obviously, simulated service testing of grain refined rotors is a necessary further step prior to their commercial utilization. A patent application has been filed on this grain refining process.

REFERENCES

1. Merrick, H.F., Maxwell, D.H., Gibson, R.C., "Fatigue in the Design of High-Temperature Alloys", Fatigue at Elevated Temperatures, ASTM STP520, American Society for Testing and Materials, 1973.

2. De Corso, S.M., Harrions, D.E., "Ceramics in Industrial Gas Turbines", ASME Report 72-GT-04, 1972.

3. Fawley, R.W., "Superalloy Progress", The Superalloys, Wiley and Sons, 1972.

4. Varin, J.D., "Microstructures and Properties of Superalloys", The Superalloys, Wiley and Sons, 1972.

5. Dahl, J.M., Danesi, W.F., Dunn, R.G., "The Partitioning of Refractory Metal Elements in Hafnium-Modified Cast Nickel-Base Superalloys", Metallurgical Transactions, Vol. 4, 1973.

6. Kotval, D.S., Venables, J.D., Calder, R.W., "The Role of Hafnium in Modifying the Microstructure of Cast Nickel-Base Superalloys", Metallurgical Transactions, Vol. 3, 1972.

7. Duhl, D.N., Sullivan, C.P., "Some Effects of Hafnium Additions on the Mechanical Properties of a Columnar-Grained Nickel-Base Superalloy", Journal of Metals, July, 1971.

8. Duhl, D.N., Erickson, J.S., Sullivan, C.P., "Advances in Directional Solidification Spur Usage in Turbine Airfoil Shapes", Metal Progress, March, 1973.

9. Sell, M., Sullivan, C.P., Ver Snyder, F.L., "Unidirectionally Solidified Superalloys", Superalloy Conference, 1972.

10. Cole, G.S., Cremiso, R.S., "Solidification and Structure Control in Superalloys", The Superalloys, Wiley and Sons, 1972.

11. VerSnyder, F.L., Guard, R.W., "Directional Grain Structures for High Temperature Strength", Transactions of the ASM, Vol. 52, 1960.

12. Piearcy, B.M., VerSnyder, F.L., "A Breakthrough in Making Turbine Components---Directional Solidification and Single Crystals", Metal Progress, November, 1966.

13. VerSnyder, F.L., et al, "Directional Solidification in the Precision Casting of Gas-Turbine Parts", Trans. Am. Found. Soc., 1967.

14. Dunlevey, F.M., Wallace, J.F., "The Effect of Thermal Cycling on the Structure and Properties of a Co, Cr, Ni-Ta-C Directionally Solidified Eutectic Alloy", Met. Trans., Vol. 5, June 1974, p. 1351.

15. Gell, M., Leverant, G.R., "Ordered Alloys: Structural Application and Physical Metallurgy", Claiter's Publishing, 1970.

16. Muzyka, D.R., "The Metallurgy of Nickel-Iron Alloys", The Superalloy, Wiley and Sons, 1972.

17. Tien, J.K., "On the Celestial Limits of Nickel-Base Superalloys", Super-Alloys--Processing, Proceedings of the Second International Conference, 1972.

18. Hockin, J., Taylor, W., "Factors Affecting the Mechanical Properties of Cast Nickel-Base Superalloys", Proceedings of the Second World Conference on Investment Casting, June 1969.

19. Form, G.W. et al, "Grain Refinement of Cast Metals", presented at the 27th International Foundry Congress, Zurich, 1960.

20. Chalmers, B., Principles of Solidification, John Wiley and Sons, 1964.

21. Chalmers, B., "Shapes and Sizes of Grains in Castings", Solidification, ASM, 1971.

22. Wallace, J.F., "Grain Refinement of Steels", Journal of Metals, 1963.

23. Private Communication, W. Garcia, Chief Metallurgist, Austenal Division of Howmet Corporation, April 23, 1975.

24. Freedman, A.H., Wallace, J.F., "The Influence of Vibration During Solidification of Castings", A.F.S. Transactions, Vol. 65 (1957).

25. Garlick, R.G., Wallace, J.F., "Grain Refinement of Solidifying Metals by Vibration", Modern Castings, June 1959.

26. Bolling, G.F., "Manipulation of Structure and Properties", Solidification, ASM, 1971.

27. Smith, C.L., et al, "A Survey of Solidification and Casting Literature up to Mid 1969", Scripta Met., Vol. 4, 1970.

28. Trunbull, G.K., et al, "Grain Refinement of Steel Castings and Weld Deposits", AFS Transactions, Vol. 69, 1961.

29. Wilson, P.F., et al, "Grain Refinement of Steel Castings", Journal of Metals, June, 1967.

30. Jackson, W.J., Hall, T., "Grain Refinement in Cast Austenitic Steels", The Solidification of Metals, 1967.

31. Tarshis, L.A., et al, "Experiments on the Solidification Structure of Alloy Castings", Metallurgical Transactions, September, 1971.

32. Letter from N. Paulucci, Metallurgical Engineer, Sherwood Refractories, Inc., Cleveland, Ohio, dated May 31, 1974.

33. International Nickel, "Alloy 713LC, Preliminary Data", July, 1964.

34. Slot, T., Stentz, R.H., Berling, J.T., "Controlled Strain Testing Procedures" in Manual on Low Cycle Fatigue Testings, ASTM, STP #465, 1969.

35. Private Communication, G. Halford, Metallurgist, NASA, Lewis Research Center, January, 1975.

36. Raske, D.T., Morrow, J., "Mechanics of Materials in Low Cycle Fatigue Testing", in Manual on Low Cycle Fatigue Testing, ASTM, STP #465, 1969.

37. Manson, S.S., "The Challenge to Unify Treatment of High Temperature Fatigue - A Partisan Proposal Based on Strainrage Partitioning", Fatigue at Elevated Temperatures, ASTM, STP #520, 1973.

38. Krempl, E., Wundt, B.M., "Hold-Time Effects in High Temperature Low-Cycle Fatigue - A literature Survey and Interpretive Report", ASTM STP #489, 1971.

39. Solomon, H.D., Coffin, L.F. Jr., "Effects of Frequency and Environment on Fatigue Crack Growth in A-286 at 1100°F", Fatigue at Elevated Temperatures, ASTM, STP #520, 1973.

40. Rudy, E., "Compendium of Phase Diagram Data-Part V", AFML-TR-65-2, Wright-Patterson AFB, Ohio.

41. Aronsson, B., Die Verfestigung Von Stahl, Institut for Metallforskning, Stockholm, Sweden, 1969.

42. Gell, M., Leverant, G.R., "The Fatigue of the Nickel-Base Alloy, MAR-M-246, in Single Crystal and Columnar Grained Forms at Room Temperature", Trans. Metl. Soc. AIME, September, 1968.

43. Leverant, G.R., Gell, M., "The Elevated Temperature Fatigue of Nickel-Base Superalloy, MAR-M-200, in Conventionally-Cast and Directionally-Solidified Forms", Met. Trans., June, 1969.

44. Leverant, G.R., Duhl, D.N., "The Effect of Stress and Temperature on the Extent of Primary Creep in Directionally Solidified Nickel-Base Superalloys", Metallurgical Transactions, Vol. 2, March, 1971.

45. Leverant, G.R., Kear, G.H., "The Mechanism of Creep in Gamma Prime Precipitation-Hardened Nickel-Base Alloys at Intermediate Temperatures", Metallurgical Transactions, Volume 1, February, 1970.

46. Coffin, L.F. Jr., "The Effect of Frequency on the Cyclic Strain and Low Cycle Fatigue Behavior of Cast Udimet 500 at Elevated Temperature", Metallurgical Transactions, Volume 2, November, 1971.

47. Belcher, P.R., et al, "Black Plague Corrosion of Aircraft Turbine Blades", Hot Corrosion Problems Associated With Gas Turbines, ASTM SRP 421, 1967.

48. Hamilton, P.F., et al, "Nickel-Base Alloys and Their Relationship to Hot Corrosive Environments", Hot Corrosion Problems Associated With Gas Turbines, ASTM STP 431, 1967.

49. Wall, F.J., Michael, S.T., "Effect of Sulfate Salts on Corrosion Resistance of Gas Turbine Alloys", Hot Corrosion Problems Associated With Gas Turbines, ASTM SRP 421, 1967.

50. Glenny, R.J.E., et al, "Materials For Gas Turbines", International Metallurgical Reviews, Vol. 20, Review 193, 1975, pp. 3-19.

51. Decker, R.F., "Strengthening Mechanisms in Nickel-Base Superalloys", International Nickel Corporation, Presented at Steel Strengthening Mechanisms Symposium, Switzerland, May 1969.

52. Brown, J.T., and Bulina, J., "W545- A New Higher-Temperature Turbine Disk Alloy", High Temperature Materials, 1957.

53. Hull, F.C., Stickler, R., "Effects of Nitrogen, Boron, Zirconium and Vanadium on the Microstructure, Tensile and Creep Properties of a Chromium-Nickel-Manganese-Molybdenum Stainless Steel", Joint International Conference on Creep, The Institute of Mechanical Engineers, London, 1963.

54. Crussard, C., et al, "The Influence of Boron in Austenitic Alloys", Joint International Conference on Creep, The Institute of Mechanical Engineers, London, 1963.

TABLE I NOTE OF ALLOYING ELEMENTS IN SUPERALLOY COMPOSITION

Elements	Ni	Co	Fe	Cr	Mo,W,V	Cb,Ta,Ti	Al	C,B,Zr,Mg
Matrix class	X	X	X	X	X			
γ' class						X	X	
Grain-boundary class								X
Carbide subclass				X	X	X		
Oxide-scale subclass				X			X	
Examples[a]								
Rene 77	58.4	15	-	14.6	4.2 Mo	3.4 Ti	4.3	0.7 C 0.016 B
Mar-M 200	58.9	10	1.5	9.0	12.5 W	2.0 Ti	5.0	0.15 C 0.015 B

[a]In weight percent

TABLE II COMPOSITION OF ALLOYS

Element	713 LC	Mar-M-246	C-103
Carbon	0.03 - 0.07	0.15	0.14 - 0.18
Chromium	11.00 - 13.00	9.00	11.2 - 11.8
Molybdenum	3.80 - 5.20	2.50	1.75 - 2.25
Columbium Tantalum	1.50 - 2.50	1.50	4.80 - 5.20
Aluminum	5.50 - 6.50	5.5	3.30 - 3.70
Titanium	0.40 - 1.00	1.5	3.80 - 4.20
Boron	0.005 - 0.015	0.015	0.010 - 0.020
Zirconium	0.05 - 0.15	0.05	0.05 - 0.12
Silicon	0.05 max.	0.05	0.30 max.
Manganese	0.50 max.	0.10	0.20 max.
Iron	0.50 max.	0.15	0.50 max.
Copper	0.50 max.	LAP*	LAP*
Sulfur	0.015 max.	LAP*	0.015 max.
Cobalt	-	10.0	8.0 - 9.0
Tungsten	-	10.0	4.8 - 5.2
Hafnium	-	-	0.80 - 1.202
Nickel	Balance	Balance	Balance

* Low as Possible

TABLE III SCHEDULE OF MECHANICAL TESTS

TEST REQUIREMENTS

Type of Test	Section	Temp. °F
1. Tensile	HUB	Room, 500
2. Tensile	RIM	Room, 1000, 1400
3. Fatigue, Mech.(1)	HUB	Room, 500
4. Fatigue, Mech.	RIM	Room, 1000, 1400(3)
5. Fatigue, Thermal	BLADE	1800°F(2)
6. Fatigue-Creep	RIM	1400
7. Stress Rupture	TUBULAR	1800
8. Stress Rupture	BLADE	1850

NOTES:

(1) Strain controlled test.

(2) Cyclically heated rapidly to 1800°F, cool rapidly to 1000°F, observe crack pattern at various intervals.

(3) Screening test.

Table IV

Free energy of formation of hafnium, titanium, and zirconium carbides and borides.

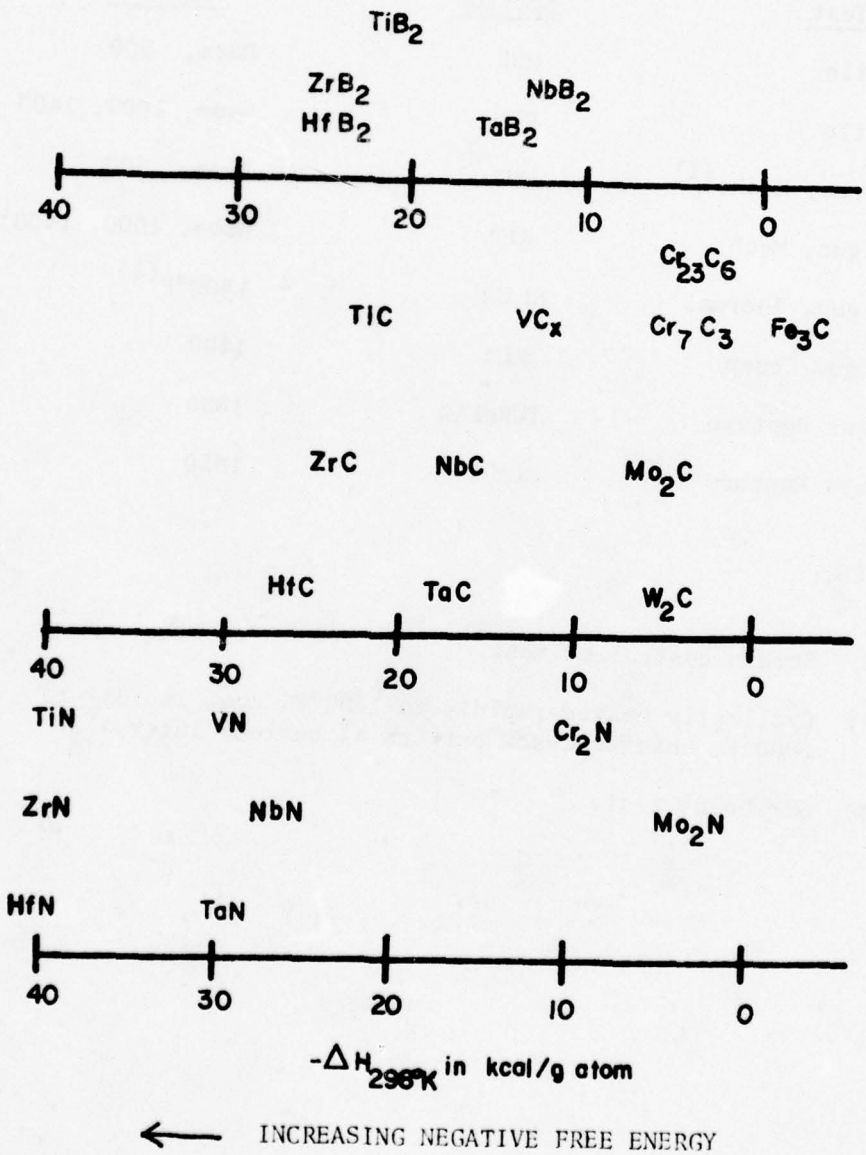

TABLE V
SUMMARY OF FIRST SERIES OF HEATS MADE ON PRODUCTION FACILITIES

HEAT NO.	1	2	3	4	5	6	7	8	9	10
MOLD*	Hub	Rim	Hub	Rim	Hub	Rim	Hub	Rim	Hub	Rim
ARGON	Yes	Yes	Yes	Yes	Yes	Yes	Yes	No	No	No
BORON	Yes	Yes	Yes	Yes	Yes	Yes	Yes	No	Yes	Yes
ZIRCONIUM	Yes	Yes	No	No	No	No	No	No	Yes	No
SUPERHEAT-°F**	50	50	50	100	>200	>200	100	100	100	100
THERMAL CYCLE** (2800°F, Freeze)	Yes	Yes	Yes	Yes	Yes	Yes	Yes	No	Yes	Yes
TYPE OF GRAINS	Columnar And Equiaxed	Columnar And Equiaxed	Equiaxed Refined	Columnar And Equiaxed	Columnar And Equiaxed	Columnar	Columnar	Columnar And Equiaxed	Columnar	Equiaxed Refined
SIZE OF GRAINS (In.)	.250 And .060	.060 And .045	.004	.200 And .125	.350 And .125	.250	.200	.125 And .060	.375	.006
COMMENTS	Mold*** Didn't Fill	-	-	-	-	-	-	Mold*** Didn't Fill	-	Mold*** Didn't Fill

*** Mold did not fill because of a mis-pour or the mold tipped over.

** Temperatures measured with optical pyrometer.

* Mold Temp = 1800°F (oven temperature).

TABLE VI
SUMMARY OF SECOND SERIES OF HEATS MADE ON PRODUCTION FACILITIES

HEAT NO.	11	12	13	14	15	16
MOLD*	Hub	Rim	Hub	Rim	Hub	Rim
ARGON	No	No	No	Yes	Yes	Yes
BORON	Yes	Yes	No	Yes	Yes	No
ZIRCONIUM	No	No	No	No	No	No
SUPERHEAT (°F)**	100	100	100	100	100	100
THERMAL CYCLE** (2900°F, Freeze)	Yes	Yes	Yes	Yes	Yes	Yes
TYPE OF GRAINS	Columnar And Equiaxed	Columnar And Equiaxed	Columnar And Equiaxed	Columnar	Columnar And Equiaxed	Columnar
SIZE OF GRAINS (In.)	.250 And .250	.100 And .060	.250 And .250	.250	.250 And .200	.250
COMMENTS	-	-		-	-	Cold Mold

* Mold Temp = 2000°F(oven temperature).

** Temperatures measured with optical pyrometer.

TABLE VII

SUMMARY OF HEATS FOR PRODUCTION FACILITY
CAST T-63 ROTORS

SERIAL NO.	J311	J269	J314	J301	J291	J289
ADDITION	NONE	B	B	B	B	B
THERMAL CYCLE	NO	YES	YES	YES	YES	YES
MAXIMUM TEMP. (°F)*	+300	+400	+400	+400	+450	+375
POURING SUPERHEAT * (°F)	+300	+10	+25	+15	+15	+25
TYPE OF GRAINS	Columnar	Equiaxed	Equiaxed	Equiaxed	Equiaxed	Equiaxed
APPROXIMATE SIZE OF GRAINS (In.)	.250"	.004"	.004"	.004"	.004"	.004"

* TEMPERATURES REFER TO HOW HIGH ABOVE THE EXPERIMENTALLY ESTABLISHED MELTING TEMPERATURE THE ALLOY WAS.

TABLE VIII TENSILE DATA - RIM MOLDS

Alloy	Grain	Temperature °F	0.2% Yield Strength	Tensile Strength	Elongation %
713 LC	Base[1]	R.T.	110,000	131,200	15.0
*713 LC	Base	1000	112,000	130,400	12.0
713 LC	Base	1400	113,200	134,700	10.2
713 LC	Ref.[2]	R.T.	120,000	130,800	12.0
*713 LC	Ref.	1000	122,000	128,200	11.8
713 LC	Ref.	1400	118,600	130,000	9.6
Mar M 246	Base	R.T.	124,000	140,800	8.7
*Mar M 246	Base	1000	125,300	143,000	5.0
Mar M 246	Base	1400	124,100	141,100	3.0
Mar M 246	Ref.	R.T.	138,100	139,000	5.4
*Mar M 246	Ref.	1000	134,600	138,500	5.0
Mar M 246	Ref.	1400	131,200	135,600	3.0
C103	Base	R.T.	133,400	142,800	6.0
*C103	Base	1000	131,700	143,900	6.1
C103	Base	1400	129,900	140,300	3.4
*C103	Ref.	R.T.	127,900	141,400	5.9
C103	Ref.	1000	127,400	136,200	5.4
*C103	Ref.	1400	127,800	133,200	3.0
*713 LC	Col.[3]	R.T.	108,600	115,600	10.8
*Mar M 246	Col.	R.T.	123,000	139,400	6.6
*C103	Col.	R.T.	127,600	132,200	8.0

[1] Baseline Heat.

[2] Refined Heat.

[3] Columnar Heat.

* Single Test.

TABLE IX TENSILE DATA - HUB MOLDS

Alloy	Grain	Temperature °F	0.2% Yield Strength	Tensile Strength	Elongation %
713 LC	Base[1]	R.T.	108,800	130,000	14.0
713 LC	Base	500	109,000	131,400	12.8
713 LC	Ref.[2]	R.T.	119,600	133,300	11.7
*713 LC	Ref.	500	120,200	132,000	11.6
Mar M 246	Base	R.T.	125,100	141,000	5.2
Mar M 246	Base	500	126,000	141,300	5.0
Mar M 246	Ref.	R.T.	137,600	139,500	5.0
*Mar M 246	Ref.	500	137,500	140,000	5.0
C103	Base	R.T.	130,400	139,000	7.0
C103	Base	500	131,500	140,000	6.3
C103	Ref.	R.T.	128,200	140,400	6.4
*C103	Ref.	500	127,900	141,000	6.0

[1]Baseline Heat.

[2]Refined Heat.

*Single Test.

TABLE X - ELASTIC CONSTANTS

Alloy	Grain	Temperature °F	E_{long} (x 10^6 psi)**	E_{diam} (x 10^6 psi)*	ν
713 LC	Ref.	R.T.	29.7	94.0	0.316
713 LC	Ref.	500°F	28.0	88.6	
713 LC	Ref.	1000°F	25.0	79.1	
713 LC	Ref.	1400°F	22.2	70.3	
Mar M 246	Ref.	R.T.	31.53	100.0	0.3155
Mar M 246	Ref.	500°F	29.1	92.2	
Mar M 246	Ref.	1000°F	26.5	84.0	
Mar M 246	Ref.	1400°F	24.3	77.0	
C103	Ref.	R.T.	32.11	101.6	0.316
C103	Ref.	500°F	30.0	94.9	
C103	Ref.	1000°F	27.2	86.1	
C103	Ref.	1400°F	25.0	79.1	

*Measured

**Calculated

TABLE XI

COMPARISON OF HARDNESS BETWEEN THE HOT TEST SECTION AND COLD GRIP PORTION OF THE FATIGUE-CREEP TEST SPECIMENS

		10 kg Vickers Hardness Converted to Rc		
Alloy	Reversals	Hot Area	Cold Area	Difference
713 LC Base	(334)	37.0	32.0	5.0
713 LC Base	(882)	37.0	33.0	4.0
713 LC Ref.	(128)	39.0	35.0	4.0
713 LC Ref.	(3262)	36.5	35.0	1.5
M M-246 Base	(24)	38.5	38.0	0.5
M M-246 Base	(10,270)	38.5	37.5	1.0
M M-246 Ref.	(126)	36.0	35.0	1.0
M M-246 Ref.	(5414)	39.0	38.5	0.5
C-103 Base	(72)	38.5	36.5	2.0
C-103 Base	(1230)	44.0	41.0	3.0
C-103 Ref.	(52)	42.5	40.0	2.5
C-103 Ref.	(1546)	41.5	40.5	1.0

TABLE XII

RESULTS OF AS CAST, TUBULAR STRESS RUPTURE
TESTS CONDUCTED AT 1800°F IN AIR

ALLOY	GRAIN STRUCTURE	σ (ksi)	LIFE (HR.)	% ELONG.	MINIMUM CREEP RATE (IN./IN./HR.)
		35.25	0.3	1.8	
		30.00	2.1	3.4	
		26.43	3.2	4.7	
713LC	Baseline	23.50	10.8	7.4	
		20.56	47.6	5.6	3.08×10^{-4}
		17.62	134.1	4.8	
		30.00	0.4	2.1	
		30.00	3.0	4.2	
		26.43	6.1	8.7	
713LC	Refined	23.50	13.5	5.5	
		20.56	25.3	4.5	8.62×10^{-4}
		17.62	72.7	3.2	
		38.18	5.4	2.4	
		35.25	10.1	2.9	
		30.00	25.0	2.4	
MAR-M 246	Baseline	30.00	41.0	3.1	1.23×10^{-4}
		26.43	119.6	4.8	
		26.43	112.6	3.6	
		38.18	7.0	3.9	
		35.25	12.8	5.7	
		30.00	28.2	5.0	
MAR-M 246	Refined	30.00	53.2	4.6	4.50×10^{-4}
		26.43	120.0	4.7	
		26.43	96.6	3.8	
		35.25	1.8	2.0	
		30.00	0.3	0.0	
		30.00	1.5	1.2	9.85×10^{-5}
C-103	Baseline	26.43	19.1	1.6	
		23.50	29.6	1.4	
		20.56	139.6	2.1	
		35.25	2.7	6.1	
		30.00	4.7	5.7	
		30.00	12.2	4.9	2.56×10^{-4}
		26.43	41.7	4.1	
C-103	Refined	23.50	57.2	3.6	
		20.56	138.2	4.1	

TABLE XIII

RESULTS OF BASELINE AND REFINED MAR-M 246 FLAT STRESS RUPTURE TESTS CONDUCTED AT 1850°F AND 20.0 KSI IN AIR

GRAIN STRUCTURE	LIFE (HR.)	% ELONG.	MINIMUM CREEP RATE (IN./IN./HR.)
Baseline*	62.8	5.2	7.35×10^{-4}
Baseline	124.0	7.3	5.60×10^{-4}
Baseline	59.5	5.1	7.36×10^{-4}
Baseline	71.4	5.9	6.57×10^{-4}
Baseline	98.7	5.2	5.13×10^{-4}
Refined	112.5	13.0	1.09×10^{-3}
Refined *	29.4	5.6	1.84×10^{-3}
Refined	72.9	9.8	1.35×10^{-3}
Refined	50.7	7.8	1.36×10^{-3}
Refined	38.5	7.5	1.68×10^{-3}
Average Baseline**	88.4	5.9	6.17×10^{-4}
Average Refined **	68.7	9.5	1.37×10^{-3}

* Broke In Grip - Invalid Test
** Average of Four Valid Tests

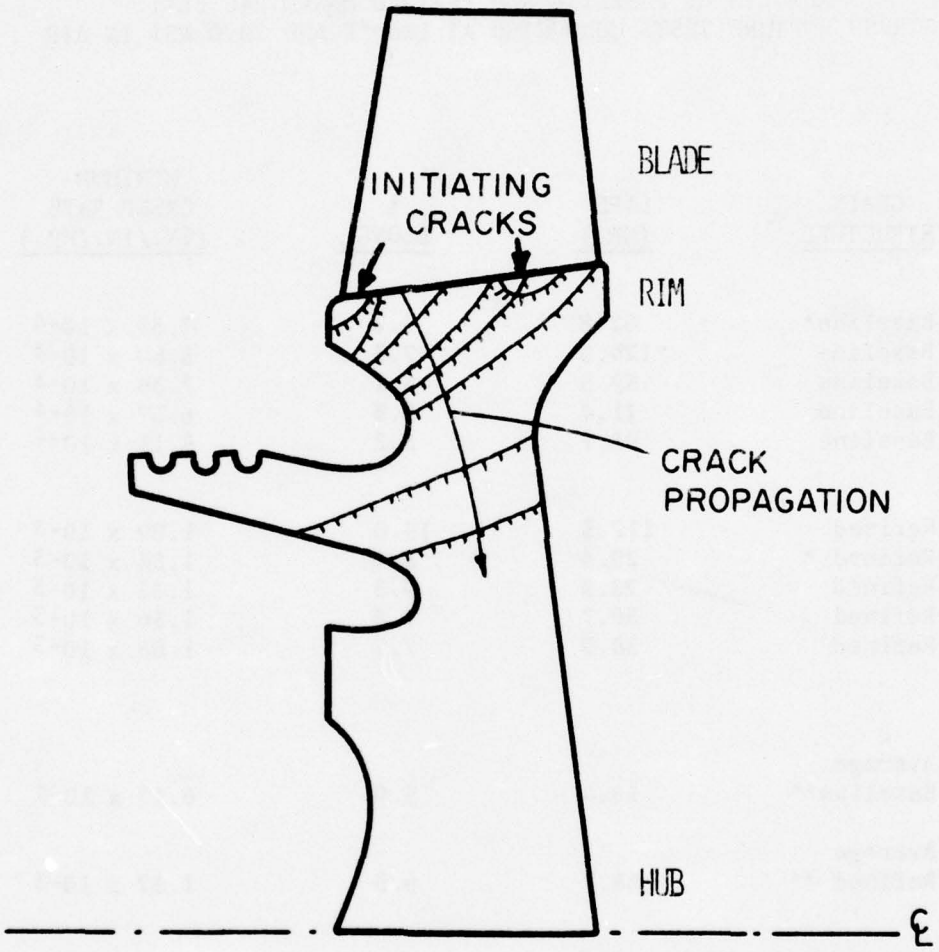

FIGURE 1: Schematic Cross Section of Turbine Rotor Showing Hub, Rim, and Blade Areas, Indicating Initiating Cracks.

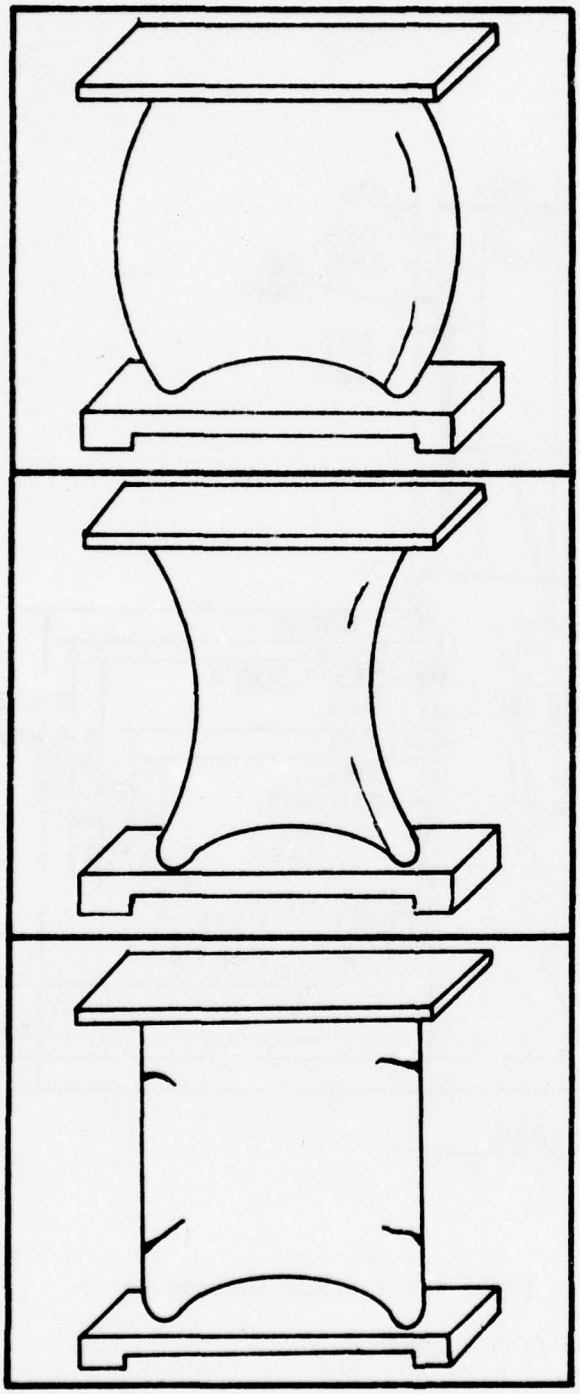

a.) ON ACCELERATION THE LEADING AND TRAILING EDGES HEAT UP FASTER AND EXPAND MORE THAN THE CENTER REGION.

b.) ON DECELERATION THE LEADING AND TRAILING EDGES COOL MORE RAPIDLY THAN THE CENTER REGION.

c.) THIS ALTERNATING CYCLE RESULTS IN THERMAL FATIGUE CRACKING OF THE LEADING AND TRAILING EDGES.

FIGURE 2: Sequence of events leading to the development of thermal fatigue cracks in gas turbine blades.[4]

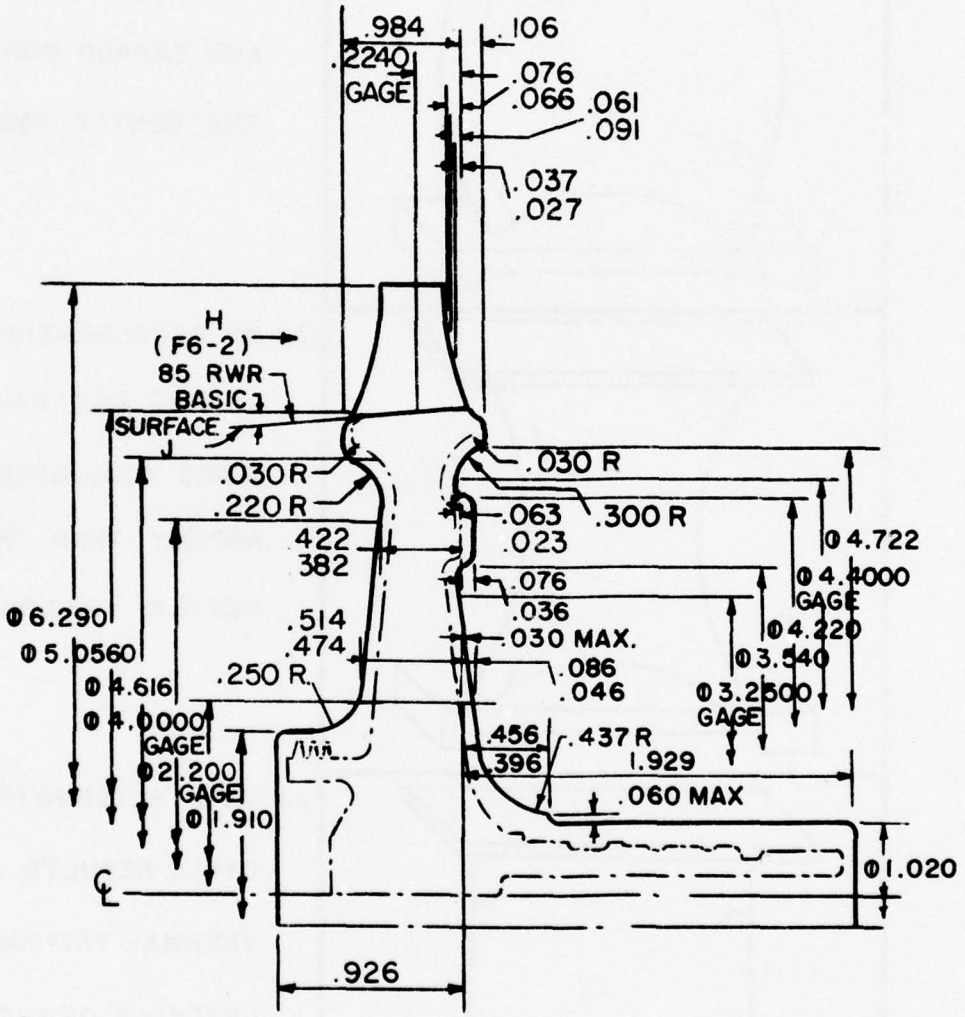

FIGURE 3: Drawing of the First Stage Turbine Rotor for the T-63 Engine.

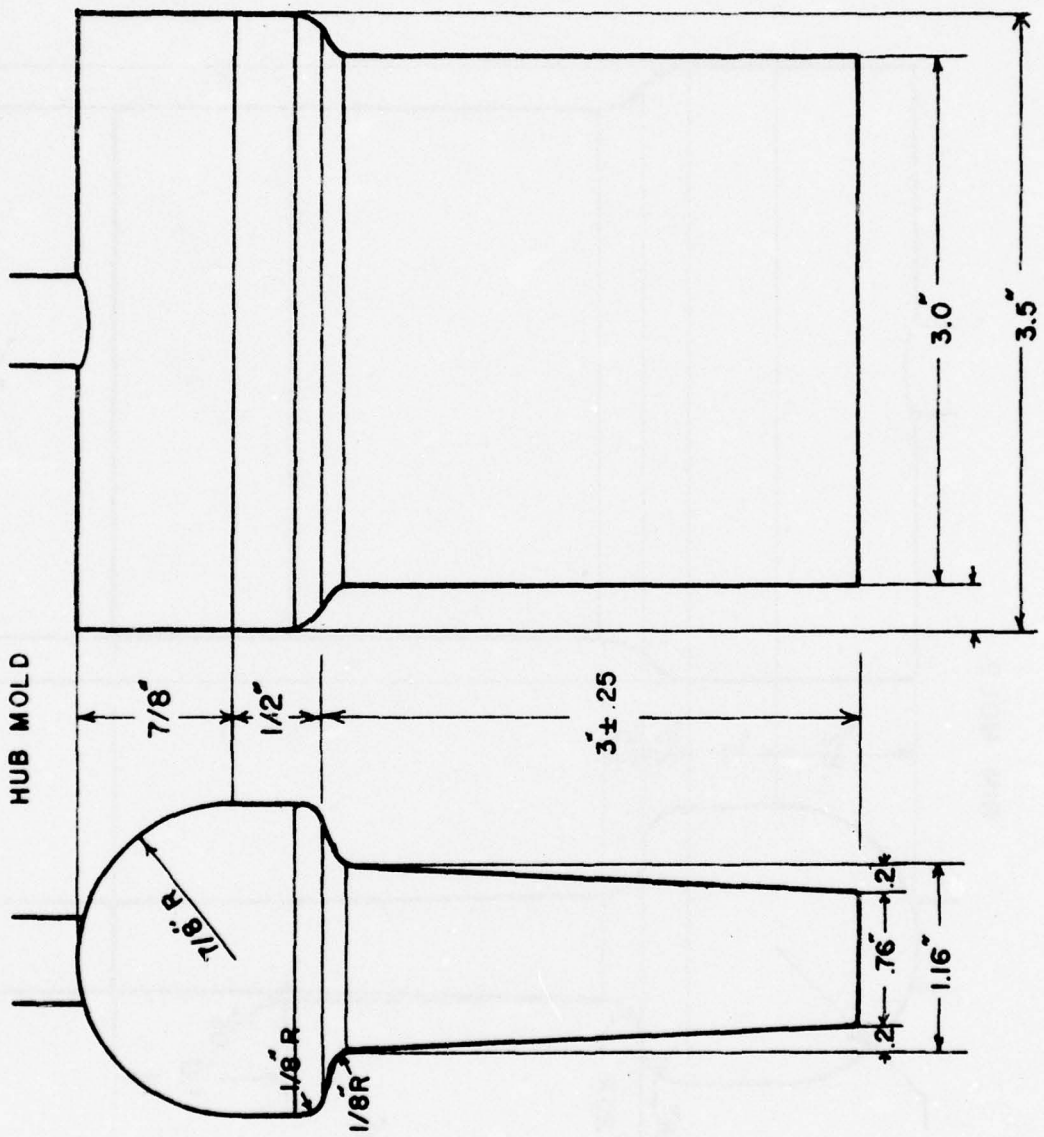

FIGURE 4: Casting used to simulate hub section of T-63 rotor.

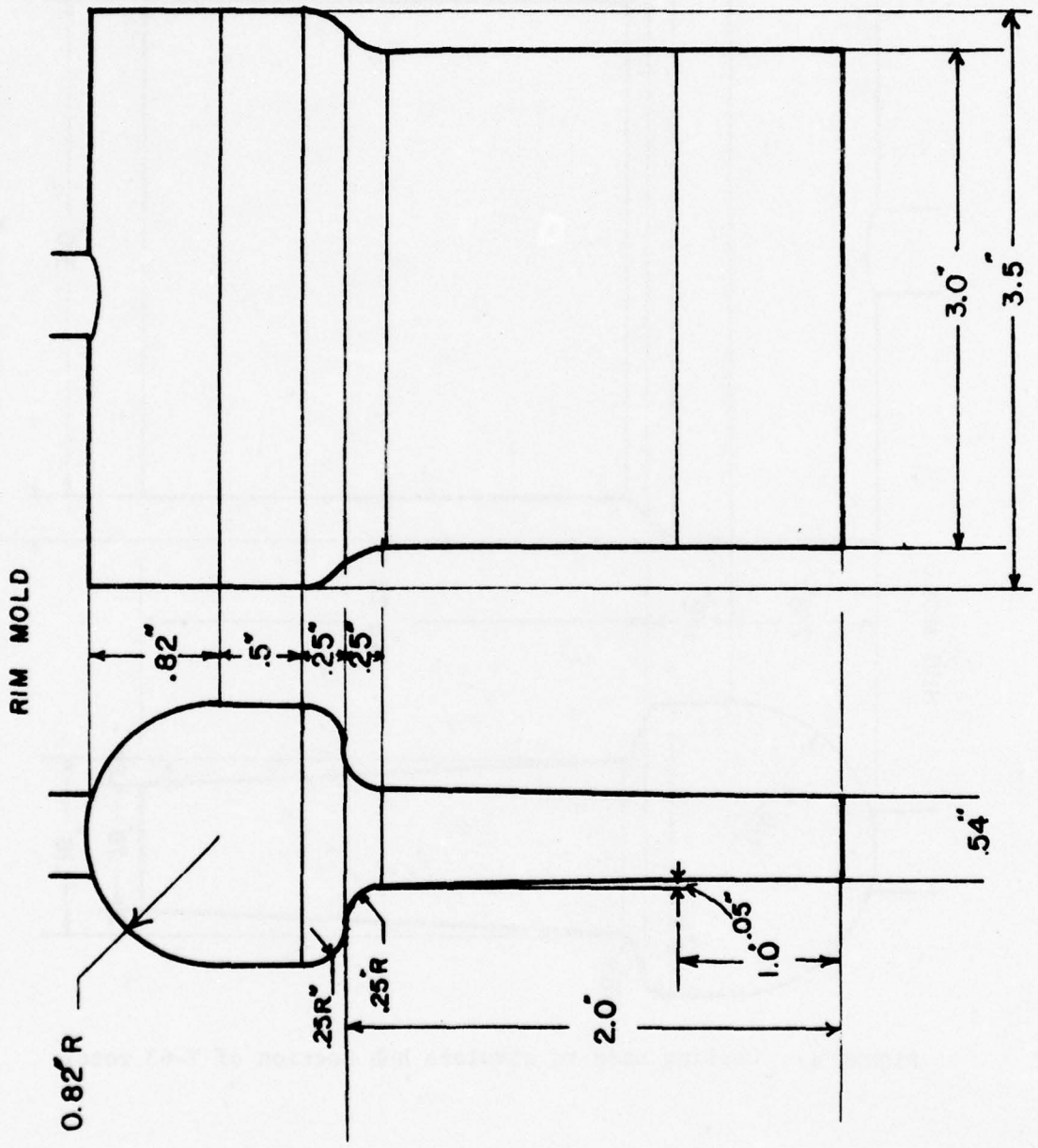

FIGURE 5: Casting used to simulate rim section of T-63 rotor.

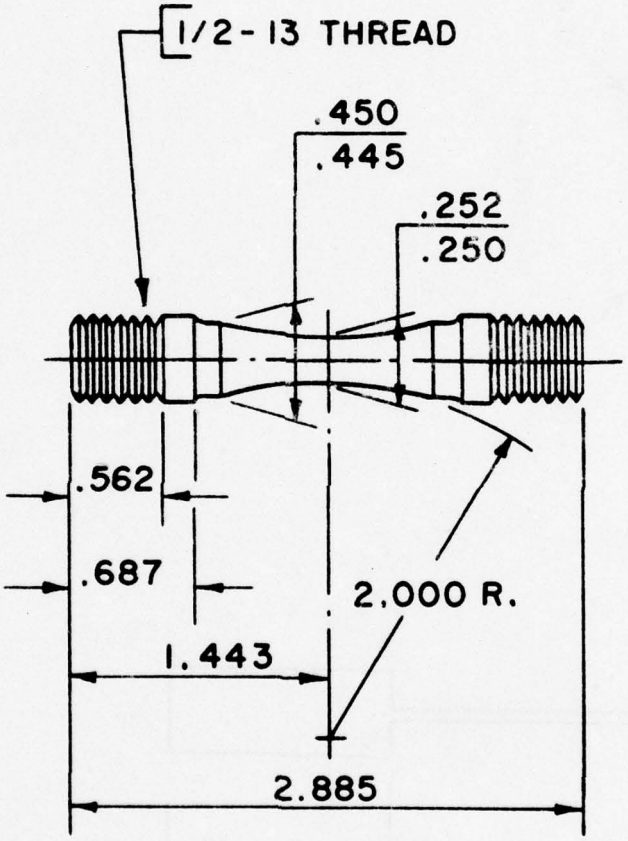

FIGURE 6: THREADED END HOURGLASS SPECIMEN FOR TENSILE, LOW CYCLE FATIGUE, AND FATIGUE-CREEP TESTING.

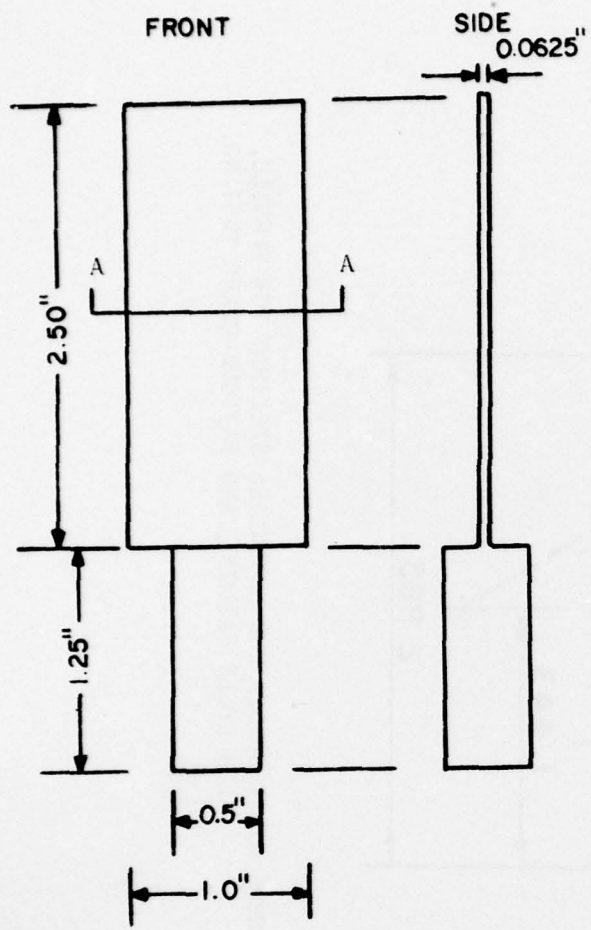

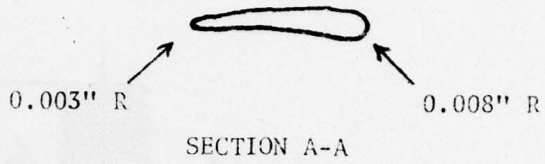

FIGURE 7: Simulated airfoil specimen used in thermal fatigue testing.

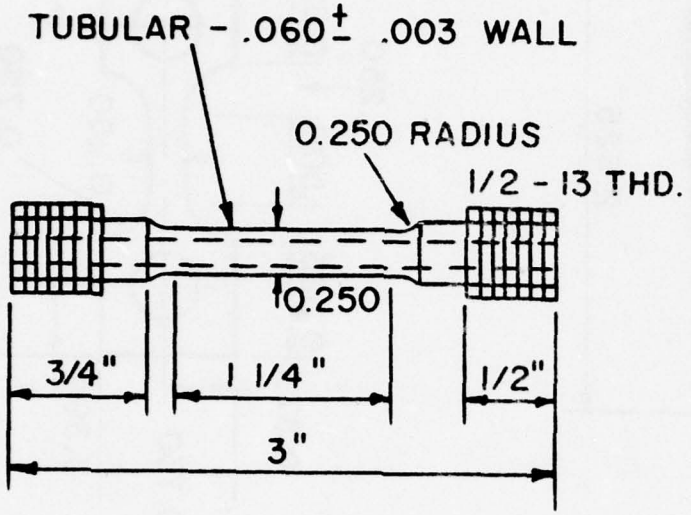

FIGURE 8: CAST TO SIZE TUBULAR STRESS RUPTURE SPECIMEN.

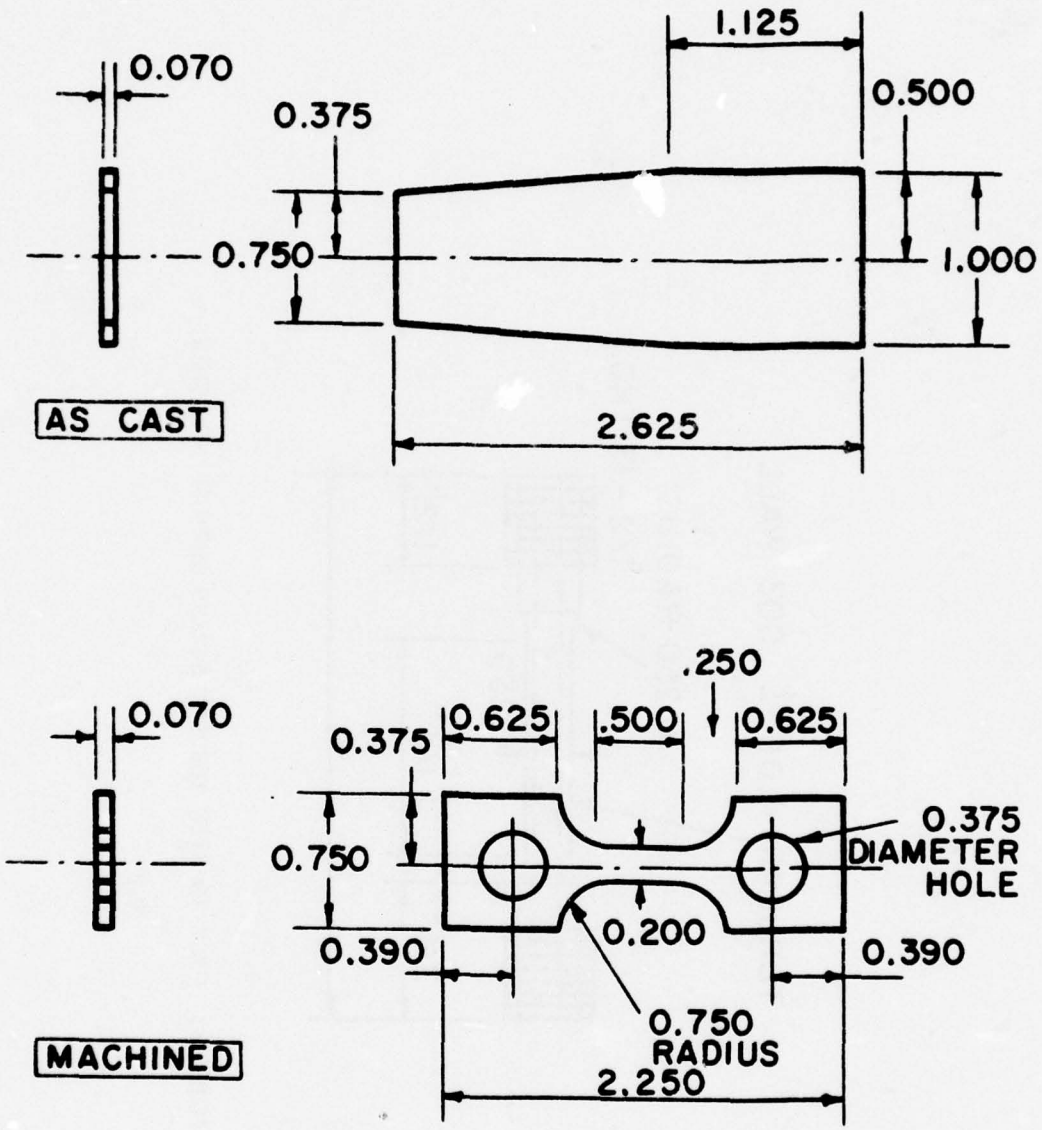

FIGURE 9: FLAT STRESS RUPTURE SPECIMEN, AS CAST AND MACHINED TO FINAL SHAPE.

FIGURE 10: MACROSTRUCTURE OF A TYPICAL COMMERCIAL ROTOR SHOWING COARSE COLUMNAR GRAINS, .75X.

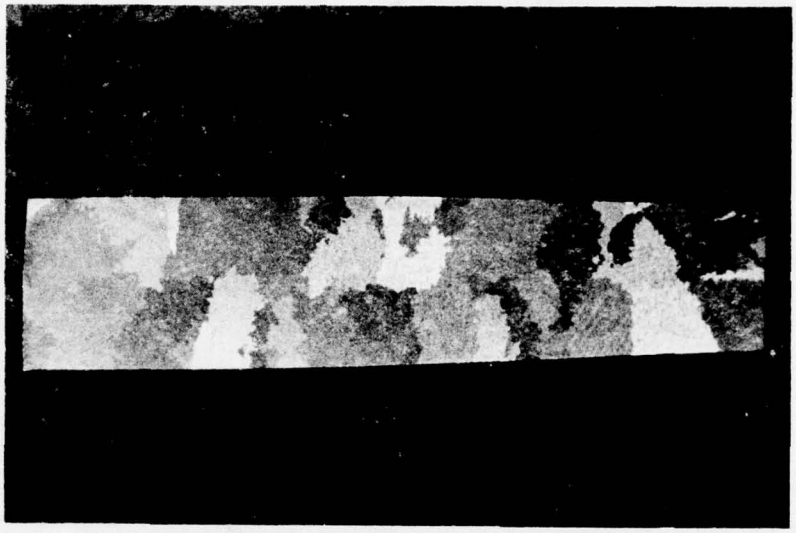

a) COARSE COLUMNAR BASELINE STRUCTURE

b) FINE COLUMNAR STRUCTURE

FIGURE 11: MACROSTRUCTURE OF COARSE COLUMNAR AND FINE COLUMNAR 713 LC CASTINGS IN A RIM MOLD, 1.5X.

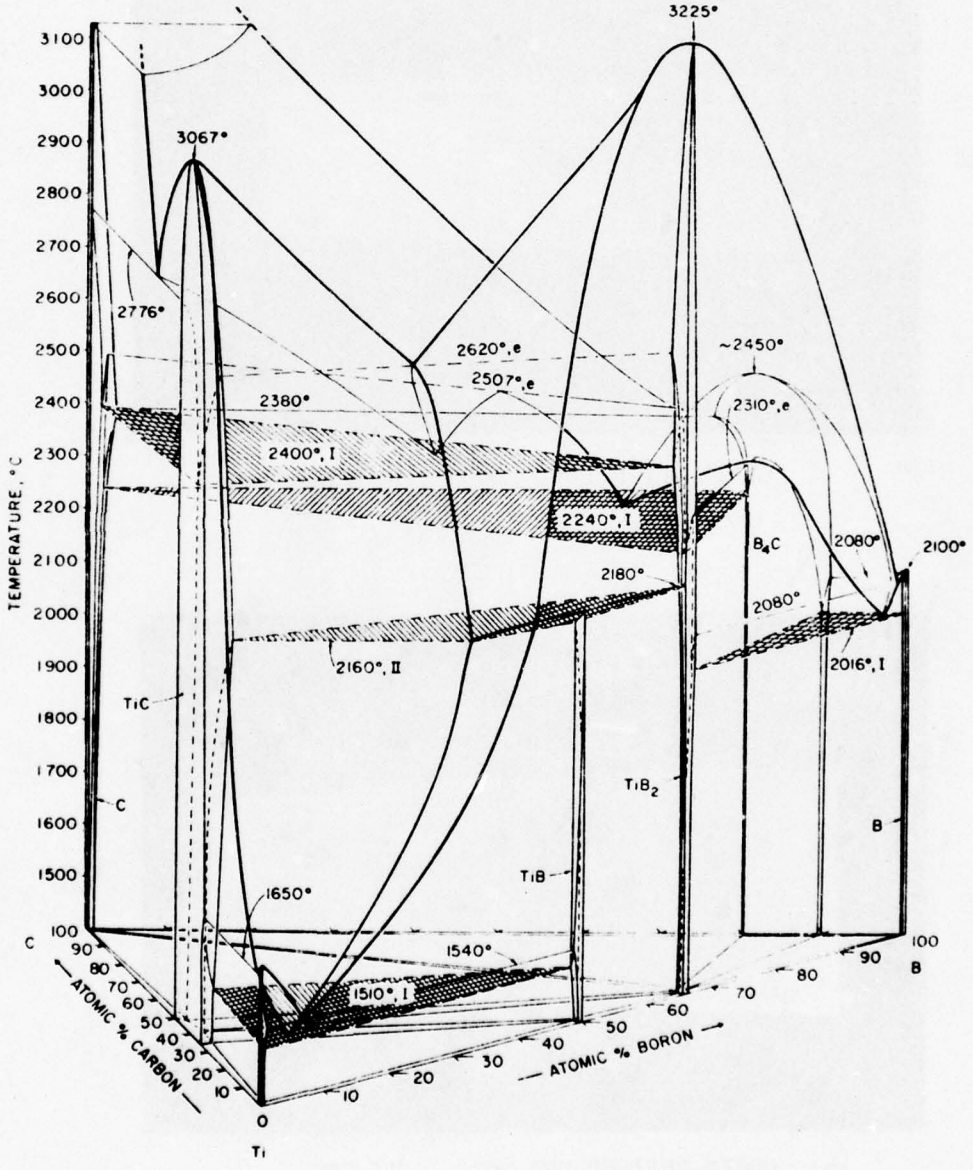

FIGURE 12: ISOMETRIC VIEW OF THE B-Ti-C SYSTEM.

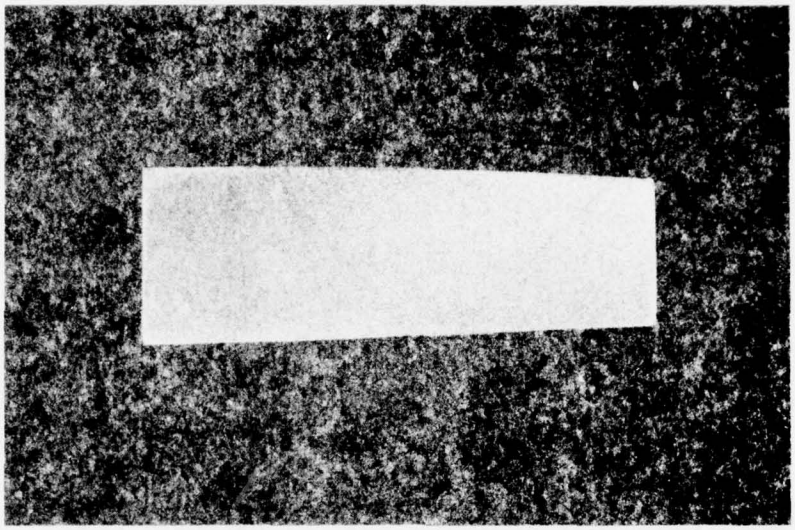

a) GRAIN REFINED RIM MOLD STRUCTURE

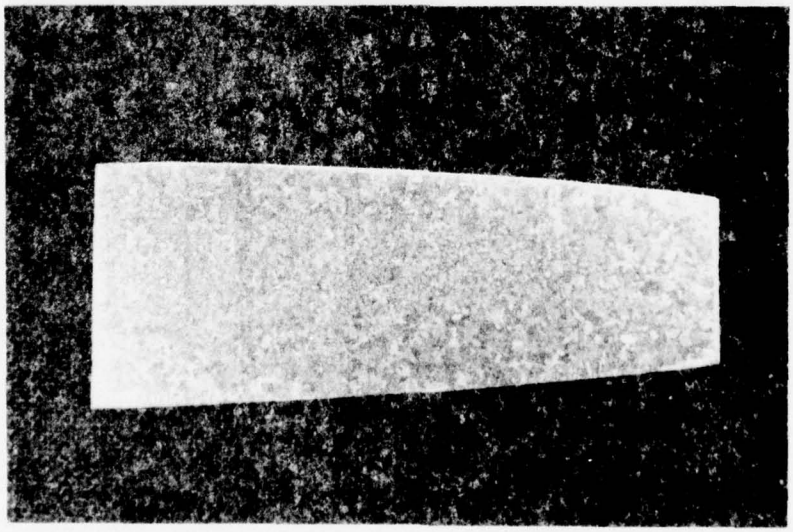

b) GRAIN REFINED HUB MOLD STRUCTURE

FIGURE 13: MACROSTRUCTURES OF GRAIN REFINED RIM MOLD AND GRAIN REFINED HUB MOLD FOR 713 LC CASTINGS, 1.5X.

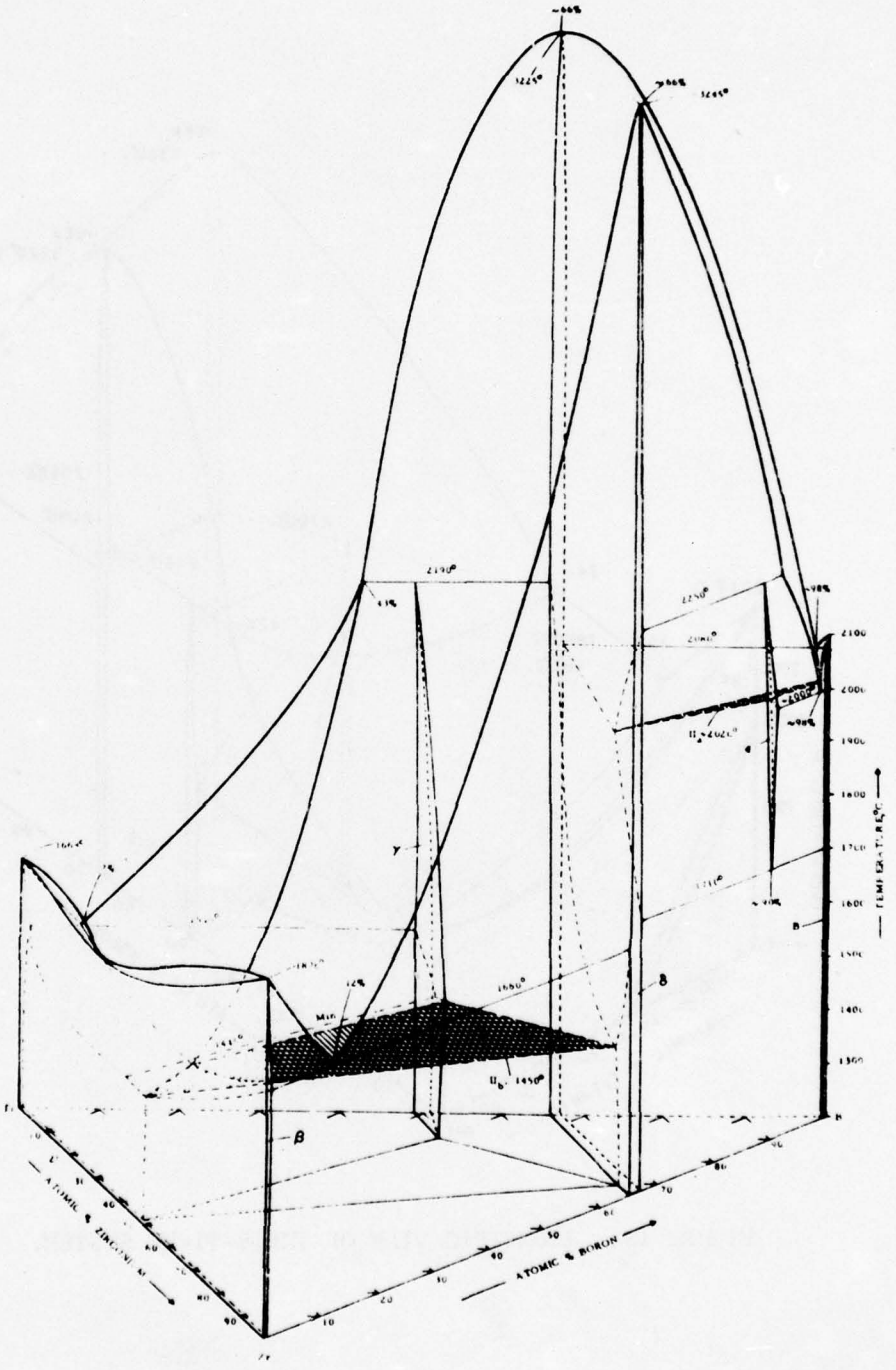

FIGURE 14: ISOMETRIC VIEW OF THE B-Zr-Ti SYSTEM.

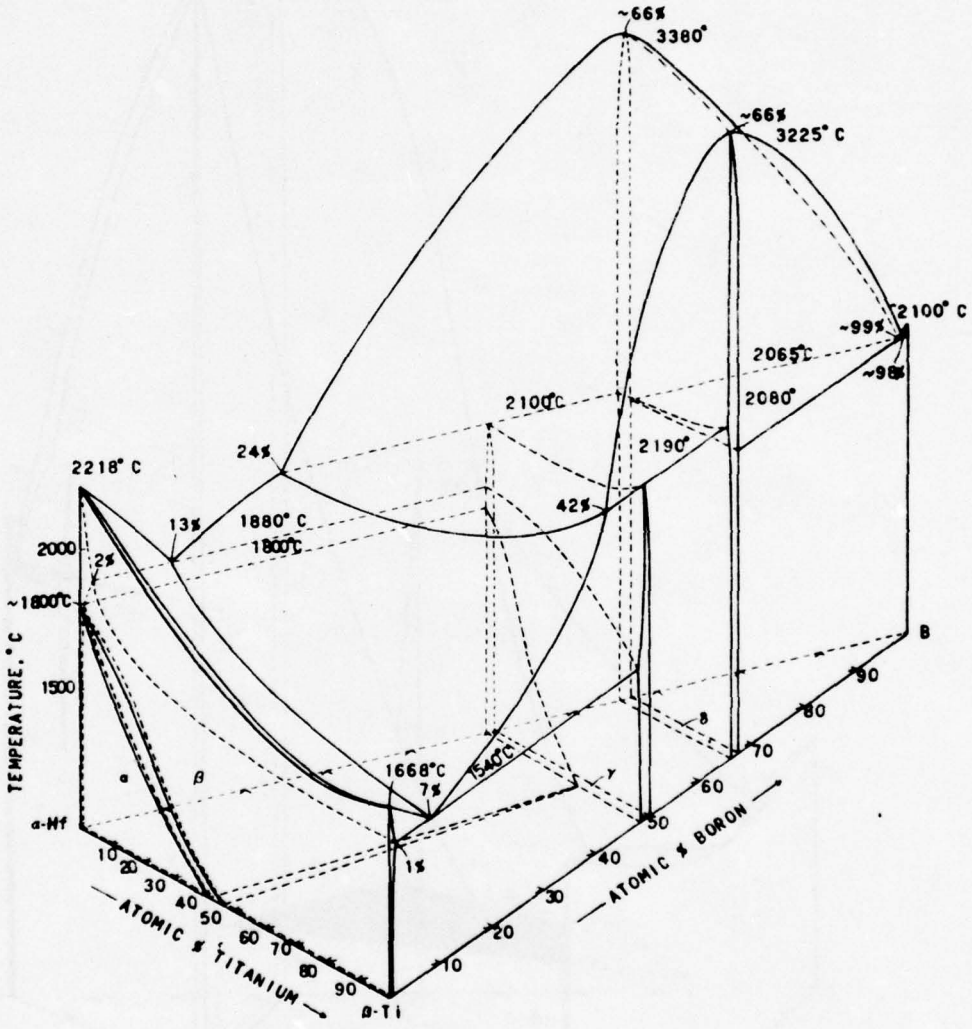

FIGURE 15: ISOMETRIC VIEW OF THE B-Ti-Hf SYSTEM.

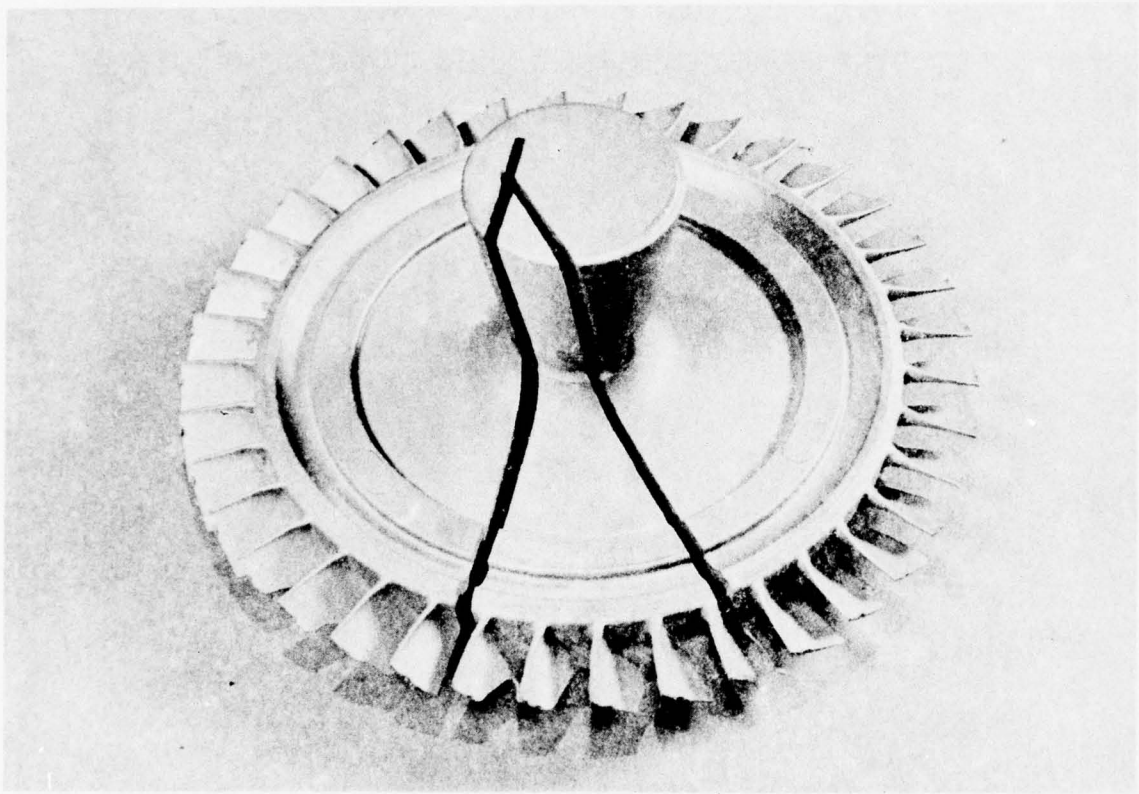

FIGURE 16: PHOTOGRAPH OF T-63 ROTOR CAST AT PRODUCTION FACILITY AND SECTIONED FOR MACROSTRUCTURAL EXAMINATION, 0.75X.

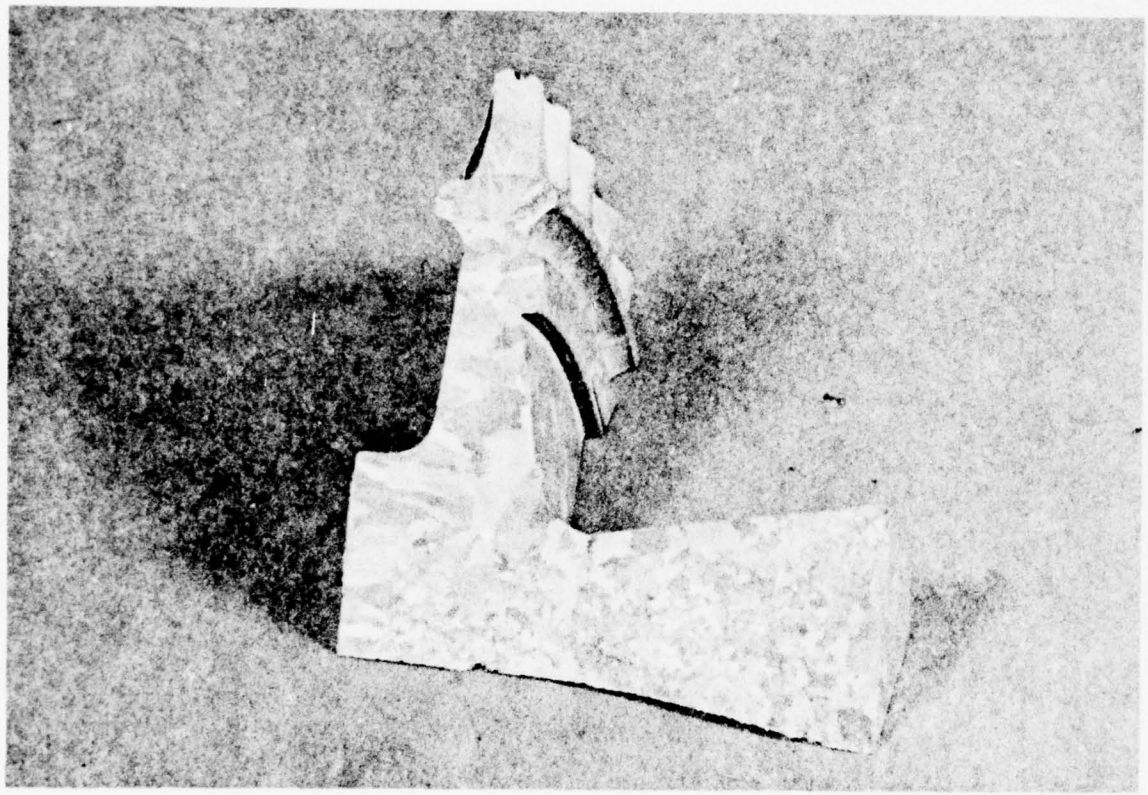

FIGURE 17: PHOTOGRAPH OF SECTIONED T-63 ROTOR CAST BY CONVENTIONAL METHODS, ETCHED 1X.

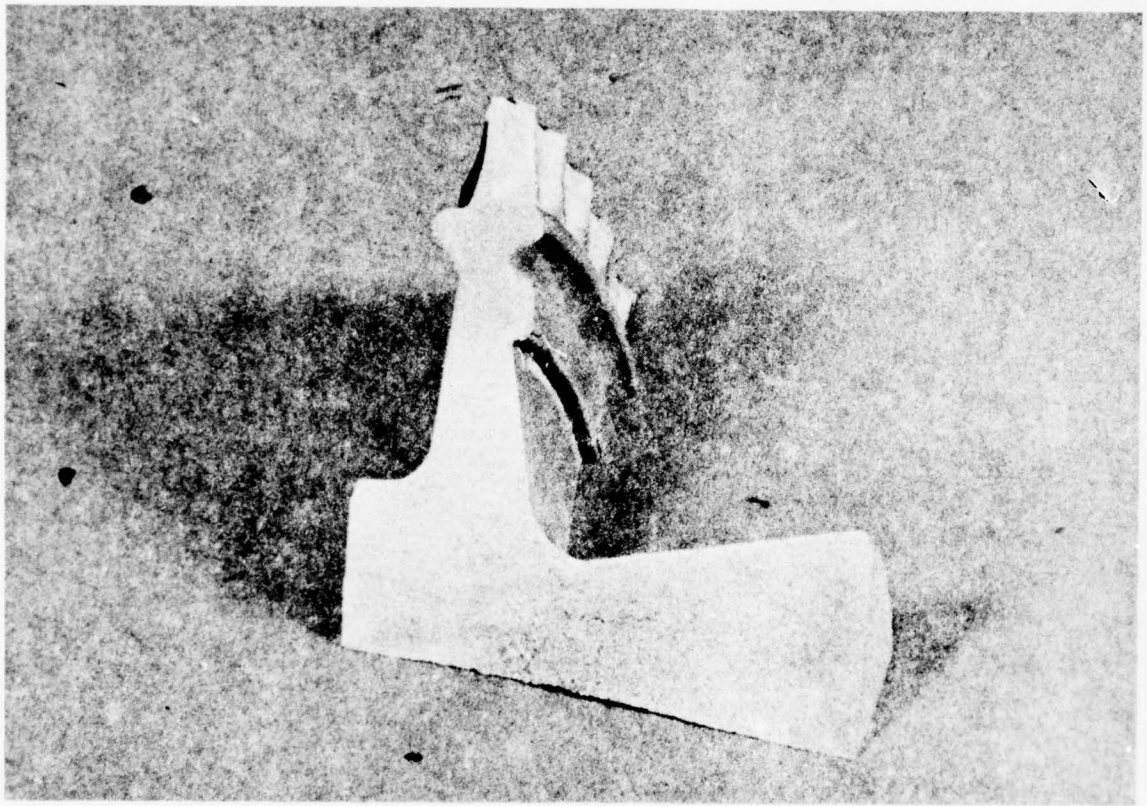

FIGURE 18: PHOTOGRAPH OF SECTIONED T-63 ROTOR CAST UTILIZING GRAIN REFINEMENT TECHNIQUE, ETCHED 1X.

a) BASELINE 713 LC AT 250X

b) BASELINE 713 LC AT 1000X

c) REFINED 713 LC AT 1000X

d) REFINED MAR-M 246 AT 1000X

FIGURE 19: MICROSTRUCTURE OF BASELINE (COARSE COLUMNAR) 713 LC AND GRAIN REFINED 713 LC AND MAR-M 246.

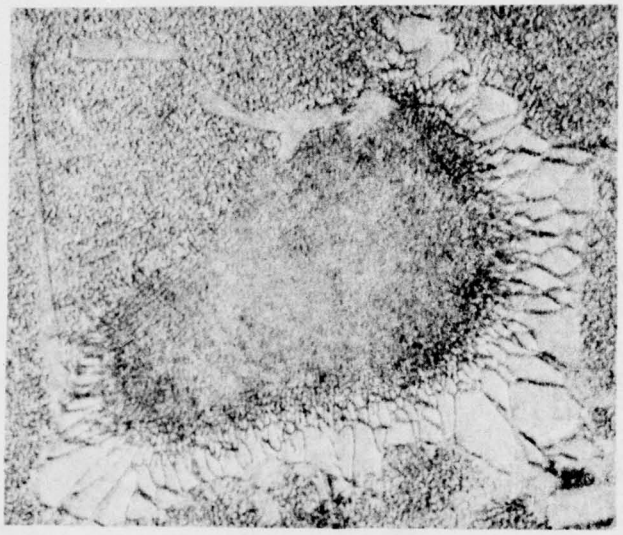

a) BASELINE C 103 SHOWING γ/γ' ISLAND AT 1000X

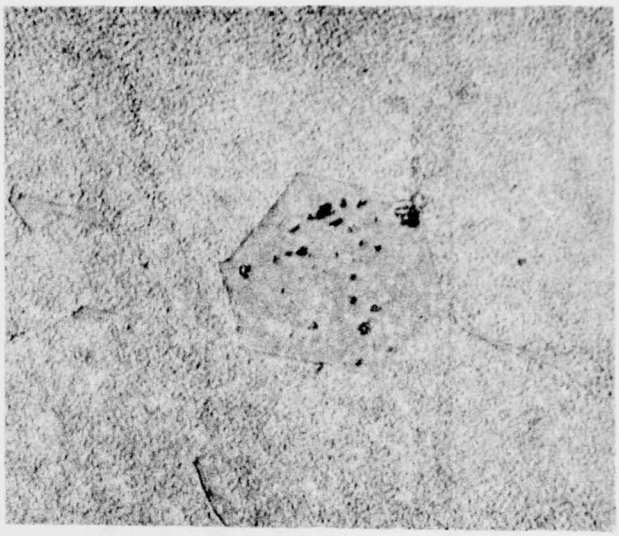

b) BASELINE C 103 SHOWING HEXAGONAL CARBIDE AT 1000X

c) REFINED C 103 SHOWING CONVOLUTED, INTERLOCKING GRAIN BOUNDARIES AT 250X.

FIGURE 20: MICROSTRUCTURES OF BASELINE (COARSE COLUMNAR) AND GRAIN REFINED C 103.

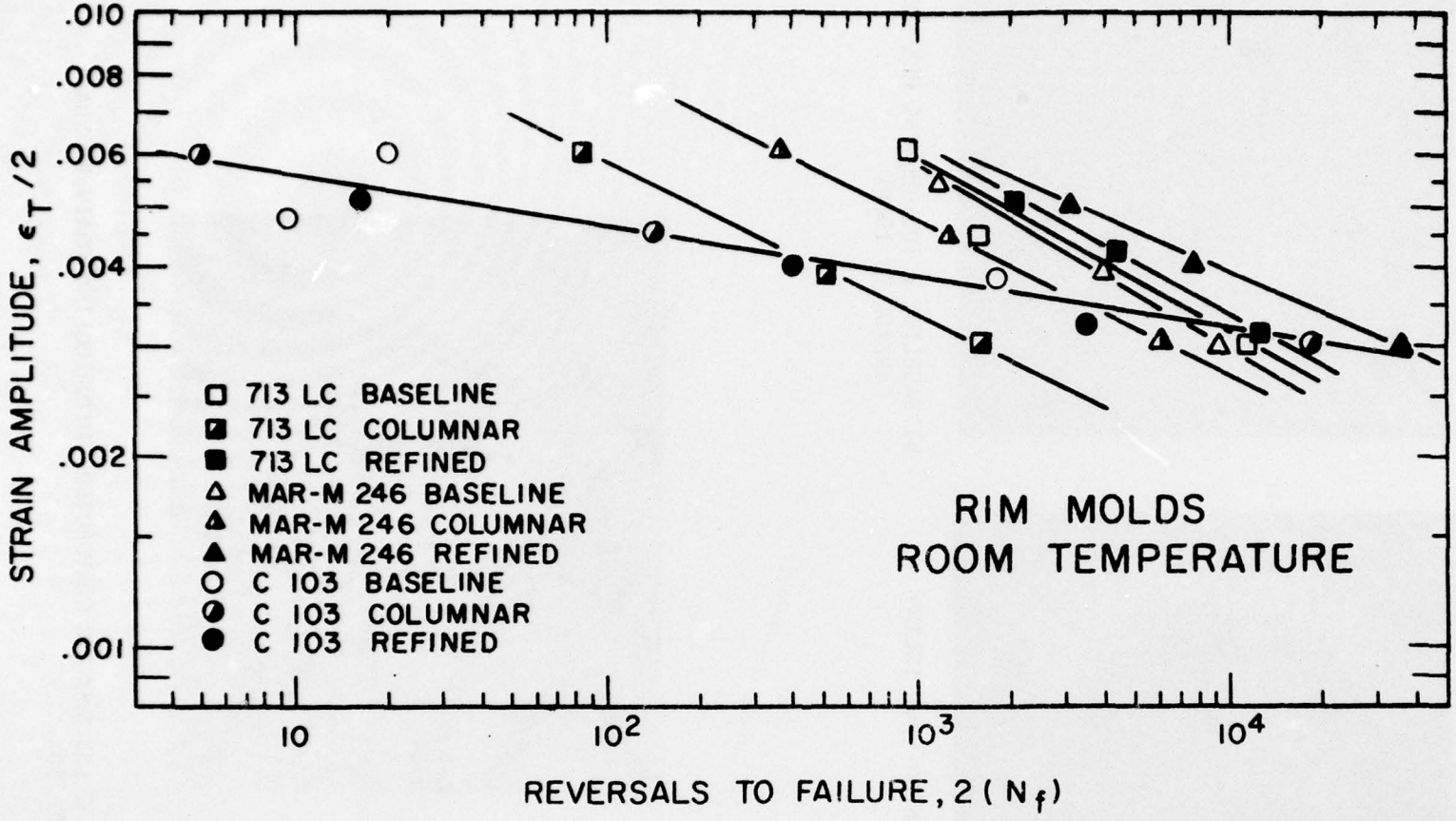

FIGURE 21: ROOM TEMPERATURE LOW CYCLE FATIGUE BEHAVIOR OF SPECIMENS FROM THE MOLD SIMULATING THE RIM OF THE ROTOR.

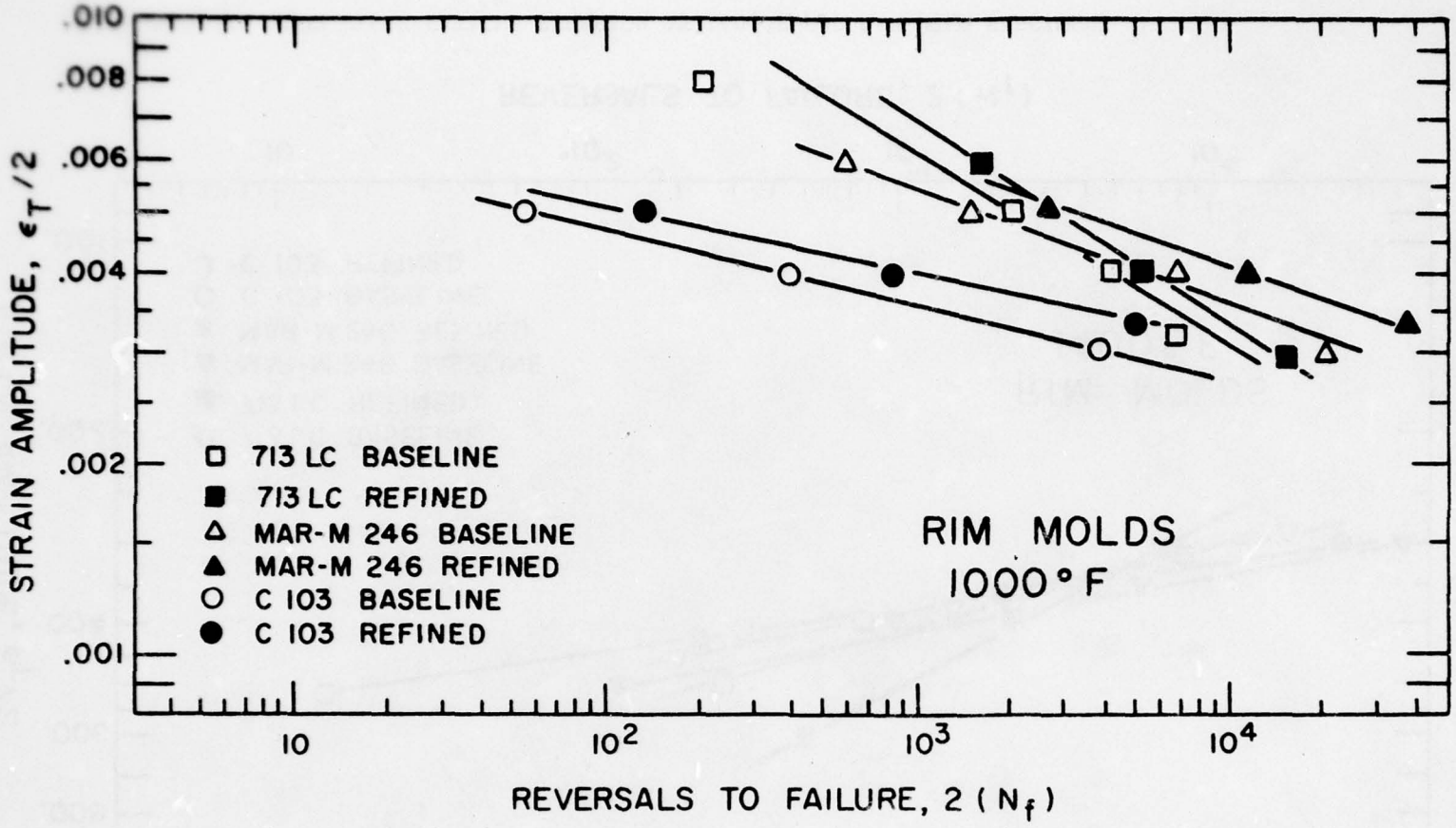

FIGURE 22: LOW CYCLE FATIGUE BEHAVIOR AT 1000°F FOR RIM MOLD SPECIMENS.

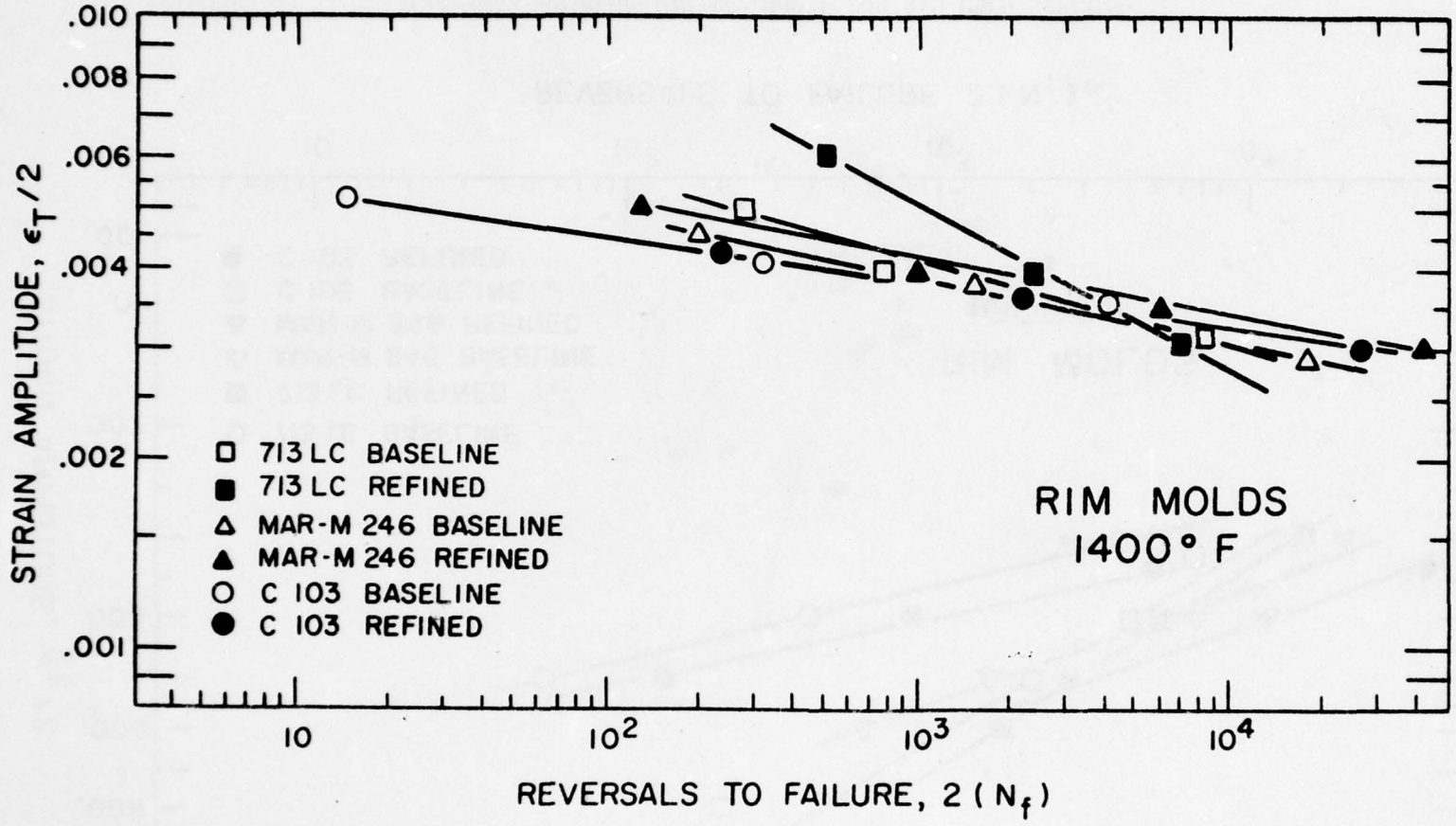

FIGURE 23: LOW CYCLE FATIGUE BEHAVIOR AT 1400°F FOR RIM MOLD SPECIMENS.

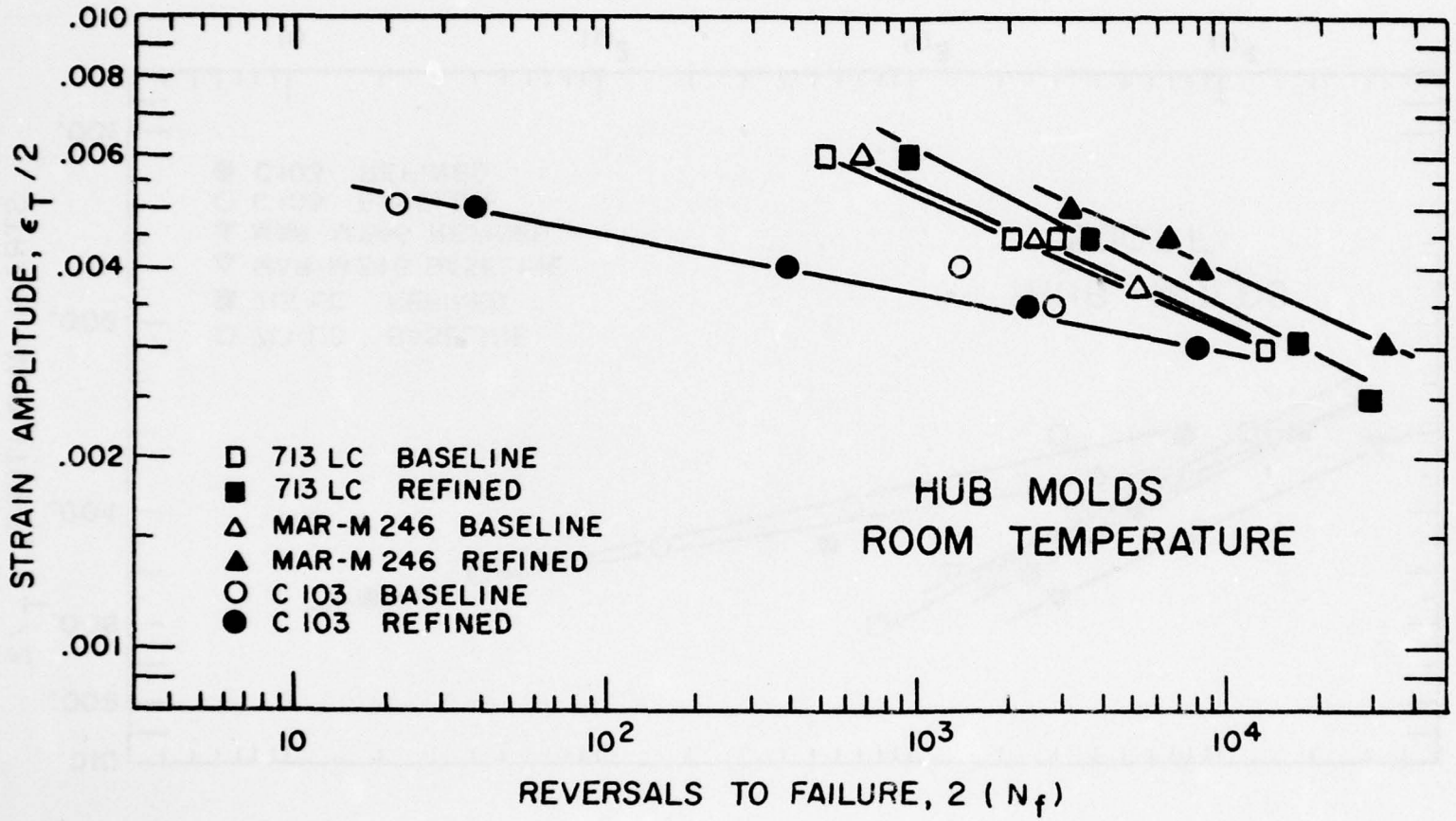

FIGURE 24: ROOM TEMPERATURE LOW CYCLE FATIGUE BEHAVIOR OF SPECIMENS FROM THE MOLD SIMULATING THE HUB OF THE ROTOR.

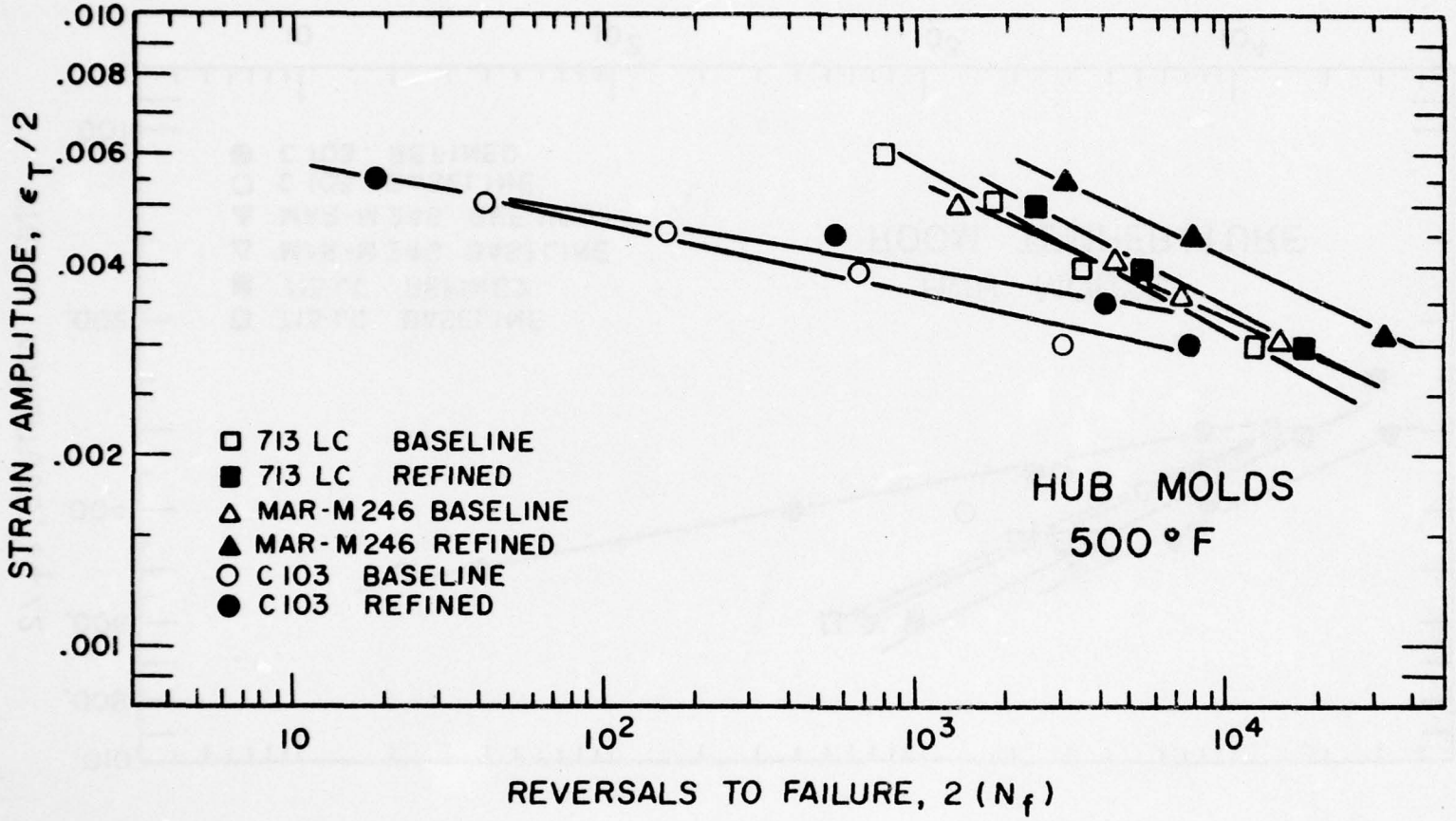

FIGURE 25: LOW CYCLE FATIGUE BEHAVIOR AT 500°F FOR HUB MOLD SPECIMENS.

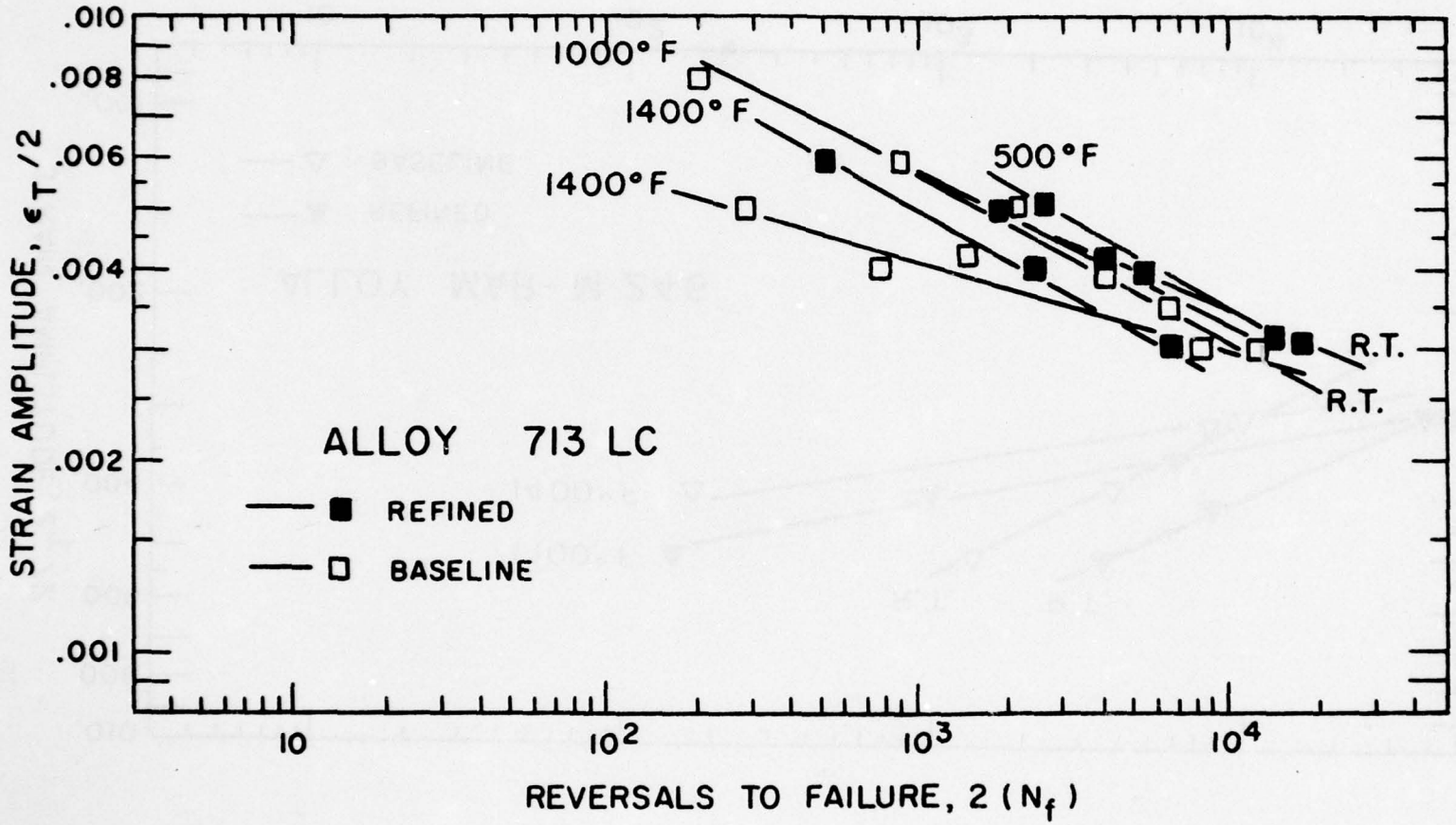

FIGURE 26: LOW CYCLE FATIGUE CURVES FOR 713 LC IN THE BASELINE, COARSE COLUMNAR AND REFINED, FINE GRAINED EQUIAXED CONDITIONS.

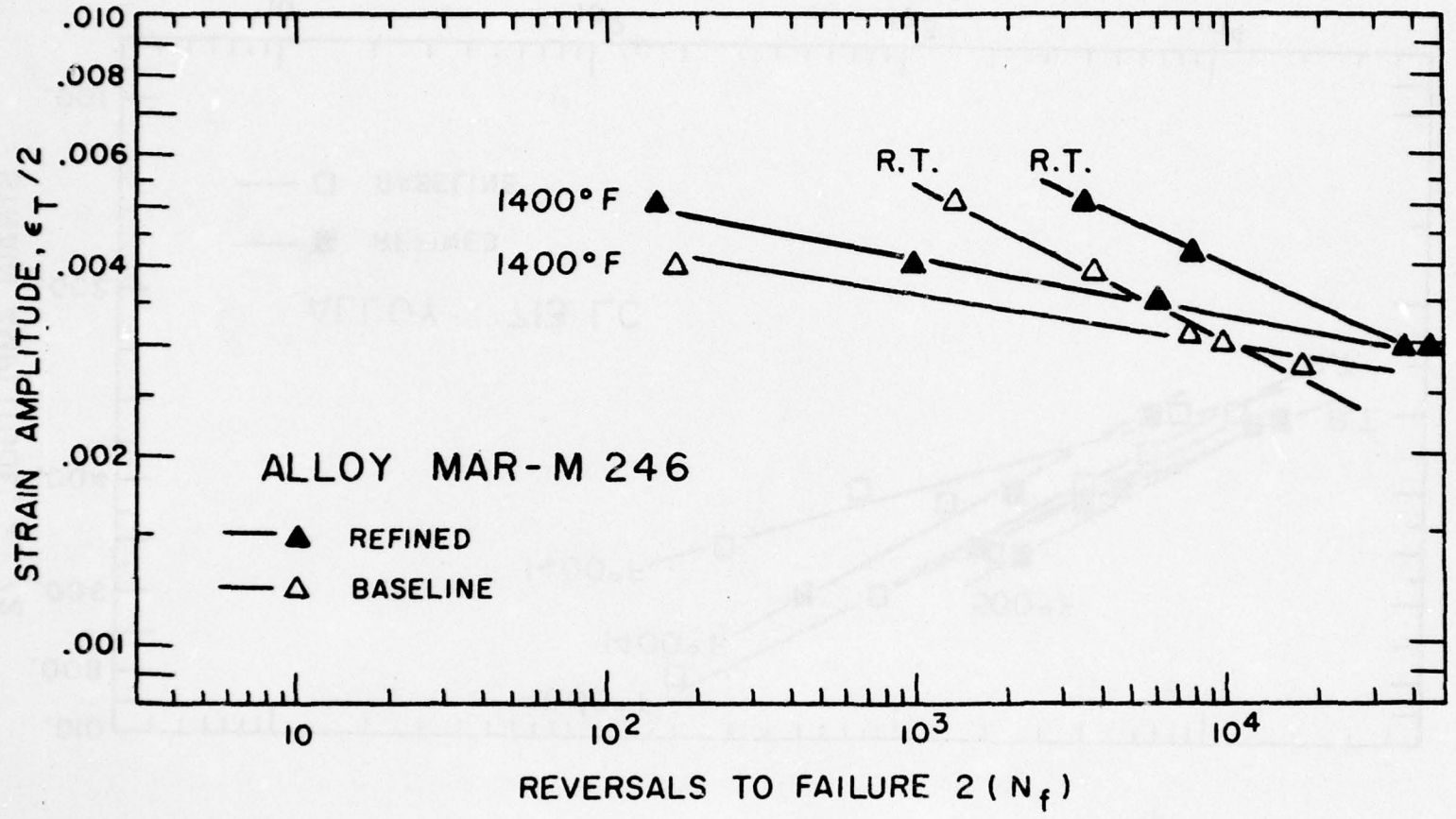

FIGURE 27: LOW CYCLE FATIGUE CURVES FOR MAR-M 246 IN THE BASELINE, COARSE COLUMNAR AND REFINED, FINE GRAINED EQUIAXED CONDITION.

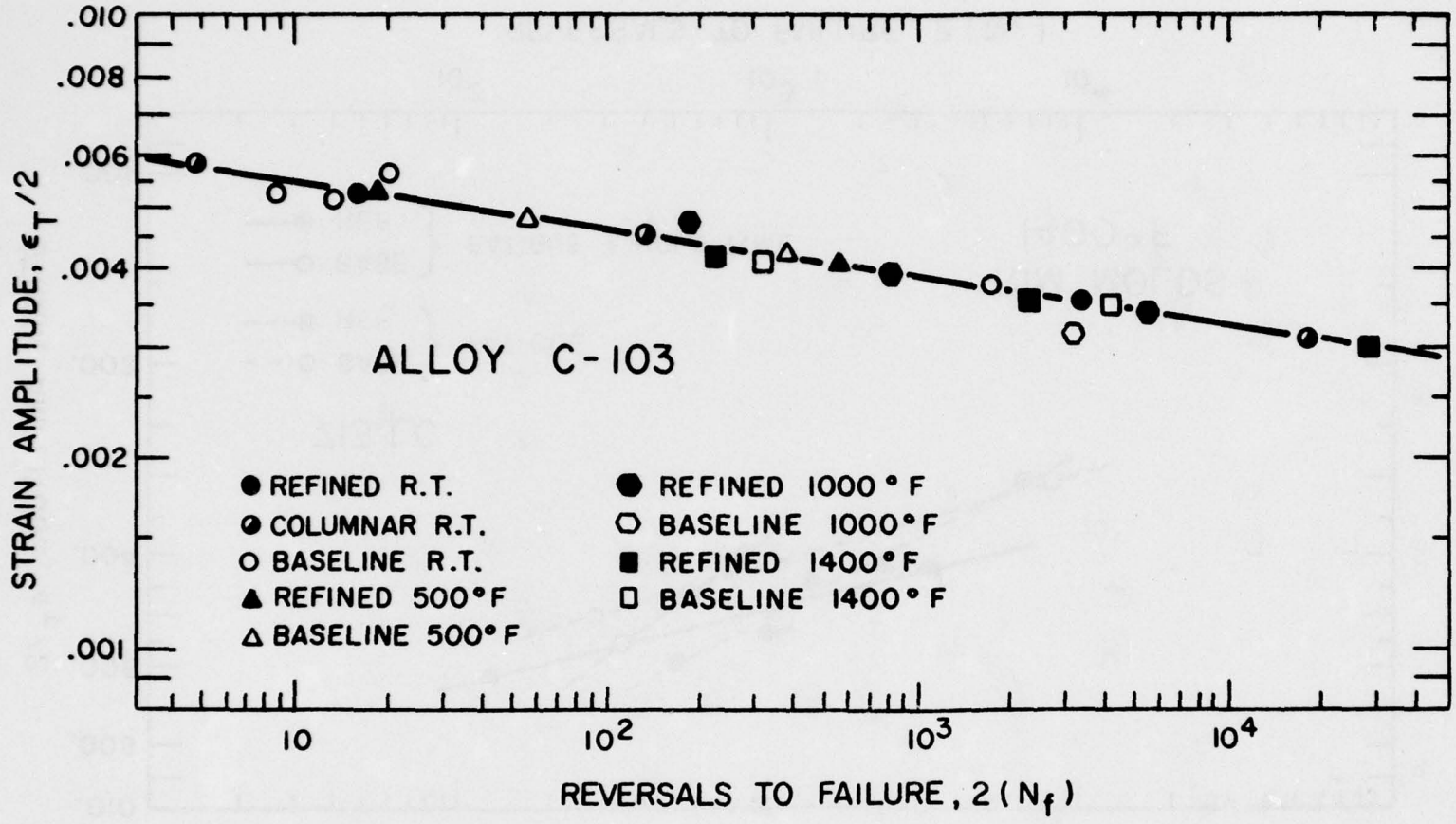

FIGURE 28: LOW CYCLE FATIGUE CURVES FOR C 103 IN THE COARSE COLUMNAR (BASELINE), FINE COLUMNAR, AND FINE GRAINED EQUIAXED CONDITION.

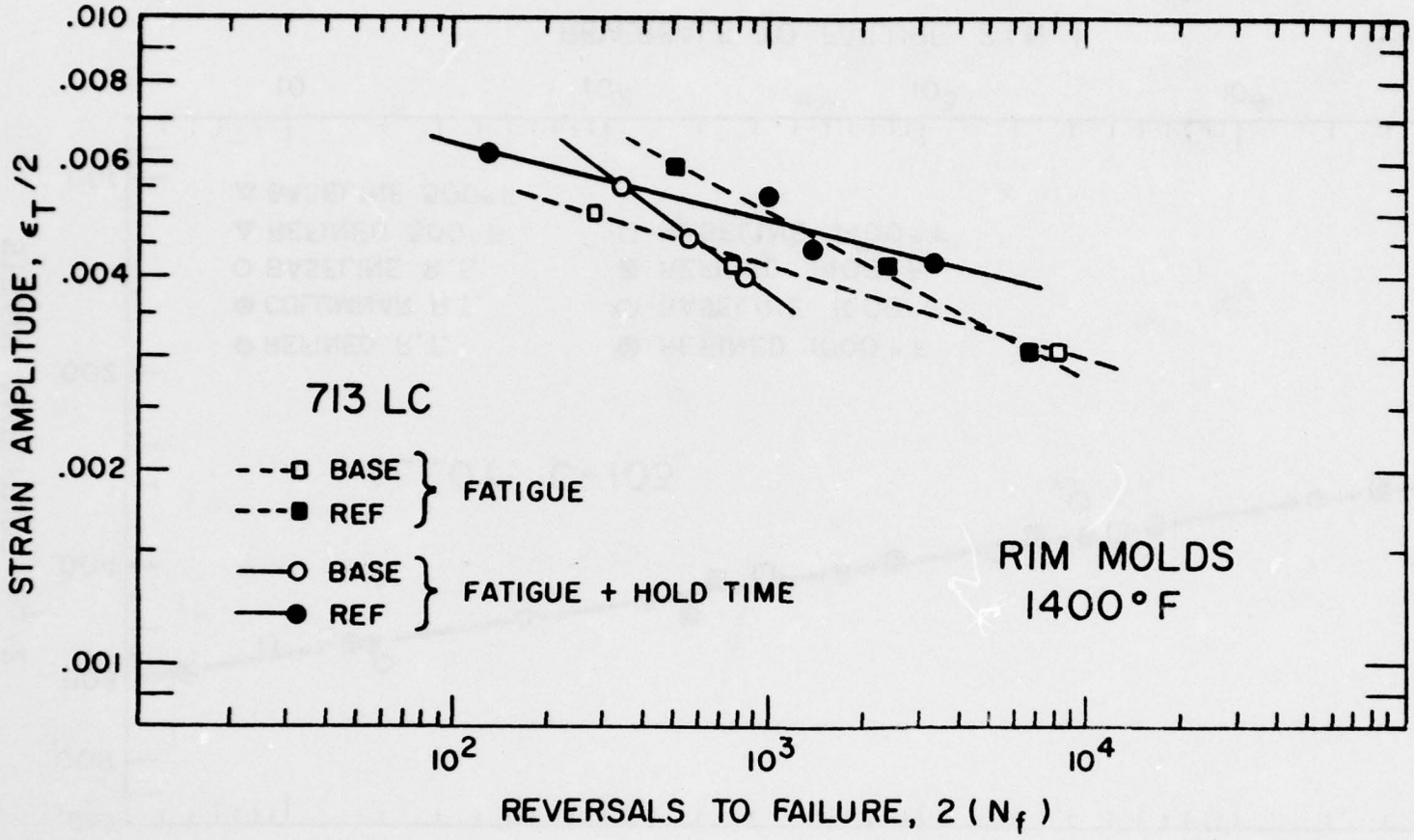

FIGURE 29: EFFECTS OF 90 SECOND HOLD TIME ON 1400°F FATIGUE PROPERTIES OF BASELINE AND REFINED 713 LC.

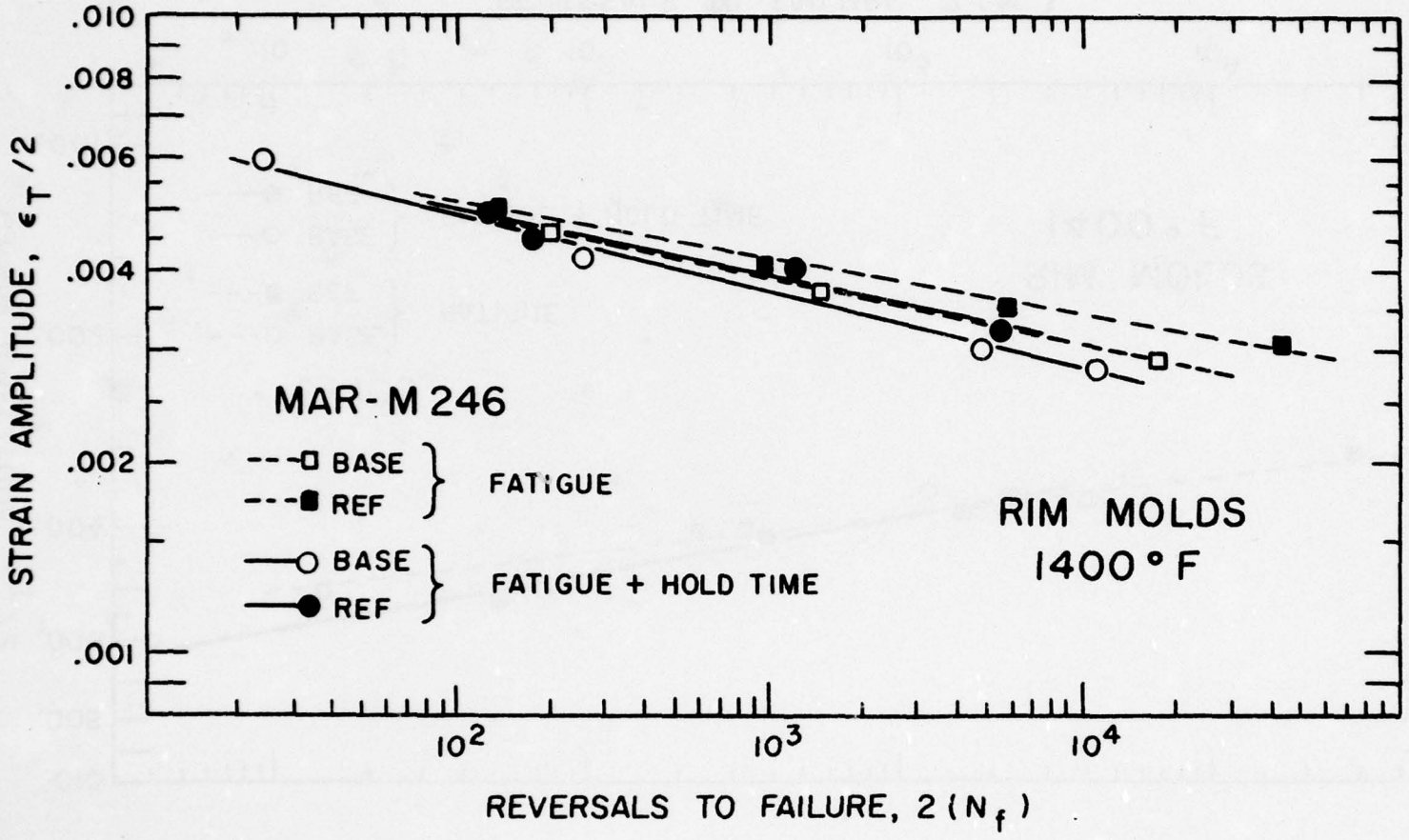

FIGURE 30: EFFECTS OF 90 SECOND HOLD TIME ON 1400°F FATIGUE PROPERTIES OF BASELINE AND REFINED MAR-M 246.

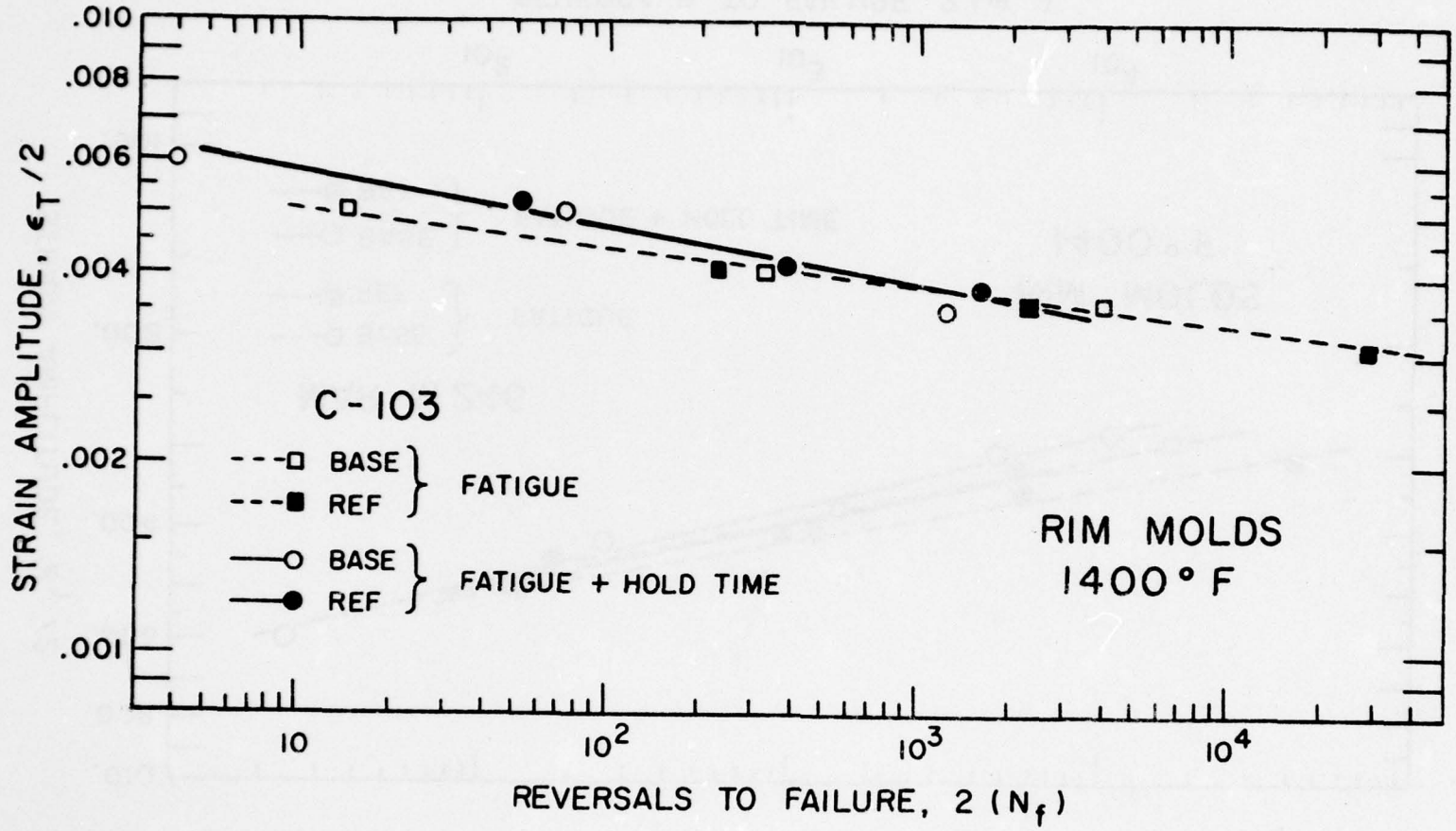

FIGURE 31: EFFECTS OF 90 SECOND HOLD TIME ON 1400°F FATIGUE PROPERTIES OF BASELINE AND REFINED C 103.

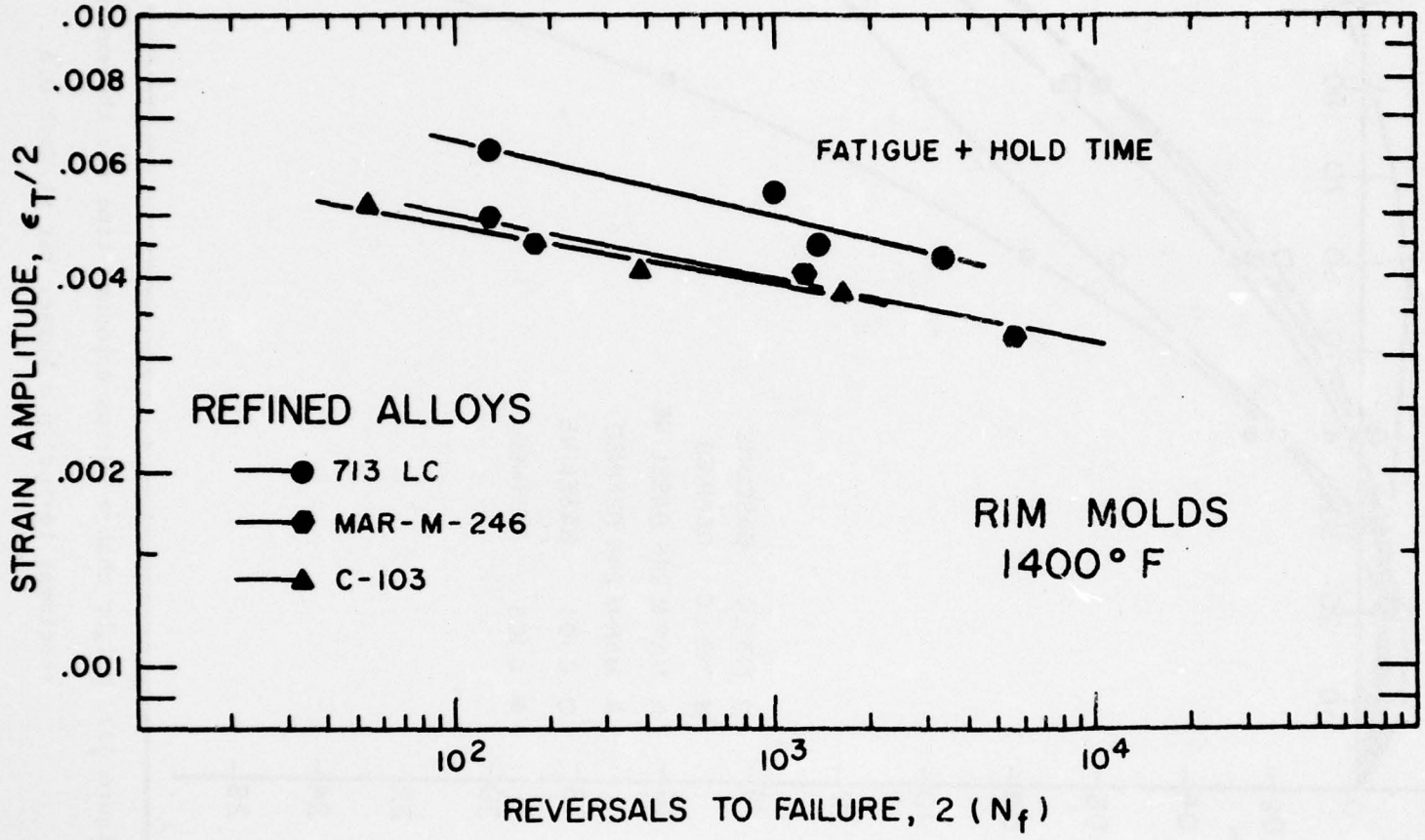

FIGURE 32: SUMMARY OF FATIGUE-CREEP PROPERTIES OF 713 LC, MAR-M 246 AND C 103 IN THE GRAIN REFINED CONDITION.

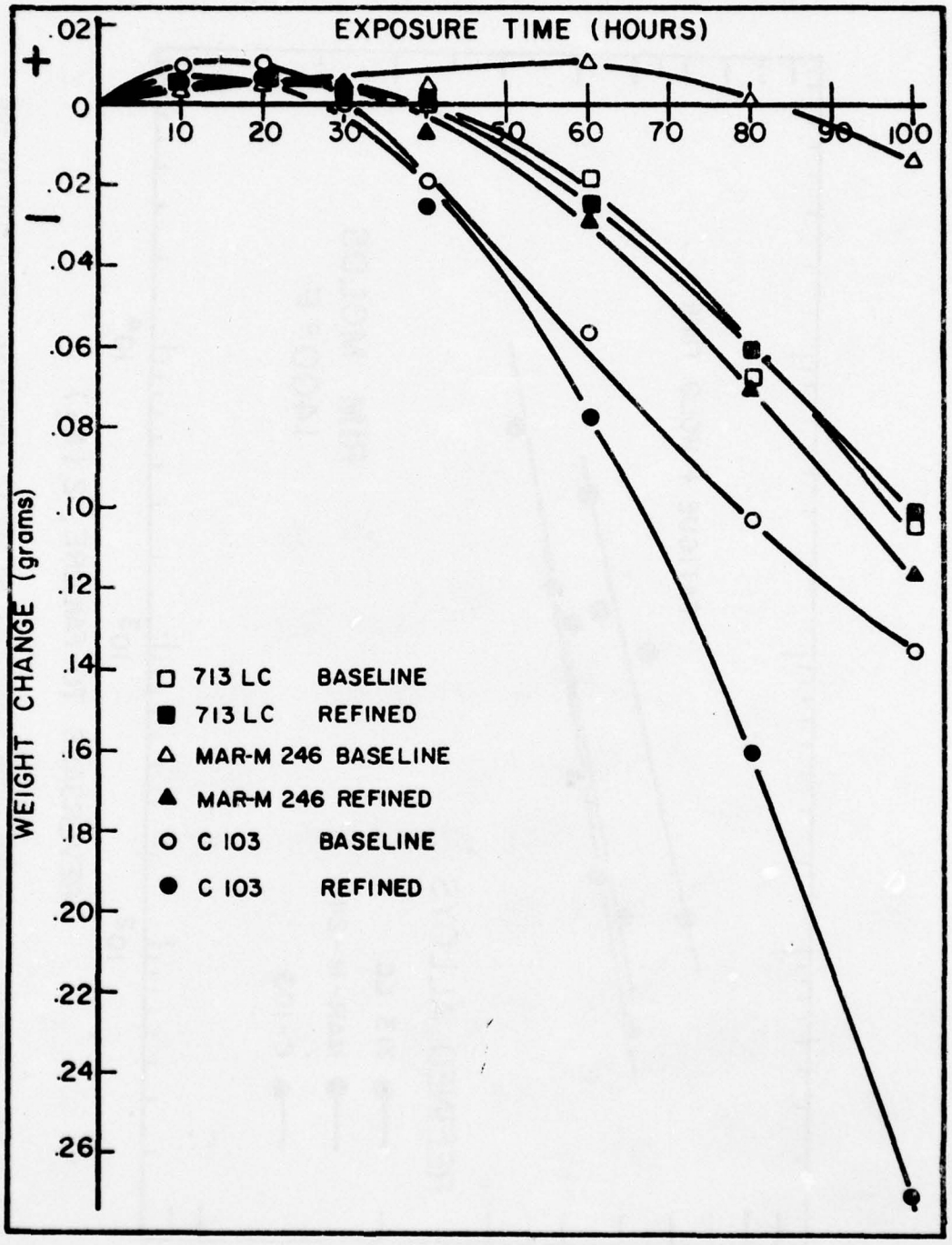

Figure 33: Weight change versus exposure time for thermal fatigue specimens tested in a burner rig at Mach 0.3 .

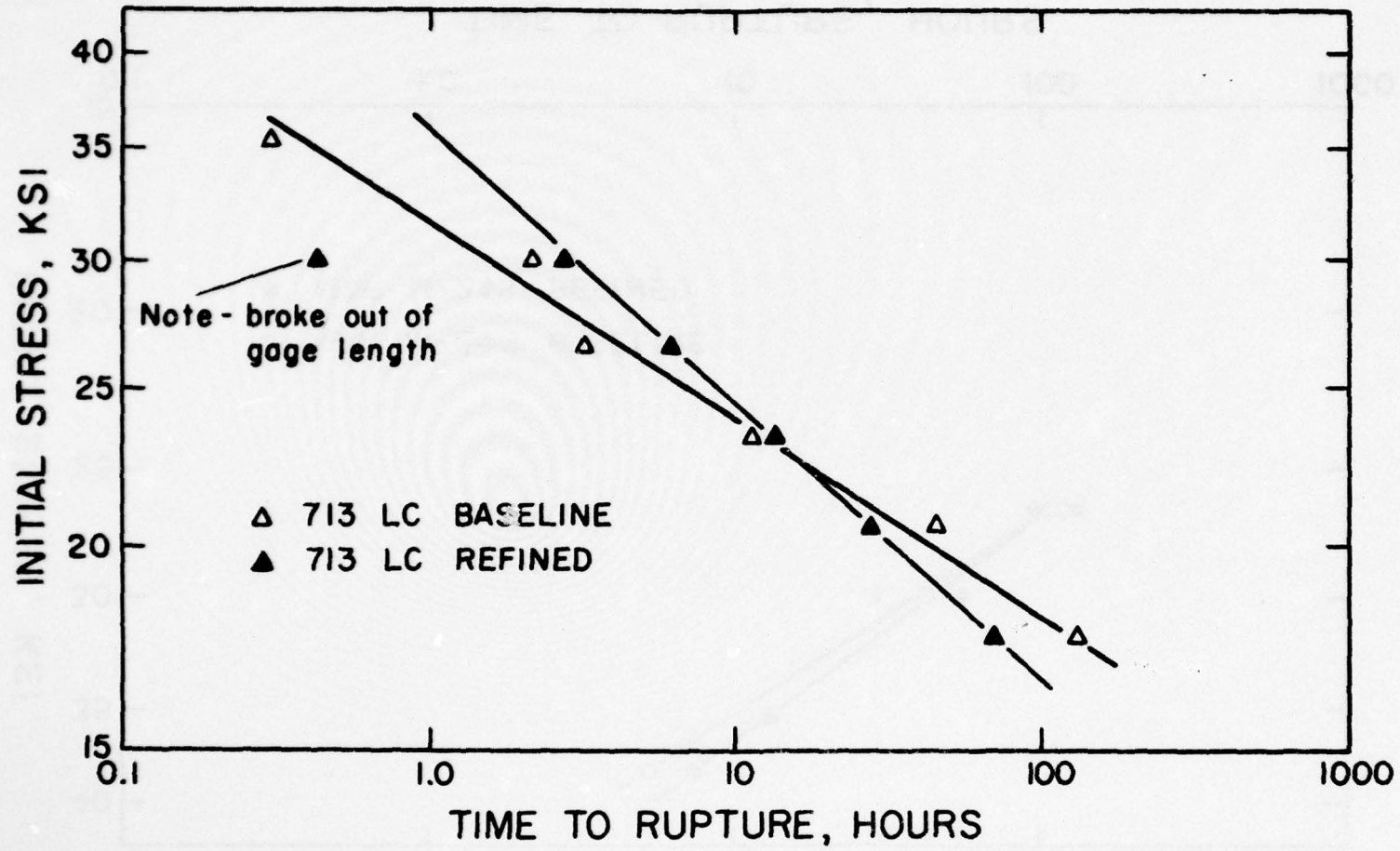

FIGURE 34: STRESS RUPTURE CURVES FOR AS CAST TUBULAR 713 LC SPECIMENS TESTED IN AIR AT 1800°F.

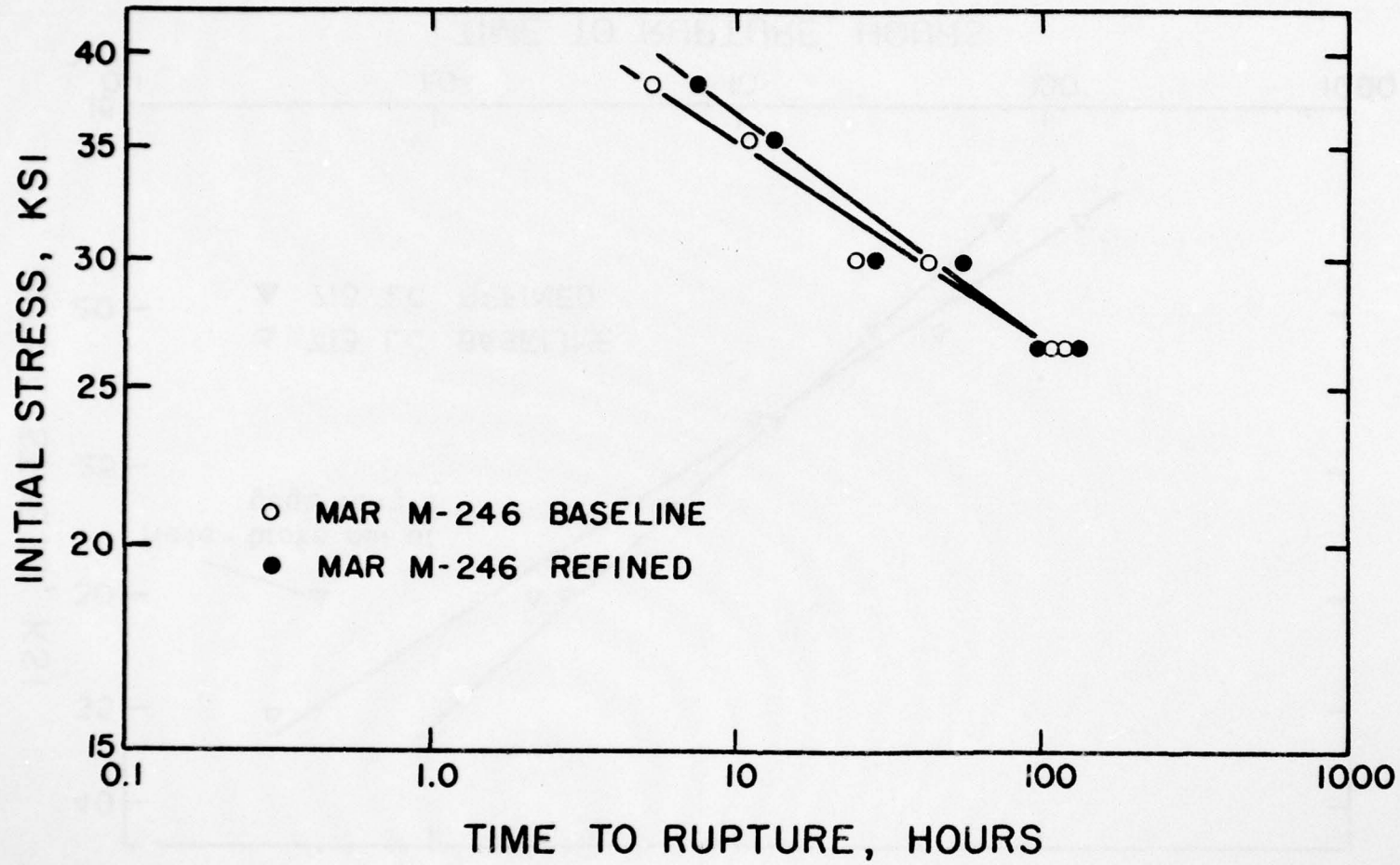

FIGURE 35: STRESS RUPTURE CURVES FOR AS CAST TUBULAR MAR-M 246 SPECIMENS TESTED IN AIR AT 1800°F.

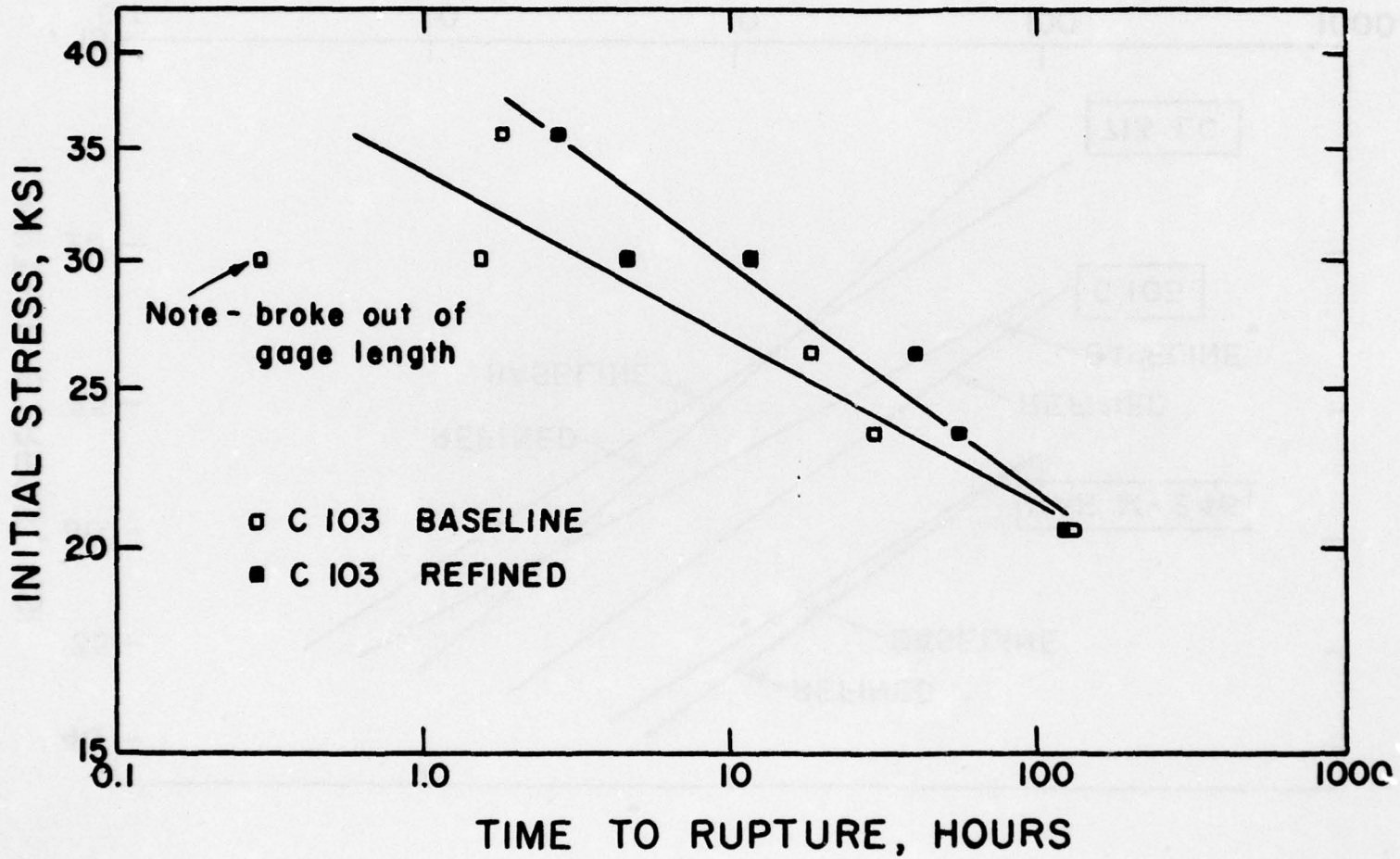

FIGURE 36: STRESS RUPTURE CURVES FOR AS CAST TUBULAR C 103 SPECIMENS TESTED IN AIR AT 1800°F.

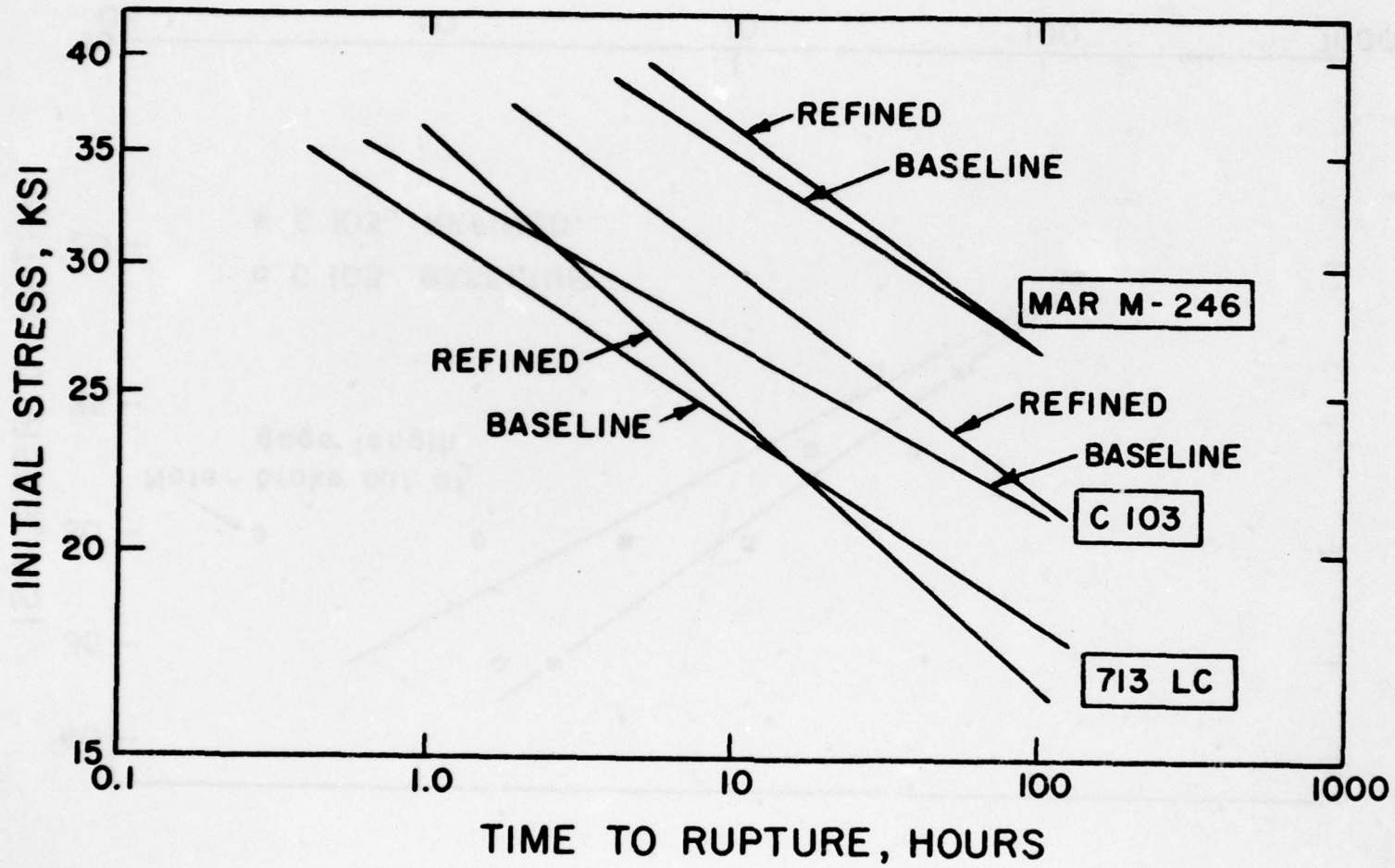

FIGURE 37: SUMMARY OF STRESS RUPTURE CURVES FOR AS CAST TUBULAR SPECIMENS TESTED IN AIR AT 1800°F.

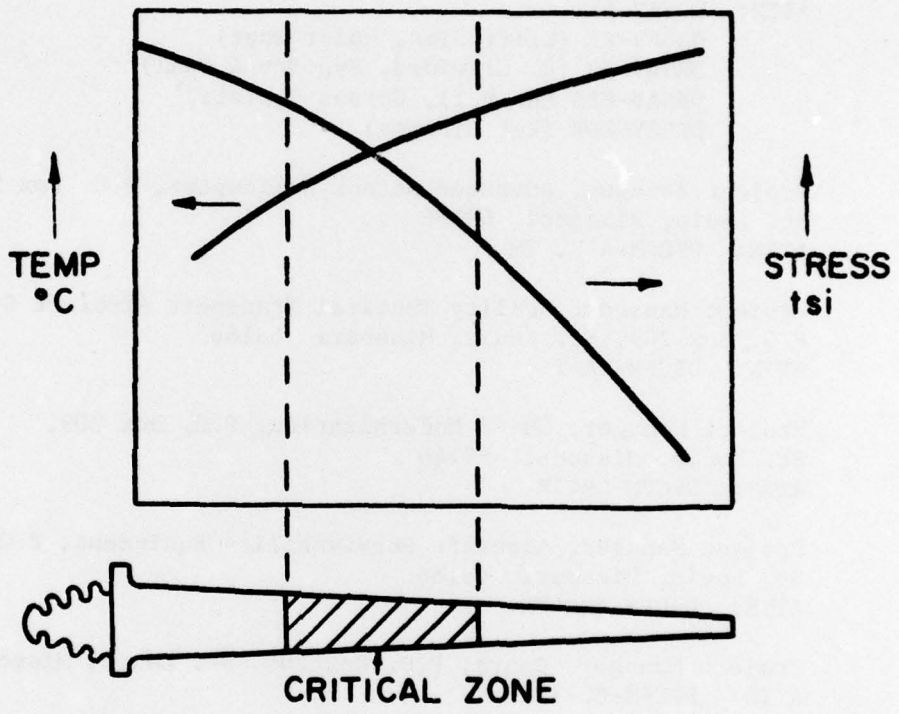

FIGURE 38: STRESS-TEMPERATURE DISTRIBUTION ALONG BLADE AEROFOIL. (REFERENCE 30)

DISTRIBUTION LIST

No. of Copies	To
	Commander, US Army Aviation Systems Command, P.O. Box 209, St. Louis, Missouri 63166
10	ATTN: DRSAV-EXT
1	DRSAV-FE (Cliff Sims, Maint Engr)
1	DRSAV-EQ (C. Crawford, Sys Dev & Qual)
1	DRSAV-FES (H. Bull, Corpus Christi)
2	DRSAV-ZDR (Ref Library)
	Project Manager, Advanced Attack Helicopter, P.O. Box 209, St. Louis, Missouri 63166
1	ATTN: DRCPM-AAH, TM
	Project Manager, Utility Tactical Transport Aircraft System, P.O. Box 209, St. Louis, Missouri 63166
1	ATTN: DRCPM-UA-T
	Project Manager, CH-47 Modernization, P.O. Box 209, St. Louis, Missouri 63166
1	ATTN: DRCPM-CH47M
	Project Manager, Aircraft Survivability Equipment, P.O. Box 209, St. Louis, Missouri 63166
1	ATTN: DRCPM-ASE-TM
	Project Manager, Cobra, P.O. Box 209, St. Louis, Missouri 63166
1	ATTN: DRCPM-CO-T
	Project Manager, Iranian Aircraft Program, P.O. Box 209, St. Louis, Missouri 63166
1	ATTN: DRCPM-IAP-T
	Commander, US Army Material Development and Readiness Command, 5001 Eisenhower Avenue, Alexandria, Virginia 22333
4	ATTN: DRCRD-TE
1	DRCLDC, Mr. R. Zentner
	Director, Eustis Directorate, US Army Air Mobility R&D Lab, Ft. Eustis, Virginia 23604
1	ATTN: SAVDL-EU-TAS
1	SAVDL-SS, Mr. J. Robinson
	Director, Ames Directorate, US Army Air Mobility R&D Lab, Ames Research Center, Moffett Field, California 94035
1	ATTN: SAVDL-AM

No. of Copies	To
	Director, Langley Directorate, US Army Air Mobility R&D Lab, Mail Stop 266, Hampton, Virginia 23365
1	ATTN: SAVDL-LA
	Director, Lewis Directorate, US Army Air Mobility R&D Lab, 21000 Brook Park Rd, Cleveland, Ohio 44135
1	ATTN: SAVDL-LE
	US Army Industrial Base Engineering Activity, Rock Island, Illinois 61201
1	ATTN: DRXIB-MT, Mr. James W. Carstens, Chief, Mftg. Tech. Division
	Air Force Materials Laboratory, Manufacturing Technology Division, Wright-Patterson Air Force Base, Ohio 45433
1	ATTN: AFML/LTM
1	AFML/LTN
1	AFML/LTE
	Commander, US Army Electronics Command, Ft. Monmouth, New Jersey 07703
1	ATTN: DRSEL-RD-P
1	DRSEL-GG-DD
	Commander, US Army Missile Command, Redstone Arsenal, Alabama 35809
1	ATTN: DRSMI-IIE
1	Technical Library
1	DRSMI-RSM, Mr. E.J. Wheelahan
	Commander, US Army Troop Support Command, 4300 Goodfellow Blvd., St. Louis, Missouri 63120
1	ATTN: DRSTS-PLC
	Commander, US Army Armament Command, Rock Island, Illinois 61201
1	ATTN: DRSAR-PPR-1W
2	Technical Library
	Commander, US Army Tank-Automotive Command, Warren, Michigan 48090
1	ATTN: DRDTA-RCM.1
2	DRDTA, Research Library
12	Commander, Defense Documentation Center, Cameron Station, Building 5, 5010 Duke Street, Alexandria, Virginia 22314

No. of Copies	To
	Hughes Helicopter, Division of Summa Corporation, M/S T-419, Centinella Avenue and Teale Street, Culver City, California 90230
2	ATTN: Mr. R.E. Moore, Bldg. 314
	Sikorsky Aircraft Division, United Aircraft Corporation, Stratford, Connecticut 06497
2	ATTN: Mr. Stan Silverstein, Section Supv., Manufacturing Technology
	Bell Helicopter Company, P.O. Box 482, Ft. Worth, Texas 76101
2	ATTN: Mr. P. Baumgartner, Chief, Manufacturing Technology
	Kaman Aerospace Corporation, Bloomfield, Connecticut 06002
2	ATTN: Mr. A.S. Falcone, Chief of Materials Engineering
	Boeing Vertol Company, Box 16858, Philadelphia, Pennsylvania 19142
2	ATTN: R. Pinckney, Manufacturing Technology
	Detroit Diesel Allison Division, General Motors Corporation, P.O. Box 894, Indianapolis, Indiana 46206
2	ATTN: James E. Knott, General Manager
	General Electric Company, 10449 St. Charles Rock Road, St. Ann, Missouri 63074
2	ATTN: Mr. H. Franzen
	AVCO-Lycoming Corporation, 550 South Main Street, Stratford, Connecticut 06497
2	ATTN: Mr. V. Strautman, Manager, Process Technology Laboratory
	United Technologies Corporation, Pratt & Whitney Aircraft Division, Manufacturing Research and Development, East Hartford, Connecticut 06108
2	ATTN: Mr. Ray Traynor
1	Mr. Louis J. Fiedler, Senior Development Engineer, Materials Laboratory, AVCO-Lycoming Division, 550 South Main Street, Stratford, Connecticut 06497
1	Mr. Barry Goldblatt, Director, Materials & Process Technology Laboratory, AVCO-Lycoming Division, 550 South Main Street, Stratford, Connecticut 06497

No. of Copies	To
1	Mr. John Petrusha, Airesearch Manufacturing Company, Dept. 93-393M, 402 South 36 Street, Phoenix, Arizona 85034
1	Mr. John A. Alexander, Manager, Materials Research Development, TRW Equipment, TRW, Inc., 23555 Euclid Avenue, Cleveland, Ohio 44117
1	Mr. W.R. Freeman, Jr., Vice President and Technical Director, Technical Center, Howmet Corporation, 699 Benston Road, Whitehall, Michigan 49461
1	Mr. Jay Vandersluis, Technical Director, Misco Technical Center, 699 Benston Road, Whitehall, Michigan 49461
1	Mrs. Elizabeth Barrett, T/M 3417, TRW Equipment, TRW, Inc., 23555 Euclid Avenue, Cleveland, Ohio 44117
1	Mr. Randy Sutscher, AMSAV-ERE, P.O. Box 209, Main Office, St. Louis, Missouri 63166
1	Mr. John Acurio, USAMRDL, 21000 Brookpark Road, Cleveland, Ohio 44135
1	Mr. Henry L. Morrow, AMRDL, Ft. Eustis, Virginia 23604
1	Mr. Ralph Tyson, DRSAV-ERP, USAVSCOM, P.O. Box 209, St. Louis, Missouri 63166
1	Mr. E. Scott Nichols, Materials Engineer, Detroit Diesel, Allison Division, General Motors Corp., P.O. Box 894, Code T2B, Indianapolis, Indiana 46206
1	Dr. Thomas S. Piwonka, Section Manager, Casting Technology, TRW Equipment, TRW, Inc., 23555 Euclid Avenue, Cleveland, Ohio 44117
1	Mr. George Cash, Manager, Precision Investment Casting Unit, Mail Drop 26804, General Electric Company, 1000 Western Avenue, Lynn, Massachusetts 01910
1	Mr. Robert Prine, Naval Air Systems Command, Jefferson Plaza, Jefferson Parkway, Washington, D.C.
1	Mr. Marvin Schmidt, Air Force Propulsion Laboratory, Wright Patterson Air Force Base, Ohio 45433
1	Dr. Gary Halford 49-1, NASA Lewis Research Center, 21000 Brookpark Road, Cleveland, Ohio 44017

No. of Copies	To
1	Dr. R.L. Ashbrook 49-3, NASA Lewis Research Center, 21000 Brookpark Road, Cleveland, Ohio 44017
	Director, Army Materials and Mechanics Research Center, Watertown, Massachusetts 02172
2	ATTN: DRXMR-PL
1	DRXMR-AG
1	DRXMR-PR
1	DRXMR-CT
1	DRXMR-X
1	DRXMR-AP
1	DRXMR-M
1	Dr. Paul J. Ahearn
12	Mr. Perry R. Smoot

y Materials and Mechanics Research Center,
Watertown, Massachusetts 02172
INFLUENCE OF GRAIN REFINEMENT ON THE
STRUCTURE AND PROPERTIES OF CAST
NICKEL-BASE SUPERALLOY TURBINE COMPONENTS
A.F. Denzine, T.A. Kolakowski,
W.M. Matlock and J.F. Wallace
Case Western Reserve University
Department of Metallurgy & Materials
Science
Cleveland, Ohio 44106

al Report AMMRC CTR 77-15, May 1977, 51 pp -
illus - tables, Contract DAAG46-74-C-0009
D/A Project 1728036, AMCMS Code 4097
Final Report, September 10, 1973 to May 15, 1977

AD _____

UNCLASSIFIED
UNLIMITED DISTRIBUTION

Key Words:

Cast Nickel Superalloys
Cast Grain Size Control
Low Cycle Fatigue
Stress Rupture Properties
Tensile Properties
Fatigue-Creep Properties

influence of refinement of the cast grains on the mechanical properties of three nickel
e superalloys (713LC, MAR-M-246 and C103) was determined. The investigation was con-
ted because improvements in the fatigue properties of integrally cast rotors for heli-
ters was desired. Grain refinement of all three alloys was accomplished by a controlled
rmal cycling technique together with a boron addition to the melt. This refinement
ctice was successfully adapted to production rotor casting. This grain refinement in-
ased by a factor of 2 to 4 the number of cycles to failure in low cycle fatigue of
LC and MAR-M-246. The fatigue behavior of C103 was insensitive to grain size. The
ld strength of 713LC and MAR-M-246 was increased 10 ksi but the tensile strength and
tility slightly decreased by grain refinement. The 1800°F stress rupture properties of
refined alloys were slightly superior to the unrefined alloys at high stress levels
equal to or slightly inferior at low stress levels. At 1850°F and lower stress levels,
stress rupture properties of MAR-M-246 were somewhat reduced compared to the unrefined
ucture.

Army Materials and Mechanics Research Center,
Watertown, Massachusetts 02172
INFLUENCE OF GRAIN REFINEMENT ON THE
STRUCTURE AND PROPERTIES OF CAST
NICKEL-BASE SUPERALLOY TURBINE COMPONENTS
A.F. Denzine, T.A. Kolakowski,
W.M. Matlock and J.F. Wallace
Case Western Reserve University
Department of Metallurgy & Materials
Science
Cleveland, Ohio 44106

Final Report AMMRC CTR 77-15, May 1977, 51 pp -
illus - tables, Contract DAAG46-74-C-0009
D/A Project 1728036, AMCMS Code 4097
Final Report, September 10, 1973 to May 15, 1977

AD _____

UNCLASSIFIED
UNLIMITED DISTRIBUTION

Key Words:

Cast Nickel Superalloys
Cast Grain Size Control
Low Cycle Fatigue
Stress Rupture Properties
Tensile Properties
Fatigue-Creep Properties

The influence of refinement of the cast grains on the mechanical properties of three nickel base superalloys (713LC, MAR-M-246 and C103) was determined. The investigation was conducted because improvements in the fatigue properties of integrally cast rotors for helicopters was desired. Grain refinement of all three alloys was accomplished by a controlled thermal cycling technique together with a boron addition to the melt. This refinement practice was successfully adapted to production rotor casting. This grain refinement increased by a factor of 2 to 4 the number of cycles to failure in low cycle fatigue of 713LC and MAR-M-246. The fatigue behavior of C103 was insensitive to grain size. The yield strength of 713LC and MAR-M-246 was increased 10 ksi but the tensile strength and ductility slightly decreased by grain refinement. The 1800°F stress rupture properties of the refined alloys were slightly superior to the unrefined alloys at high stress levels and equal to or slightly inferior at low stress levels. At 1850°F and lower stress levels, the stress rupture properties of MAR-M-246 were somewhat reduced compared to the unrefined structure.

y Materials and Mechanics Research Center,
Watertown, Massachusetts 02172
INFLUENCE OF GRAIN REFINEMENT ON THE
STRUCTURE AND PROPERTIES OF CAST
NICKEL-BASE SUPERALLOY TURBINE COMPONENTS
A.F. Denzine, T.A. Kolakowski,
W.M. Matlock and J.F. Wallace
Case Western Reserve University
Department of Metallurgy & Materials
Science
Cleveland, Ohio 44106

al Report AMMRC CTR 77-15, May 1977, 51 pp -
illus - tables, Contract DAAG46-74-C-0009
D/A Project 1728036, AMCMS Code 4097
Final Report, September 10, 1973 to May 15, 1977

AD _____

UNCLASSIFIED
UNLIMITED DISTRIBUTION

Key Words:

Cast Nickel Superalloys
Cast Grain Size Control
Low Cycle Fatigue
Stress Rupture Properties
Tensile Properties
Fatigue-Creep Properties

influence of refinement of the cast grains on the mechanical properties of three nickel
e superalloys (713LC, MAR-M-246 and C103) was determined. The investigation was con-
ted because improvements in the fatigue properties of integrally cast rotors for heli-
ters was desired. Grain refinement of all three alloys was accomplished by a controlled
rmal cycling technique together with a boron addition to the melt. This refinement
ctice was successfully adapted to production rotor casting. This grain refinement in-
ased by a factor of 2 to 4 the number of cycles to failure in low cycle fatigue of
LC and MAR-M-246. The fatigue behavior of C103 was insensitive to grain size. The
ld strength of 713LC and MAR-M-246 was increased 10 ksi but the tensile strength and
tility slightly decreased by grain refinement. The 1800°F stress rupture properties of
refined alloys were slightly superior to the unrefined alloys at high stress levels
equal to or slightly inferior at low stress levels. At 1850°F and lower stress levels,
stress rupture properties of MAR-M-246 were somewhat reduced compared to the unrefined
ucture.

Army Materials and Mechanics Research Center,
Watertown, Massachusetts 02172
INFLUENCE OF GRAIN REFINEMENT ON THE
STRUCTURE AND PROPERTIES OF CAST
NICKEL-BASE SUPERALLOY TURBINE COMPONENTS
A.F. Denzine, T.A. Kolakowski,
W.M. Matlock and J.F. Wallace
Case Western Reserve University
Department of Metallurgy & Materials
Science
Cleveland, Ohio 44106

Final Report AMMRC CTR 77-15, May 1977, 51 pp -
illus - tables, Contract DAAG46-74-C-0009
D/A Project 1728036, AMCMS Code 4097
Final Report, September 10, 1973 to May 15, 1977

AD _____

UNCLASSIFIED
UNLIMITED DISTRIBUTION

Key Words:

Cast Nickel Superalloys
Cast Grain Size Control
Low Cycle Fatigue
Stress Rupture Properties
Tensile Properties
Fatigue-Creep Properties

The influence of refinement of the cast grains on the mechanical properties of three nickel base superalloys (713LC, MAR-M-246 and C103) was determined. The investigation was conducted because improvements in the fatigue properties of integrally cast rotors for helicopters was desired. Grain refinement of all three alloys was accomplished by a controlled thermal cycling technique together with a boron addition to the melt. This refinement practice was successfully adapted to production rotor casting. This grain refinement increased by a factor of 2 to 4 the number of cycles to failure in low cycle fatigue of 713LC and MAR-M-246. The fatigue behavior of C103 was insensitive to grain size. The yield strength of 713LC and MAR-M-246 was increased 10 ksi but the tensile strength and ductility slightly decreased by grain refinement. The 1800°F stress rupture properties of the refined alloys were slightly superior to the unrefined alloys at high stress levels and equal to or slightly inferior at low stress levels. At 1850°F and lower stress levels, the stress rupture properties of MAR-M-246 were somewhat reduced compared to the unrefined structure.